MODELING AND SIMULATION OF FLEXIBLE FRAMES FOR PROPER MODELING OF HEAVY TRUCK DYNAMICS

M TANVEER RAHMAN KHAN

Modeling and Simulation of Flexible Frames for Proper Modeling of Heavy Truck Dynamics

By

© M Tanveer Rahman Khan

A thesis submitted to the School of Graduate Studies

In partial fulfillment of the requirements for

The degree of Master of Engineering

Faculty of Engineering and Applied Science

Memorial University of Newfoundland

July 2009

St. John's Newfoundland & Labrador Canada

Acknowledgements

First of all, I am so deeply grateful and would like very much to thank my parents, for giving me the opportunity to come to Canada to pursue a Master of Engineering degree at Memorial University, and also for their fabulous encouragement, genuine love and magnificent support. Moreover, my very special thanks are due to my brother and my sister, for their concerns regarding all aspects about me.

This Master's thesis could not have been completed without the brilliant continued supervision, wonderful help and great contributions of Dr. Geoff Rideout, my Supervisor. I am tremendously grateful to him with great regard and respect.

My warm and lovely thanks are due to my friends here in St. John's who always helped me a lot for settling down mentally over this new atmosphere in the early date of stay.

I sincerely would like to thank Dr. R. Seshadri, Dr. Glyn George, Dr. Seshu Adluri, Dr. Leonard Lye, and Dr. Geoff Rideout, for the knowledge I have gained from the courses, in which they were instructors.

I would like to give special thanks to Mrs. Moya Crocker for her recommendations, suggestions and help always.

Finally, my thanks go to the Faculty of Engineering and Applied Science, Memorial University of Newfoundland for providing facilities and services.

Table of Contents

List of Tables

List of Figures

List of Symbols

ω = Angular velocity

f =Frequency in Hz

T = Time is sec

ω'=Spatial frequency

A = Bump height

L= Length of bump

E=Modulus of Elasticity

ρ = Density

t = Thickness

h = Height

b= Width

P= Instantaneous power

A=Activity

A_{max} = Maximum Activity

V= velocity

F = Force

w= Displacement

κ = slip ratio

Abstract

The goal of the proposed research is to determine the range of validity of rigid body models of trucks depending on the severity of road inputs, and the mass and location of the payload. A "half car" model of a Class VI truck was constructed using the bond graph modeling representation, for which power flow among elements has been employed to determine whether or not frame flexibility affects vehicle motion, or can be neglected. Bond graph based proper modeling and partitioning methods were used to systematically and quantitatively determine whether or not frame flexibility effects were negligible. A proposed algorithm based on Design of Experiments and response surface analysis showed promise in more efficiently searching the design space to generate the range of parameters with fewer simulation runs than were required with a "brute force" method. The feasibility of the power-based partitioning method and response surface algorithm were demonstrated with a simple free-free beam case study.

Flexible frame modal parameters were calculated from theory, and with a finite element model, for inclusion in half-car (pitch plane) bond graph models. Application of the partitioning algorithm to a nonlinear half-car model with vertical and longitudinal dynamics resulted in a range of payloads and road roughnesses for which a rigid model may be assumed valid. The metric for assessing suitability of a rigid model, which was called "relative activity", was correlated with accuracy of a rigid model. Rigid models within the range of validity performed well. The results of this thesis support the use of energy-based partitioning to automate the reduction of truck models. Unnecessary

complexity can be avoided while predictive ability is maintained, with less reliance on intuition and assumption.

Chapter 1

Introduction

1.1 Introduction

Simulating the dynamic response of trucks requires that a model be constructed and subject to road inputs. Inclusion or omission of flexible frame effects is often based on intuition or assumption, with for example one or two lower modes retained for trucks with a long span between axles and a significant load at mid-span. If frame vibration is assumed to significantly affect rigid body outputs such as sprung mass acceleration at the driver's seat or pitch response at the driver's head level, flexibility is typically incorporated in one of two ways. Either a finite element model of the frame is used, for which complexity and computation time can be prohibitive, or a simplified linear lumped-parameter or modal expansion model (which often assumes small motions) is employed.

The goal of the proposed research is to determine the range of validity of rigid body models of trucks depending on the severity of road inputs, and the mass and location of the payload. A "half-car" model of a Class VI truck is constructed using the bond graph modeling representation, for which power flow among elements will be employed to determine whether or not frame flexibility affects vehicle motion, or can be neglected. The flexible frame modal parameters will be calculated from theory and used in a model expansion bond graph model. A simple finite element model will also be

generated to predict the modal natural frequencies. A parametric study will be undertaken to determine the envelope of road inputs and vehicle parameters (including payload) for which flexible frame dynamics are decoupled from gross vehicle motion.

The decoupling will be assessed using a bond graph-based proper modeling and partitioning method which will be discussed in a later chapter. The Response Surface Method will also be to studied as a possible means of more efficiently determining the parameter ranges over which a rigid model is sufficient. The response surfaces are generated with Design of Experiments (DOE) software. The goal of the response surface analysis is to more efficiently search the design space to generate the range of parameters with fewer simulation runs than are required with a "brute force" method. The feasibility of the response surface approach is demonstrated with a simple free-free beam case study.

Section 1.2 gives background information on truck ride quality, focusing on the potential importance of flexibility effects on driver comfort and vehicle handling, as well as approaches to truck frame modeling. In Section 1.3 there will be short description of the fundamentals of finite element analysis. The finite element method will be used to estimate natural frequencies of a simple truck frame model. In Section 1.4 there will be a summary of the bond graph method. In Section 1.5 there will be a short description of Design of Experiments, the statistical tool used to generate the response surfaces. Section 1.6 will describe model partitioning and proper modeling. Section 1.7 will describe the scope of research work in this thesis.

1.2 Truck Ride Quality

Ride quality refers to the degree of protection offered vehicle occupants from uneven elements in the road surface or terrain. A car with very good ride quality is also a comfortable car to ride in. Cars that disturb vehicle occupants with major or minor road irregularities would be judged to have low ride quality.

For vehicles such as trucks, load bearing capability interferes with ride quality - suspension settings are very stiff so the vehicle doesn't change pitch when loaded, meaning that most trucks do not ride particularly comfortably (especially when empty). In passenger vehicles, self-leveling suspension has been introduced to counteract this effect [Jiang, 2001].

Road construction quality and maintenance have a direct impact on ride quality. In jurisdictions with smooth road surfaces, the vehicle can be optimized for a higher degree of handling. In most industrialized countries, as well as in many developing countries, pavement condition is scanned on the road network level using laser/inertial road profilometers. The profilometer records road geometry and condition while driving at highway speed. Results from profilometry can be used to design an optimal geometric pavement repair, eliminating all long wave unevenness, roughness, erroneous cross slope magnitudes and undesired cross slope variance, with the least road grinding and paving efforts [Liu,1997] . The outcome is a surface with superior ride quality.

Gillespie (1985) states that ride quality is a subjective perception normally associated with the level of comfort experienced when traveling in a vehicle. So in a

broad sense the visible ride is the collective result of many factors. Flexibility of the frame is one of the major factors that can affect ride quality. Ibrahim (2004) shows a comparison between the response of the rigid and flexible body models in which the frame flexibility strongly affects the driver vertical acceleration, the cab pitch acceleration, the acceleration of a point on the frame under the cab and the acceleration of a point on the frame under the center of gravity of the truck body. The root mean square acceleration values of these variables for the flexible body model were increased by 18, 125, 64 and 52%, respectively over the rigid body model. He also shows from the response spectra of these variables that in the case of the flexible body model, lightly damped peaks are observed at frequencies corresponding to the first three natural frequencies of the frame flexible modes, particularly at the fundamental frequency of 7.25 Hz.

The analysis presented covers the range 0-40 Hz and is not affected by the inclusion of structural modes higher than the three lowest which have been selected. The inclusion of higher modes would, therefore, only be necessary if the frequency range of interest was extended beyond 40 Hz. The sensitivity of the ride performance to the structural damping of the frame is summarized in which he shows the root mean square values of the truck responses. Significant improvements occur in some aspects of performance, e.g. driver/cab vertical acceleration, but other outputs, e.g. cab suspension working space and longitudinal acceleration are unaffected.

1.3 Finite Element Method

Finite element analysis has been utilized in almost all stages of vehicle design and development, and has played more and more important roles in vehicle durability analysis, crashworthiness and occupant safety analysis, and noise, vibration and harshness (NVH) analysis. Fewer applications were found in the vehicle dynamics area, in which the most commonly used models assume rigid body kinematics and dynamics.

One of the obvious advantages of conducting rigid body dynamics analysis is speed. The solutions can be obtained fast and thus much iteration can be done in a relatively short time period. The most important assumption in using the rigid body approach is that the global effect of the very small component deformations, which are one or two orders less than that of the springs, shocks, bushings etc., to the vehicle dynamic behavior is negligible. The rigid body approach is widely used, and the vehicle dynamics analysis and results of many such applications have been acceptable and even good,

1.4 Bond Graphs

A bond graph is a graphical description of a physical dynamic system. It is an energy-based graphical technique for building mathematical models of dynamic systems. A bond graph depicts the energy flow between components used to model a system [Gawthrop and Ballance, 1999]. Bond graphs have a number of advantages over conventional block diagram and computer simulation techniques. Since they work on the principle of conservation of energy, it is difficult to accidentally introduce extra energy

into a system. Virtually any type of physical system (mechanical, electrical, electro-mechanical, etc.) can be modeled using the bond graph technique. Since each bond represents a bi-directional flow, systems which produce a "back force" (e.g., back emf in a motor) on the input are easily modeled without introducing extra feedback loops [Gawthrop and Ballance, 1999]. Bond graphs are based on the principle of continuity of power. If the dynamics of the physical system to be modeled operate on widely varying time scales, fast continuous-time behaviors can be modeled as instantaneous phenomena by using a hybrid bond graph.

The fundamental idea of a bond graph is that the power transmitted between connected components is the product of generalized "effort" and "flow". In the case of mechanical systems, effort is force and flow is velocity; in the case of torsion systems, effort is torque and flow is angular velocity. Bond graphs consist of elements and junctions. To introduce bond graphs, simple examples of two different physical domains, namely an RLC circuit (electrical domain) and a damped mass–spring system (mechanical domain, translation) are discussed here.

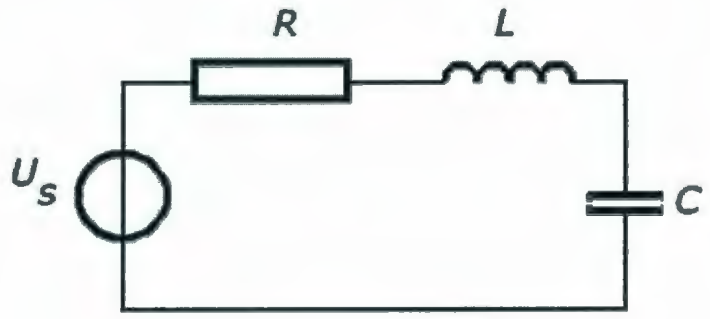

Fig. 1.1: The RLC Circuit [Broenink, 1999]

In electrical networks, the port variables of the bond graph elements are the electrical voltage over the element port and electrical current through the element port. Note that a port is an interface of an element to other elements; it is the connection point of the bonds. The power being exchanged by a port with the rest of the system is the product of voltage and current. In order to facilitate the conversion to bond graphs, the different elements of the electric domain are drawn in such a way that their ports become visible (Figure 1.2). To this port, a power bond was connected or bond for short. This bond denotes the energy exchange between the elements. A bond is drawn as an edge with half an arrow. The direction of this half arrow denotes the positive direction of the energy flow. In principle, the voltage source delivers power and the other elements absorb power.

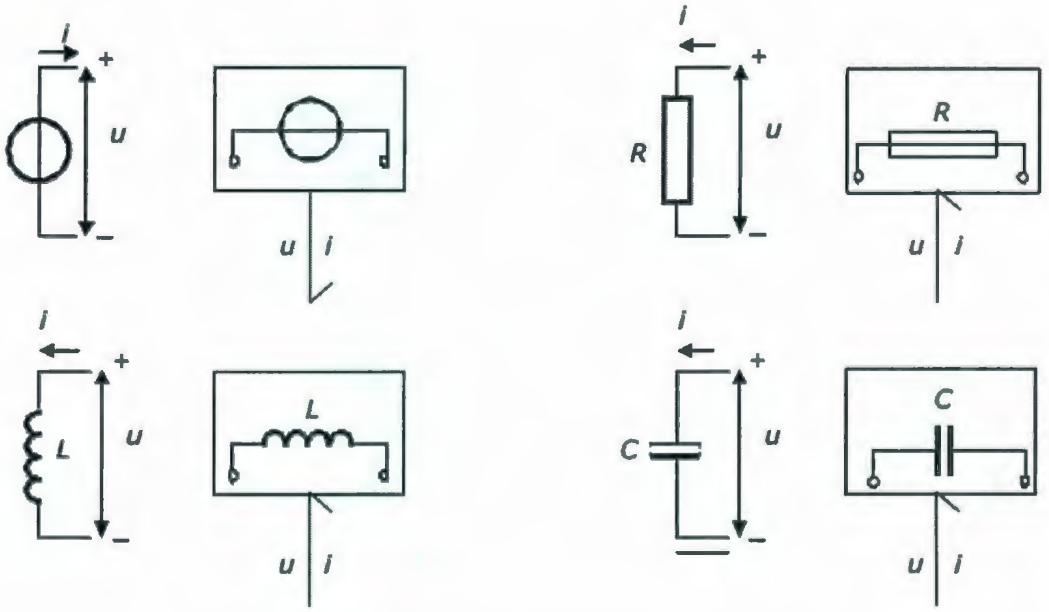

Fig. 1.2: Electrical Elements with Power Ports [Broenink, 1999]

Consider the circuit of Figure 1.1, in which the voltage over the elements is different and through all elements flow the same current. Changing the electric symbols into corresponding bond graph elements results in the bond graph of the electrical circuit. The common current is changed to a '1', which is called 1-junction. Writing the specific variables along the bonds makes the bond graph an electric bond graph. The voltage is mapped onto the domain–independent effort variable and the current maps onto the domain–independent flow variable (the current always on the side of the arrow). 1-junction means that the current (flow) through all connected bonds is the same, and that the voltages (efforts) sum to zero, considering the sign. This sign is related to the power direction (i.e. direction of the half arrow) of the bond. This summing equation is the Kirchhoff voltage law.

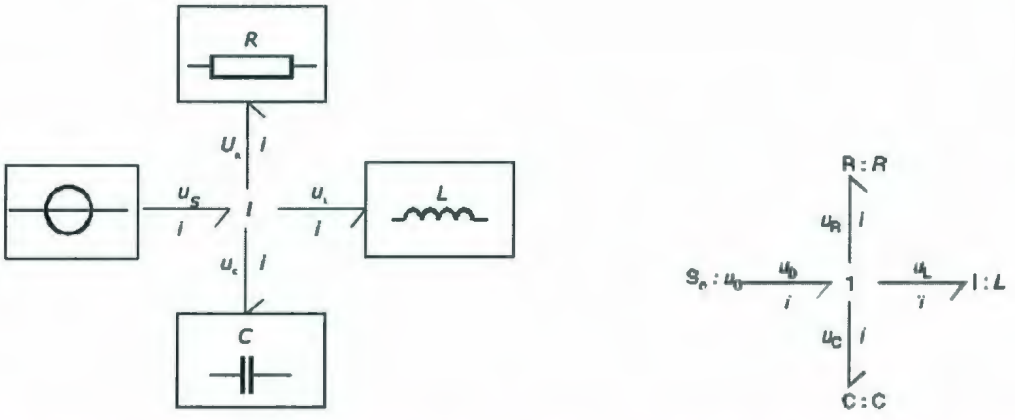

Fig. 1.3: Bond graph with Electrical Symbols (Left) and with Standard Symbols (Right) [Broenink, 1999]

Parallel connections, in which the voltage over all connected elements is the same, are denoted by a 0–junction. A 0–junction means that the voltage (effort) over all connected

bonds is the same, and that the currents (flows) sum to zero, considering the sign. This summing equation is the Kirchhoff current law.

The second example is the damped mass–spring system, a mechanical system shown below in Figure 1.4.

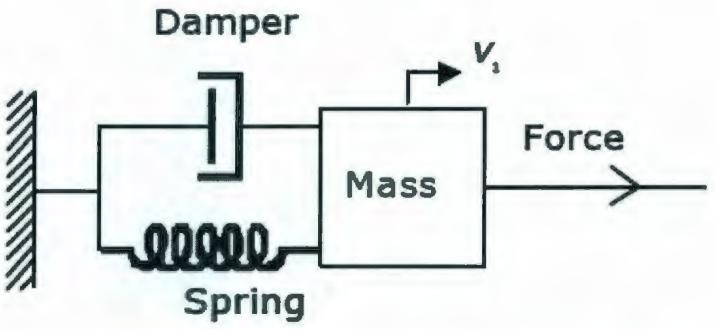

Fig.1.4: Mass-Spring-Damper System [Broenink, 1999]

In mechanical diagrams, the port variables of the bond graph elements are the force on the element port and velocity of the element port. For the rotational mechanical domain, the port variables are the torque and angular velocity. Again, two variables are involved. The power being exchanged by a port with the rest of the system is the product of force and velocity. All elements in the mechanical example have the same velocity. These elements can be connected to a 1-junction, which also implies that the forces sum up to zero (Newton's Law), considering the algebraic sign (related to the power direction). The force is mapped onto an effort and the velocity onto a flow. For the rotational mechanical domain, the torque is mapped onto an effort and the angular velocity onto a flow. This implies that force is analogous to electric voltage and that velocity is analogous to electric current.

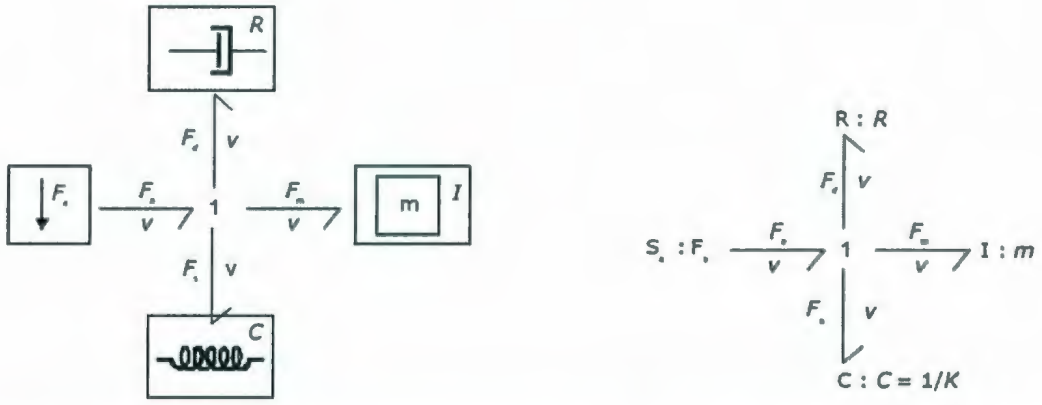

Fig. 1.5: Bond Graph with Mechanical Symbols (Left) and with Standard Symbols (Right) [Broenink, 1999]

From the above discussion it can be declared that in bond graphs, the damper is analogous to the resistor, spring is analogous to the capacitor, mass is analogous to the inductor, force source is analogous to the voltage source, common velocity is analogous to the loop current.

Besides points with common velocity, also points with common force exist in mechanical systems. Then forces are all equal and velocities sum up to zero, considering the sign (related to the power direction). These common force points are denoted as 0-junctions in a bond graph (an example is a series connection of a spring and a damper.

Bond graph elements are drawn as letter combinations indicating the type of element. "C" elements have a generalized displacement energy variable (typically denoted as "q"), e.g. capacitor (stores charge), spring (stores displacement). "I" elements store energy in proportion to their generalized momentum "p", e.g. inductor (stores flux linkage), mass (stores linear momentum). "R" resistor elements dissipate free energy, e.g.

electric resistor, mechanical friction. "Se" and "Sf" elements are sources, e.g. electric mains (voltage source), gravity (force source), and pump (flow source).

Through these two examples, most bond graph symbols were introduced and indicated how in two physical domains the elements are transformed into bond graphs. The electrical and mechanical bond graphs were identical, suggesting that the systems are dynamically equivalent. Bond graphs allow different types of subsystems, such as motors, linkages and pumps, to be easily combined into a single simulation model.

Some bond graph elements did not appear in the previous example models. An ideal transformer is represented by TF and is power continuous (i.e. no power is stored or dissipated). The transformation can occur within the same domain (toothed wheel, lever) or between different domains (electromotor, winch). Efforts are transduced to efforts and flows to flows. The parameter n is the transformer ratio. Due to the power continuity, only one dimensionless parameter, n, is needed to describe both the effort transduction and the flow transduction.

An ideal gyrator is represented by GY, and is also power continuous (i.e. no power is stored or is dissipated. Examples are an electromotor, a pump and a turbine. Real–life realizations of gyrators are mostly transducers representing a domain–transformation. The parameter r is the gyrator ratio. Since r is a relation between effort and flow, it has the same dimension as the parameter of the R element. If r is not constant, the gyrator is a modulated gyrator, a MGY. Table 1.1 summarizes the symbols and constitutive laws of bond graph elements.

Table 1.1: Bond Graph Elements [Rideout et.al. 2007]

	SYMBOL	CONSTITUTIVE LAW (LINEAR)	CAUSALITY CONSTRAINTS
SOURCES			
Flow	Sf ⊢→	f = f(t)	fixed flow out
Effort	Se →⊣	e = e(t)	fixed effort out
ENERGETIC ELEMENTS			
Inertia	→⊣ I ⊢→ I	$f = \frac{1}{I}\int e\,dt$ $e = I\frac{df}{dt}$	preferred integral
Capacitor	⊢→ C →⊣ C	$e = \frac{1}{C}\int f\,dt$ $f = C\frac{de}{dt}$	preferred integral
Resistor	⊢→ R →⊣ R	$e = Rf$ $f = \frac{1}{R}e$	none
2-PORT ELEMENTS			
Transformer	1 →⊣ TF ⊢→ 2 n	$e_2 = n\,e_1$ $f_1 = n\,f_2$	effort in-effort out or flow in-flow out
Modulated Transformer	↓ θ →⊣ MTF →⊣ n(θ)	$e_2 = n(\theta)\,e_1$ $f_1 = n(\theta)\,f_2$	
Gyrator	1 ⊢→ GY →⊣ 2 n	$e_2 = n\,f_1$ $e_1 = n\,f_2$	flow in-effort out or effort in-flow out
Modulated Gyrator	↓ θ ⊢→ MGY →⊣ n(θ)	$e_2 = n(\theta)\,f_1$ $e_1 = n(\theta)\,f_2$	
CONSTRAINT NODES			
1-junction	1 →⊣ 1 ⊢→ 2 ↓ 3	$e_2 = e_1 - e_3$ $f_1 = f_2$ $f_3 = f_2$	one flow input
0-junction	1 ⊢→ 0 ⊢→ 2 ↓ 3	$f_2 = f_1 - f_3$ $e_1 = e_2$ $e_3 = e_2$	one effort input

1.5 DOE Method

Design of Experiments (DOE) is the design of all information-gathering exercises where variation is present, whether under the full control of the experimenter or not (the latter situation is usually called an observational study). Often the experimenter is interested in the effect of some process or intervention (the 'treatment') on some objects (the 'experimental units'), which may be people. Design of experiments is thus a discipline that has very broad application across all the natural and social sciences. It is also called experimental design at a slight risk of ambiguity (it concerns designing experiments, not experimenting in design).

Response Surface Methods (RSM) offer statistical design of experiment (DOE) tools that lead to peak process performance. RSM produces precise maps based on mathematical models. It can put all your responses together via sophisticated optimization approaches, which ultimately lead to the discovery of sweet spots where you meet all specifications at minimal cost.

The development of response surface methods began with the publication of a landmark article by Box and Wilson (1951) entitled "On the Experimental Attainment of Optimum Conditions." In a retrospective on events leading up to this paper, Box (2000) recalled observing process improvement teams in the United Kingdom at Imperial Chemical Industries in the late 1940s. Box and Wilson realized that, as a practical matter, statistical plans for experimentation must be very flexible and allow for a series of iterations. Box and other industrial statisticians, notably Hunter (1958-59) continued to

hone the strategy of experimentation to the point where it became standard practice in chemical and other process industries in the UK and elsewhere. In the United States, Du Pont took the lead in making effective use of the tools of DOE, including RSM. Via their Management and Technology Center they took an in-house workshop called "Strategy of Experimentation" public and, over the last quarter of the 20th century, trained legions of engineers, scientists, and quality professionals on these statistical methods for experimentation.

This now-proven strategy of experimentation, illustrated in Figure 1.2, begins with standard two-level fractional factorial design, mathematically described as "2k-p" [Box and Hunter, 1961], which provides a screening tool. During this phase experimenters seek to discover the vital few factors that create statistically significant effects of practical importance for the goal of process improvement. To save time at this early stage where a number (k) of unknown factors must be quickly screened, the strategy calls for use of relatively low-resolution ("Res") fractions (p).

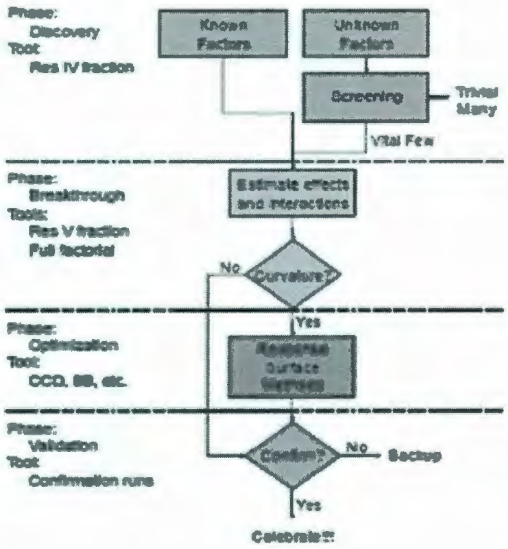

Fig. 1.6: Strategy of Experimentation [Box and Hunter 1961]

After discarding trivial factors (preferably by holding them fixed or blocking them out), the experimental program should enter the breakthrough phase where interactions become evident. This requires higher-resolution, or possibly full, two-level factorial designs. By definition, traditional one-factor-at-a-time (OFAT) approaches will never uncover interactions of factors that often prove to be the key to success, so practitioners of statistical DOE often generate a huge return-on-investment (ROI) at this breakthrough phase.

Eighty percent (or more) of all that can be gained in yield and quality from the process might be accomplished at this point, despite having invested only 20 percent of the overall experimental effort. However, high-tech industries facing severe competition cannot stop here. If curvature is detected in their systems, they must optimize their processes for the remaining 20 percent to be gained. As indicated in the flowchart on

Figure 1.2, this is the point where response surface methods (RSM) come into play. The typical tools used for RSM, which are detailed later in this thesis, are the central composite design (CCD) and Box-Behnken design (BBD).

1.6 Proper Modeling and Partitioning

According to Rideout et.al. (2007) "Proper Modeling" can be defined as the systematic determination of the model of minimal complexity that satisfies the modeling objectives and retains physically meaningful design parameters and variables. Methodologies compatible with the proper modeling philosophy should be systematic and algorithmic, minimizing the need for a domain expert to override the algorithms and leverage his or her experience and intuition to generate the optimally deduced or reduced model. The methodologies are to be applicable to multi-domain models, i.e., models comprised of electrical, hydraulic, thermal and multi-body mechanical components. To ensure that underlying assumptions remain valid throughout the process, the required complexity of the model should be reevaluated as the system parameters and environment change.

In this research problem a half-car bond graph model will be simulated to determine which flexible modes (if any) to eliminate from the model. Once those are identified then a rigid body model can be created, those modes can be partitioned, and thus a proper model can be achieved. More details of the partitioning method will be given in Chapter 4.

1.7 Scope of the Work

Frame flexibility is sometimes an important factor that affects ride quality. Other times, it can be neglected. To improve the efficiency of ride quality modeling it will be much helpful if it is possible to eliminate the flexible effects for a certain payload and road profile. The validity of a rigid model should be determined systematically and quantitatively. The proposed research strives to determine the range of validity of rigid body models for varying vehicle payloads and road profiles. First, a finite element model of the truck frame rails has been modeled using ANSYS to observe the mode shapes and determine the natural frequencies. Due to the suspension of the ANSYS site license at Memorial University and the lack of availability of the software, a complete frame model could not be constructed. The primary role of the finite element analysis was, therefore, to generate approximate estimates of the natural frequencies for transverse vibration, and to compare these with natural frequencies derived from beam theory. Frame rail dimensions were taken from a Sterling truck that is similar to an International Class VI truck for which a complete parameter set is available.

A model of a free-free beam was then created to derive the theoretical modal properties and demonstrate the use of bond graphs for continuous systems. The free-free beam model was incorporated into a nonlinear half-car truck model which contains both vertical and longitudinal dynamics. Bond graph partitioning was performed to find the range of validity of a rigid frame model. A range of payloads and sinusoidal road profile frequencies was determined, for which a rigid model is acceptable. The free-free beam

was also used to investigate the usefulness of the response surface method for determining the range of parameters for which flexible modes did not contribute significantly to system response. An algorithm was developed based on response surface analysis, to reproduce the range of validity results with fewer simulation runs.

Chapter 2

Literature Review

2.1 Introduction

Ride comfort is mainly influenced by whole body vibration and postural position. Exposure to whole body vibration induces effects on vehicle operators from short-term bodily discomfort and inefficient performance to long-term physiological damage. This problem is especially severe for long-distance truck drivers and off-road vehicle drivers, such as agricultural tractor drivers. These drivers are generally more likely to experience large doses of vibration [Jiang, 2001].

The exact degree of ride comfort is extremely difficult to determine due to the numerous factors involved, which include vibration amplitude, frequency, road profile, direction, input position, posture and different subjects. In spite of the complexity involved in evaluating ride comfort, a large body of research gives us considerable information on the general effects of whole body vibration. Those effects are related to ride comfort, interference, health and motion sickness.

Predicting ride for truck models varies on different model criteria. Flexibility and rigidity play an important role in this regard. Different components of truck models such as springs, shocks, suspension linkages and bushings are represented in different ways. Most of the modelers use masses, springs and dampers to represent these components. Moreover rigidity and flexibility are important to keep in mind for a modeler working on

truck frame vibration prediction. In this literature review different aspects are discussed. Section 2.2 gives background information on different methods of ride quality assessing. Section 2.3 will explain factors which affect ride. Section 2.4 will specifically discuss heavy trucks. Section 2.5 will describe applications of rigid and flexible models. In Section 2.6 road profiles for ride simulation will be discussed.

2.2 Ride Quality Assessment Methods

Ride quality boundaries are difficult to determine because of the variations in individual sensitivity to vibration and the lack of a generally accepted approach to the assessment of human response to vibration. Considerable research has, however, been conducted by a number of investigators in an attempt to define ride comfort limits. A variety of methods for assessing ride quality have been developed over the years [Jiang, 2001].

Subjective Ride Measurement

This is the traditional technique for comparing vehicle ride quality in the automotive industry. With a large enough trained jury and a well-designed evaluation scheme, vehicles driven over a given road section are compared. This method can provide a meaningful comparison of the ride quality of different vehicles. However, the difference between vehicles cannot be quantitatively determined by this type of subjective evaluation.

Shaker Table Tests

This is a laboratory test in which vehicle wheels are supported by controlled hydraulic actuators. This test can produce sinusoidal force or displacement excitation in the vertical direction. These tests intend to identify ride quality in terms of vibration, amplitude, velocity or acceleration in the vertical, lateral and longitudinal directions. The longitudinal and lateral vibration cannot be generated; hence this method cannot precisely reproduce the real vibration environment.

Ride Simulator Tests

In this kind of test, the actuator can replicate the vibration in all three directions when the vehicle travels through different road profiles. The actual vehicle body is directly mounted on hydraulic actuators, which will reproduce the vehicle pitch, roll and bounce motion. In this case, it is possible to establish human subjective tolerance limits. The simulator is very expensive and its capability to imitate the real ride simulation will have a great influence on the test results.

2.3 Factors Affecting Ride

There are several design factors affecting vehicle ride [Jiang, 2001]. The most significant factor is the axle (primary) suspension. Wheels, tires, and the suspension are almost completely responsible for the ride of the vehicle in automobile design. When designing heavy trucks, however, other factors also play significant roles. Relative to their smaller mass, cars are much stiffer than trucks. With trucks, their relatively flexible

frames can create a major source of ride problems depending on payload, road input, and frame flexibility. In addition, trucks have many large masses such as exhaust stacks, fuel tanks, and battery boxes that have their own dynamics at different frequencies. Many trucks use a secondary suspension to mount the cab to the frame to better isolate the occupants from the dynamics of the components mounted to the truck frame.

2.4 Heavy Trucks

Originally, cars were built using body-on-frame design. As the name implies, the body was built separately from the frame and then the two were joined together near the end of the manufacturing process. Almost all of the structural rigidity came from the frame. The main advantage of this type of design is ease of manufacturing. Today, most cars and many SUVs are built utilizing a unibody design: the body and frame form a single unit. Unlike body-on-frame designs, the body of a unibody vehicle contributes significantly to structural strength. Unlike cars, however, trucks never made the transition to unibody design. This is because unibody designs lack flexibility of function. The same basic truck chassis design must accomplish many different tasks. One chassis might be used with different truck bodies ranging from cement mixers to moving trucks. The same chassis would also have to accommodate wheelbases (the distance between the front and rear axles) differing by feet. In addition, while cross-country haulers from the same manufacturer may look similar, they are often significantly different from each other. Manufacturers often use the same chassis with several different cabs. Even trucks with the same cab can have different wheelbases. To accommodate these major differences –

not to mention hundreds of other options, such as fuel tank size, transmissions, and body aerodynamics – dozens of separate unibody designs would be required. Combined with the low production numbers of heavy trucks, body-on-frame designs are much more cost-efficient. As mentioned earlier, with a body-on-frame design, the frame is responsible for most of the vehicle's rigidity. This frame consists of two long frame rails connected to each other with cross members every few feet. In addition, the engine, transmission, and fifth wheel double as structural members. The frames of highway trucks are about 20-30 feet long, 1 foot high, and 3 feet wide. Just as with the suspension, there are natural frequencies associated with the frame. The frame has an infinite number of vibration modes, occurring at different frequencies. The most important of these is the first bending mode, which is also called "beaming." The beaming frequency is usually the first mode of vibration, occurring less than 20 Hz [Cao, 2005]. Truck beaming is the first order, full vehicle vertical bending vibration mode. The vertical vibration of the chassis frame rail predominately determines it. Rear axle input is the major source of beaming. By changing frame material properties the beaming frequency can be varied without significant changes in mode shape. Increasing the Young's modulus by 10 percent, the peak vertical frequency response could be reduced by about 10 percent while its beaming frequency was increased by 5 percent [Cao, 2005]. The truck frames are long compared to their height, so they are relatively flexible along their length. If the end of a diving board is held down and then released, it will oscillate up and down at its bending natural frequency. Truck frames behave in the same way in that when a system is excited at its natural frequency, the motion of the input is greatly amplified. In the same manner, when

the truck frame is excited (by the primary suspension) at its beaming frequency, the frame becomes very active. The large displacements that occur at the beaming resonance are a possibly major source of ride deterioration, even when compared to the vibrations caused by the resonances of other components. With suspensions, low natural frequencies are desirable. With structures such as frames, good ride quality is obtained with high natural frequencies. If the frame's modal frequencies are much higher than that the road inputs, the modes will not be excited because the road escalation frequency to the frame (in other words, the output vibrations from the suspension) will be low. Additionally, high frequency vibrations are less important because the human body is less sensitive to them.

2.5 Rigid and Flexible Models

A rigid body is an idealization of solid body of finite size in which deformation is neglected. In other words, the distance between any two given points of a rigid body remains constant in time regardless of external forces exerted on it. The position of a rigid body is determined by the position of its center of mass and by its orientation. On the other hand, in models with flexibility, deformation is considered. A number of researchers have discussed flexible and rigid models. Some researchers considered flexibility in their models whereas others did not.

Ledesma (1998) worked on ride quality of heavy trucks where two models were considered for experiment. In the first model the chassis was assumed to be infinitely

rigid so that the multibody system consists only of rigid bodies. On the second model, the compliance of the chassis frame was considered in the formulation.

Shabana (1989) shows that a chassis frame can be represented by a rigid body or by a flexible body. A rigid frame can be described by its mass, center of gravity and mass moment of inertia about its center of gravity. A flexible body representation can be described by its mass distribution, natural frequencies, damping ratio and mode shapes. These properties can be obtained from a modal analysis of the finite element model of chassis frame or from modal testing. These modal and inertia properties are then included in the formulation of the equations of motion for the mechanical system which consists of rigid and flexible bodies [Shabana, 1989]. Shabana modeled off-frame components such as the engine and transmission as lumped masses which are supported by the chassis frame through mountings. The mountings can be represented as springs with viscous dampers.

Ibrahim (1994) worked on both rigid and flexible models in order to observe the effect of rigidity versus flexibility, and compare simulation results for different road profiles. Ibrahim used a rigid body model with six degree of freedom two-dimensional structures consisting of four rigid body masses (truck body mass, front and rear wheel and axle assemblies). The frame flexibility was taken into consideration in the truck mathematical model. The first three flexible vibration modes were considered and the other modes were assumed to be outside the frequency range of interest which was 0-40 Hz. Flexibility effects arising from the cab and engine structure have also been assumed

to be outside this frequency range and therefore these subsystems have been modeled as rigid bodies [Ibrahim, 1994].

Tong (2000) worked with both rigid and flexible models. His main intention of the simulation was to show the major differences of two flexible frame models and a rigid body model. All the models he compared were simulated using the same boundary conditions. The study by Tong (2000) shows the differences in the system response when the chassis flexibility is considered. Although the elastic deformation was small, the simulation results of flexible models varied significantly from the rigid model.

Jalali (2006) studied the influence of frame flexibility on ride comfort of long vehicles. He used a parametric and simple model which was able to consider frame flexibility. In order to understand the flexibility effects, the behavior of the flexible model has been compared with the behavior of a classical lumped mass model without body flexibility terms.

Dahlberg (1979), Michelberger (1988) and Abdollahi (2001) conducted research on rigidity and flexibility effects on ride quality behavior. But, they modeled the whole body structure as a rigid beam and completely ignored the vehicle body flexibility. Jalali (2006) shows that considering only the rigid frame results in very poor accuracy of the results.

Gadal (1986) and Baum (1977) suggests modeling the whole vehicle using the finite element method. Jalali (2006) shows that this is a very complex and time-consuming modeling approach. So, for considering body flexibility effects in a simple

and parametric manner, Jalali (2006) developed a new ride model that contained both rigidity and flexibility.

In summary, the literature shows that while in many applications, rigid truck models give acceptable results (especially early in the design stage), flexibility effects can often contribute significantly to overall vehicle response. What is missing from the literature is a systematic and quantitative method for determining if flexibility is required. Including flexibility when it does not significantly affect the outputs of interest creates models that are needlessly complex, increases the number of parameters that must be estimated, and typically slows down simulation time. The research in this thesis addresses this limitation.

2.6 Road Profiles for Ride Simulation

The most fundamental excitation variable in the road transport process is the road profile. In the absence of surface defects, any vertical acceleration experienced by a road vehicle would emanate from engine vibrations, wheel imbalance and other deterministic sources of excitation. Therefore, it makes sense to attempt to characterize road profiles and classify them in relevant categories. Road classification method is mainly based on spatial power spectral density (PSD) [Yamada, 1985]. The road surface profiles are stochastic in nature and can be represented by their statistical properties. One of the most useful and compact representations is the PSD of the road profile, which is found by taking the Fourier transform of the road's autocorrelation function, which essentially represents the measured time signal as a series of sinusoidal functions with varying

amplitudes and phases. The PSD represents the power in the signal at a particular frequency, and is typically plotted versus ω (in rad/s) or f (in Hz). Note that $2\pi f = \omega$ and for a vehicle moving at a constant longitudinal velocity, u_0, the distance traveled and the time, t are related by $x = u_0 t$. Thus, one can define a spatial frequency, $\omega' = \omega / u_0$ (in rad/m or rad/ft) or $f' = f / u_0$ (in cycles/m or cycles/ft). Sometimes it is convenient to express the road input excitation as a velocity or acceleration input rather than a displacement (or elevation). A completely random signal is characterized by a flat PSD versus frequency plot. This fact can be used to advantage in simulating road profiles by treating the road profile as the output of the linear filter $G(s=j\omega)$ (i.e., dynamic system with transfer function G(s).Thus one can utilize a random number generator available on a computer system as the basis for generating various road profiles.

The road profile that will be used in this research is sinusoidal, with variable amplitude and wavelength. This allows the road input severity to be varied incrementally, by changing either the bump height or the distance between bumps. Fig 2.1 shows a schematic diagram of the road profile.

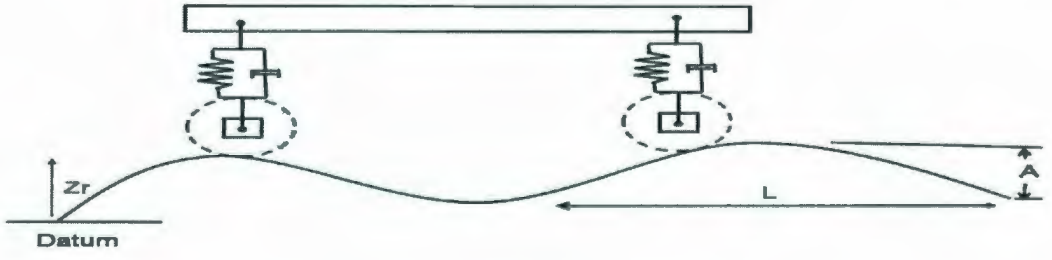

Fig. 2.1: Road Profile Schematic Diagram

In the figure, it shows two parameters that will varied to vary road roughness. For a fixed bump height A, roughness will change if length, L is varied. As length, L is decreased roughness will increase. The governing equation is

$$y = A\sin(\frac{2\pi}{L})x \tag{2.1}$$

Chapter 3

Finite Element Model of Single Rail Frame

3.1 Scope of Analysis

Many studies have been done on vibration of trucks, mainly from the viewpoint of ride quality. Recently, computer aided engineering techniques have been introduced to study this phenomenon [Matsushita et.al. 1979]. Experimental vibrations of vehicles involve complex apparatus and structural components of the vehicle, not to mention diverse types of complicated exciting forces. Since it is very difficult to analyze the vibration phenomena in the design stage, the practice so far has been to make test vehicles and then go on improving them by repeated experiments. However, the use of vehicles is being diversified year by year, and the vehicle itself is being diversified to keep pace with this demand. The pressure is now to design and develop a large variety of vehicles with minimum development time. This is forcing a drastic cut on the time involved in the design- experiment cycle. It is necessary to estimate the various dynamic phenomena accurately in the design stage in order to cut downtime in this cycle. Moreover, it is also necessary to develop practical simulation techniques with a high degree of accuracy.

The phenomenon of vibration, which is considered a big problem in trucks, is affected primarily by the vibration characteristics of the frame. In an actual vehicle, cab and power plant with large mass and moment of inertia are connected with rubber to the frame, along with tires and suspension. Because of this, all the components interplay with each other, thereby setting up a coupled vibration system with multiple degrees of freedom. Analysis of these vibrations calls for not only a highly accurate model of the frame, but also accurate models of the suspension, cab and power plant, etc. The finite element method (FEM) can be considered for analyzing such overall vibration of vehicles after preparing model for a whole vehicle, but the snag for conventional FEM technique is the calculation time and capacity of the computer. Moreover, verifying calculation accuracy of individual parts is also not that easy.

A free-free beam (for which transverse vibration is not constrained at either end) is comparable to a truck frame. There are some limitations of the finite element modeling in this thesis. The ANSYS license became unavailable during the course of the research. Therefore, only a single frame rail could be modeled.

3.2 Basic Concepts in Finite Element Method

The finite element method (FEM) (sometimes referred to as finite element analysis) is a numerical technique for finding approximate solutions of partial differential equations (PDE) as well as of integral equations. The solution approach is based either on eliminating the differential equation completely (steady state problems), or rendering the

PDE into an approximating system of ordinary differential equations, which are then solved using standard techniques such as Euler's method, Runge-Kutta, etc.

In solving partial differential equations, the primary challenge is to create an equation that approximates the equation to be studied, but is numerically stable, meaning that errors in the input data and intermediate calculations do not accumulate and cause the resulting output to be meaningless [Gilbert,1973]. There are many ways of doing this, all with advantages and disadvantages. The Finite Element Method is a good choice for solving partial differential equations over complex domains (like cars and oil pipelines), when the domain changes (as during a solid state reaction with a moving boundary), when the desired precision varies over the entire domain, or when the solution lacks smoothness. For instance, in a frontal crash simulation it is possible to increase prediction accuracy in "important" areas like the front of the car and reduce it in its rear (thus reducing cost of the simulation).

A variety of specializations under the umbrella of the mechanical engineering discipline (such as aeronautical, biomechanical, and automotive industries) commonly use integrated FEM in design and development of their products. Several modern FEM packages include specific components such as thermal, electromagnetic, fluid, and structural working environments. In a structural simulation, FEM helps tremendously in producing stiffness and strength visualizations and also in minimizing weight, materials, and costs. FEM allows detailed visualization of where structures bend or twist, and indicates the distribution of stresses and displacements. FEM software provides a wide

range of simulation options for controlling the complexity of both modeling and analysis of a system. Similarly, the desired level of accuracy required and associated computational time requirements can be managed simultaneously to address most engineering applications. FEM allows entire designs to be constructed, refined, and optimized before the design is manufactured. This powerful design tool has significantly improved both the standard of engineering designs and the methodology of the design process in many industrial applications. The introduction of FEM has substantially decreased the time to take products from concept to the production line. It is primarily through improved initial prototype designs using FEM that testing and development have been accelerated. In summary, benefits of FEM include increased accuracy, enhanced design and better insight into critical design parameters, virtual prototyping, fewer hardware prototypes, a faster and less expensive design cycle, increased productivity, and increased revenue.

3.3 Modal Analysis Using FEM

The goal of modal analysis in structural mechanics is to determine the natural mode shapes and frequencies of an object or structure during free vibration. It is common to use the finite element method (FEM) to perform this analysis. . The types of equations which arise from modal analysis are those seen in eigensystems. The physical interpretation of the eigenvalues and eigenvectors which come from solving the system are that they represent the frequencies and corresponding mode shapes. Sometimes, the

only desired modes are the lowest frequencies because they can be the most prominent modes at which the object will vibrate, dominating all the higher frequency modes.

It is also possible to test a physical object to determine its natural frequencies and mode shapes. This is called an Experimental Modal Analysis. The results of the physical test can be used to calibrate a finite element model to determine if the underlying assumptions made were correct (for example, correct material properties and boundary conditions were used).

3.4 Finite Element Model for Single Rail Frame

A single rail frame was modeled using the finite element method (which is comparable to a free-free beam). The natural frequency theoretically was obtained from the Equation 3.1, where β comes from solution of a trigonometric frequency equation, ℓ is the length of the beam and I is the area moment of inertia

$$\omega^2 = (\beta l)^2 \sqrt{EI / \rho A l^4} \tag{3.1}$$

The dimensions were obtained from a Sterling truck cab and chassis vocational reference guide published in January 2002 [Sterling, 2002].

Dimensions:

Length, L= 5.283 m

Width, b = 0.162 m

Height, h = 0.2604 m

Thickness, t = 0.0508 m

Parameters:

Modulus of Elasticity, E = 200e9 N/ m^2

X-Sectional Area, A = 0.032633 m^2

Density, ρ = 76812.3 N/m^3

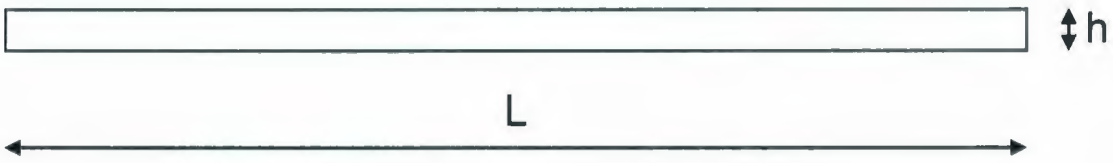

Fig. 3.1: Schematic Diagram of Free Free Beam

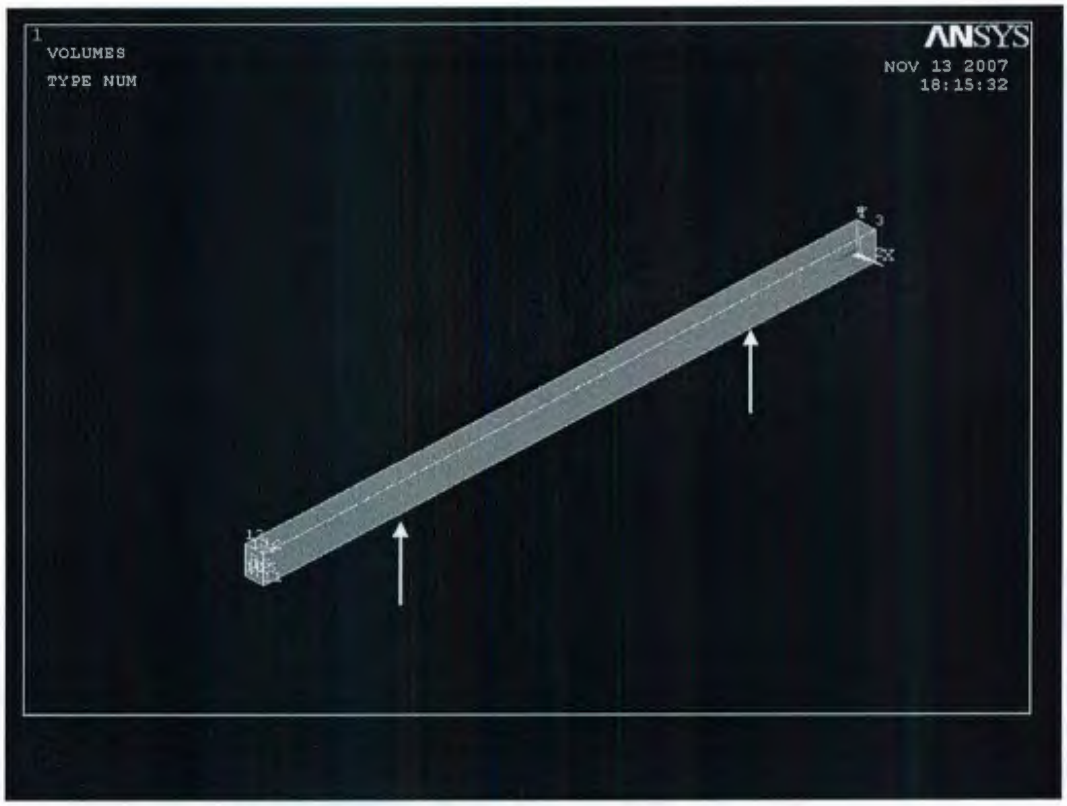

Fig. 3.2 ANSYS Model of a Free Free Beam

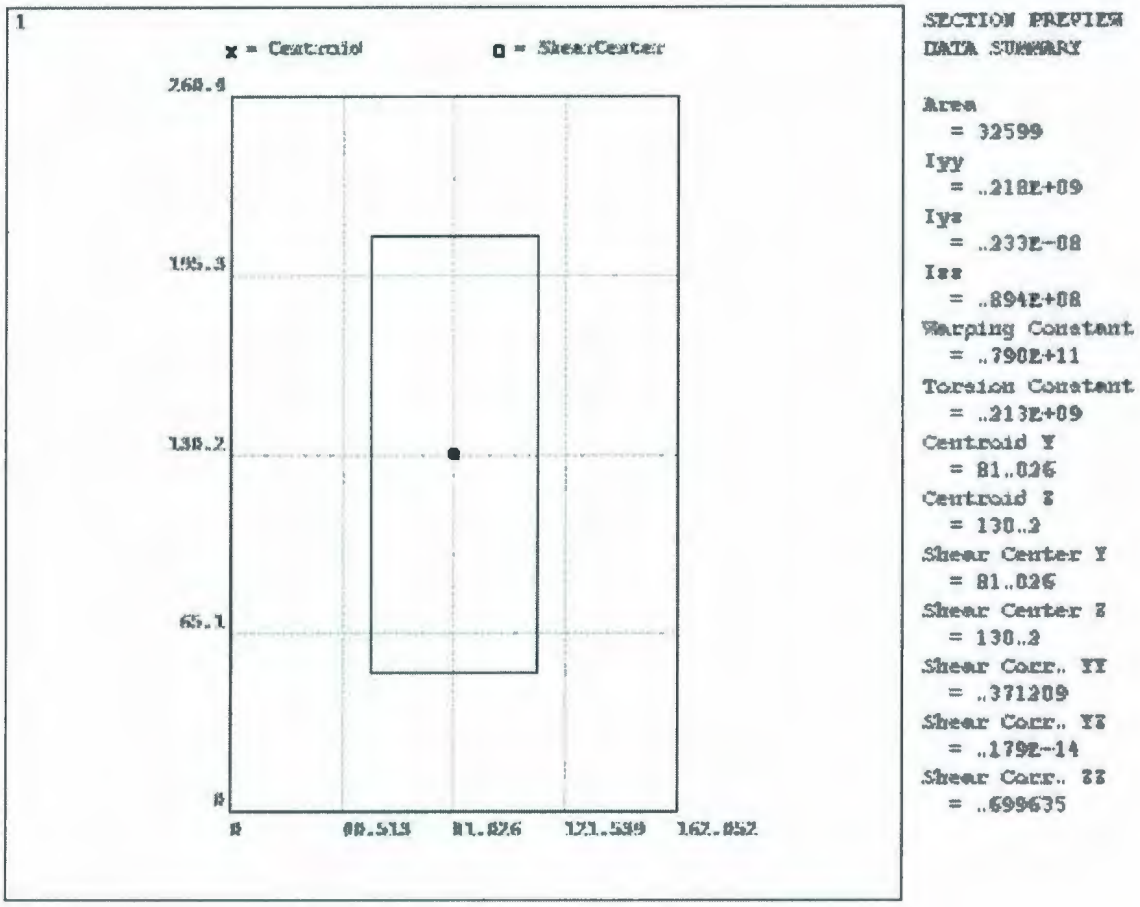

Fig. 3.3: Section Diagram of Free Free Beam

The natural frequencies obtained theoretically were 10.27 Hz, 17.05 Hz and 30.69 Hz respectively for first, second and third flexible mode shapes. The theoretical values were obtained using Equation 3.1. Then a free-free beam was modeled using "beam 3" elements in ANSYS environment. Because it was a free-free beam, no constraints were needed for the FEA model but the suspension mounting points were used as shown in Figure 3.2. The beam was modeled as a box beam cross section to input the real

geometric parameters. After modeling the beam, modal analysis was done to get the natural frequencies of the flexible modes. The simulation results obtained were 10.930 Hz, 16.979 Hz and 30.041 Hz.

A simplified version of a real truck frame with consideration of flexible modes has been shown in this Finite Element Model. Adding cross members in the model would make it more realistic, with increased stiffness. Some other factors should be included in future FEA modeling efforts like welds and joints of the cross members, location and orientation of cross members and suspension mounting points.

While the free-free beam is geometrically an oversimplification of the truck frame, the bending natural frequencies are similar to those of actual compliant truck frames with long spans. In Chapter 4, the single rail free-free beam modal parameters, including frequencies determined numerically in this chapter, will be derived.

Chapter 4 also develops theory for the partitioning algorithm. Chapter 5 applies partitioning to a nonlinear half-car truck model, the flexible portion of which is based on the free-free beam from Chapter 4 (same basic modal bond graph) and Chapter 6 will take the simple free-free beam model, and find range of validity two ways: using "brute force", and using DOE.

Chapter 4

Free-Free Beam Bond Graph, Partitioning and Relative Activity

4.1 Introduction

A free-free beam with force inputs at two discrete points is comparable to an automobile frame with front and rear suspension mounting points. A model of a free-free beam consisting of two rigid body modes and three flexible modes was constructed to represent the vehicle frame in the 20SIM bond graph software environment [20SIM, 2006]. The first two modes are rigid body translation and rotation, and the other three are flexible modes. Here in this case study a bond graph model was created and then simulated for different road frequencies and payloads to determine the range of parameters for which a rigid model is accurate. Front and rear suspensions are included. Road inputs are sinusoidal as per Figure 2.1. The model was implemented as a bond graph in 20SIM, to facilitate use of a partitioning algorithm. The partitioning algorithm will be described in Section 4.3. The partitioning algorithm will be used to find a range of parameters for which flexible modes do no significantly affect the rigid body modes and connected suspension elements. Range of validity will be plotted as a response surface. The Z axis will be maximum Relative Activity (RA) of the flexible modes, which must be below a certain threshold if the modes are negligible. Relative Activity will be defined

in Section 4.2. The X and Y axes will be the two parameters of interest that can influence the contribution of flexible modes, in this case road roughness and payload mass. A threshold value of 0.05 was set for the relative activity (RA). Then an Excel 3D Surface plot was created using the data obtained from the simulation to get the zone which was below the threshold value and also to show a graphical representation of the range over which the rigid models are valid.

Section 4.4 describes a modal expansion model of a free-free beam, and Section 4.5 shows the bond graph implementation of that model for use in later simulations.

4.2 Relative Activity

The link between constitutive law variables of energetic elements in a model is through constraint equations. Rideout *et.al.* [2007] shows how the power conserving constraint equations represented by the junction structure (0 and 1 junctions) of a bond graph model link the constitutive law variables of energetic elements, and thus can give insight into the location of weak coupling within a system. To find negligible constraint equation terms at each 0- or 1- junction a new term called "relative activity" was used. A mode can be decoupled if constraint equations involving it have negligible relative activity. In flexible systems represented by modal bond graphs, a mode is decoupled if it contributes terms with relative activity negligible compared to all the constraint equations involving it [Rideout *et al.*, 2007].

Activity A [Louca *et al.*, 1997] of an element or bond over the time interval $[t_1,t_2]$ is defined as:

$$A = \int_{t_1}^{t_2} |P| \, dt \tag{4.1}$$

P is instantaneous power (product of effort and flow) of the element or bond. The activity of a bond (constraint equation term) attached to a 0- or 1-junction (constraint equation), compared to the activities of the other bonds at that junction, is a measure of the relative importance of the term compared to the other terms in the equation. Relative activity RA_i of bond i at a junction is defined as the ratio of bond activity A_i to maximum bond activity A_{max} at the junction:

$$RA_i = \frac{A_i}{A_{\max}} \tag{4.2}$$

Low relative activity of bond i at a junction implies that:

i) for a 0-junction with n bonds, the flow f_i can be neglected in the flow constraint equation

$$\sum_{j=1}^{n} f_j = 0 \tag{4.3}$$

ii) for a 1-junction with n bonds, the effort e_i can be neglected in the effort equation

$$\sum_{j=1}^{n} e_j = 0 \tag{4.4}$$

4.3 Model Partitioning

A power bond with low relative activity at a 0-junction (1-junction) can be "conditioned", or converted to a modulated effort (flow) source. The modulating signal is the effort (flow) from the junction. The effort (flow) is applied to the node at the other end of the bond, i.e., the end that is not adjacent to the 0-junction (1-junction) at which the bond is inactive. The half-arrow direction (direction of algebraically positive power

flow) of the modulated source is the same as that of the original low-activity bond. Table 4.1 illustrates the conversion.

Table 4.1 - Interpretation of Locally Inactive Bonds [Rideout et al., 2007]

Scenario (i)	Case A, $A_1 << A_{m+1,\ldots n}$	Case B, $A_1 << A_{2,\ldots m}$
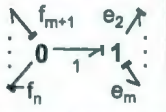	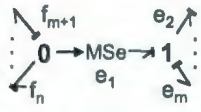	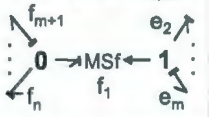
Scenario (ii)	Case A, $A_1 << A_{2,\ldots m}$	
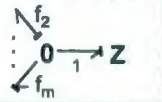	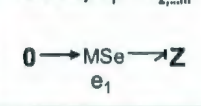	
Scenario (iii)	Case A, $A_1 << A_{2,\ldots m}$	
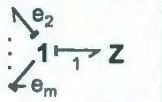	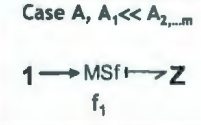	

The activity of an "internal" junction structure bond (between two junction structure elements) must be compared to the activities of the other bonds connected to both elements, as shown in Scenario (i) of Table 4.1. If both Cases A and B apply, then the original bond can be eliminated. If the local activity of an "external" junction structure bond (between a junction and an energy storage or dissipative element) is negligible, a trivial driven partition results as shown in Scenarios (ii) and (iii) of Table 4.1. The generalized impedance *Z* (representing an *I, C,* or *R* element) can then be eliminated from the model. Other possible internal bond connections are shown in Table 3 where the internal bond connects a 1- or 0-junction to an *(M)TF* or *(M)GY* element. If both bonds are locally inactive compared to their respective junctions, then the transformer or gyrator can be eliminated. If one bond is locally inactive, a modulated

source in sequence with an *(M)TF* or *(M)GY* results. The transformer or gyrator can be incorporated into the source, resulting in the equivalent conditioned junction structure shown in Table 4.2.

Table 4.2 - Transformer and Gyrator Conditioning [Rideout et al., 2007]

Transformer	Case A, $A_{1a} << A_{m+1,\ldots n}$	Equivalent
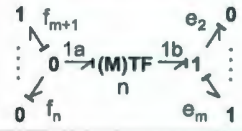	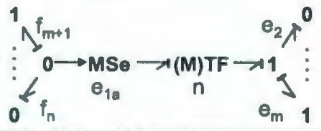	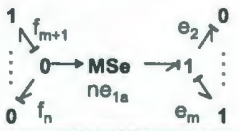
	Case B, $A_{1b} << A_{2,\ldots m}$	Equivalent
	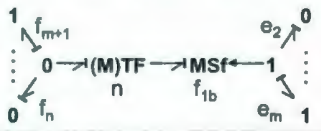	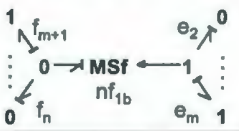
Gyrator	$A_{1a} << A_{m+1,\ldots n}$	Equivalent
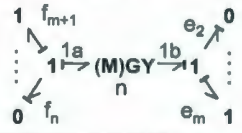	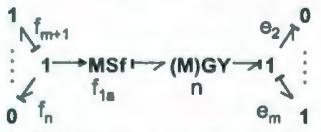	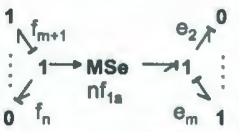
	$A_{1b} << A_{2,\ldots m}$	Equivalent
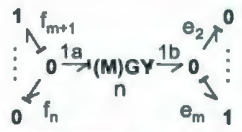	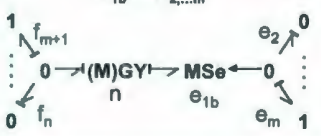	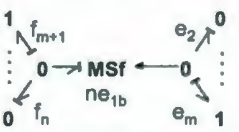

Given a conditioned bond graph (a bond graph with all locally negligible power bonds converted to modulated sources or eliminated), a *subgraph S* is a set of elements from that bond graph (including sources, energetic elements, and junction structure) that has no power bonds connected to any bond graph element outside the set.

When all *new* modulating signals (due to bond conditioning) between two subgraphs are directed from one subgraph to another subgraph, the subgraph from which

the signals originate is the *driving subgraph* $S^{\rightarrow}$, and the other is the *driven subgraph* $S^{\leftarrow}$ as shown in Figure 4.1.

A *driving partition* is a subgraph $P^{\rightarrow}$ that is connected to at least one other subgraph *strictly* by modulating signals directed outwards from $P^{\rightarrow}$ to that subgraph. See Figure 4.2 for examples.

A *driven partition* is a subgraph $P^{\leftarrow}$ that is connected to at least one other subgraph *strictly* by modulating signals directed inwards towards $P^{\leftarrow}$ from that other subgraph (Figure 4.2).

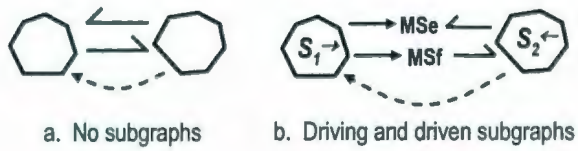

Figure 4.1: Subgraph Example Schematic [Rideout et al., 2007]

In the case studies that follow, negligible modes of a modal bond graph are eliminated if they can be shown to be driven partitions. A rigid model is assumed valid if the rigid elements are in a driving partition and the flexible modes are driven partitions.

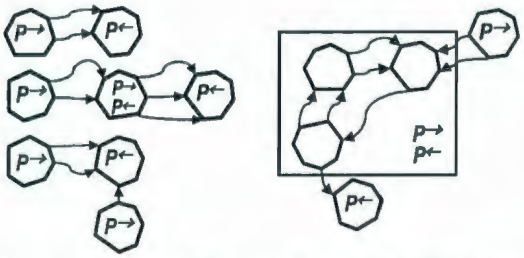

Figure 4.2: Driving and Driven Partitions [Rideout et al., 2007]

4.4 Modal Expansion Theory

A free-free beam was considered to compare the mode shape and frequencies with the finite element model which was described in an earlier chapter. To create a free-free beam model in a bond graph environment some basics of theory will be described here. The reader is referred to the text by Karnopp, Margolis and Rosenberg (2006) on which the following derivations are based.

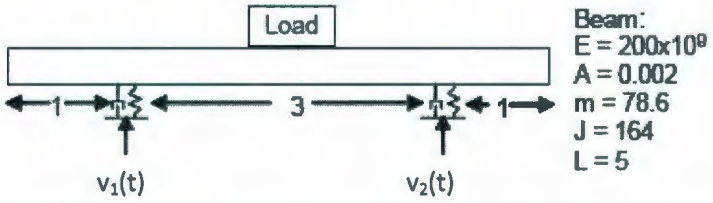

Fig. 4.3: Schematic Diagram of Free-Free Beam

The above figure shows a Bernoulli-Euler beam [Karnopp, Margolis and Rosenberg, 2005] with two external forces from the suspensions. The inertia force acting on the element of the beam is

$$\rho A \Delta x \frac{\partial^2 \omega}{\partial t^2} \tag{4.5}$$

From Newton's Second Law for the element,

$$V(x+\Delta x) - V(x) = \rho A \Delta x \frac{\partial^2 \omega}{\partial t^2} \tag{4.6}$$

The model can be reduced to a continuum representation by letting $\Delta x \to 0$ and letting small differences divided by Δx become derivatives. Thus, from Eq. (4.6),

$$\lim_{\Delta x \to 0} \frac{V(x+\Delta x) - V(x)}{\Delta x} = \frac{\partial V}{\partial x} \tag{4.7}$$

And

$$\frac{\partial V}{\partial x} = \rho A \frac{\partial^2 \omega}{\partial t^2} \tag{4.8}$$

As the point velocity $v_1(t)$ and $v_2(t)$ are acting on the Bernoulli-Euler beam at locations x_1 and x_2, respectively, along the beam, we can write,

$$F_1 \delta(x - x_1) + F_2 \delta(x - x_2) = EI \frac{\partial^4 \omega}{\partial x^4} + \rho A \frac{\partial^2 \omega}{\partial t^2} \tag{4.9}$$

The force-free boundary conditions are that no shear force and no moment exist at x=0 and x=L. So boundary conditions can be written in terms of $w(x,t)$ for the zero moment constraint as

$$\frac{\partial^2 \omega}{\partial x^2}(0,t) = \frac{\partial^2 \omega}{\partial x^2}(L,t) = 0 \tag{4.10}$$

And for the zero-shear constraint

$$\frac{\partial^3 \omega}{\partial x^3}(0,t) = \frac{\partial^3 \omega}{\partial x^3}(L,t) = 0 \tag{4.11}$$

The solution can be found using the method of separation of variables for the homogenous form of Eq. (4.9) and assuming

$$w(x,t) = Y(x) f(t) \tag{4.12}$$

Substituting into Eq. (4.8) gives

$$EI \frac{d^4 Y}{dx^4} f + \rho A Y \frac{d^2 f}{dt^2} = 0 \tag{4.13}$$

Diving each term by $\rho A Y \; f$ gives

$$\frac{EI}{\rho A} \frac{1}{Y} \frac{d^4 Y}{dx^4} + \frac{1}{f} \frac{d^2 f}{dt^2} = 0 \tag{4.14}$$

This equation can be satisfied at all x and all t only if both terms equal the same constant. Putting the second term equal to $-\omega^2$, gives

$$\frac{d^2 f}{dt^2} + \omega^2 f = 0 \tag{4.15}$$

And

$$\frac{d^4 Y}{dx^4} - \frac{\rho A}{EI}\omega^2 Y = 0 \tag{4.16}$$

Or it can be written as,

$$\frac{d^4 Y}{dx^4} - k^4 Y = 0 \tag{4.17}$$

Where

$$k^4 = \frac{\rho A}{EI}\omega^2 \tag{4.18}$$

Equation (4.16) is a total differential equation which, when solved subject to the boundary conditions (4.9) and (4.10), will yield the mode shapes and associated modal frequencies. Using Eq. (4.11) in the boundary condition yields

$$\frac{d^2 Y}{dx^2}(0) = \frac{d^2 Y}{dx^2}(L) = \frac{d^3 Y}{dx^3}(0) = \frac{d^3 Y}{dx^3}(L) = 0 \tag{4.19}$$

The spatial equation (4.16) has the general solution

$$Y(x) = A\cosh kx + B\sinh kx + C\cos kx + D\sin kx \tag{4.20}$$

Using (4.19) yields the frequency equation

$$\cosh k_n L \cos k_n L = 1 \tag{4.21}$$

The mode shape functions

$$Y_n(x) = (\cos k_n L - \cosh k_n L)(\sin k_n x + \sinh k_n x) - (\sin k_n L - \sinh k_n L)(\cos k_n x + \cosh k_n x) \tag{4.22}$$

Solving Eq. (4.20) for special values of $k_n L$ and using these in Eq. (4.17) mode frequencies gives,

$$\omega_n^2 = \frac{EI}{\rho A}\frac{(k_n L)^4}{L^4} \tag{4.23}$$

The modal masses are

$$m_n = \int_0^L \rho A Y_n^2 dx, \qquad \text{n=1,2,....,} \tag{4.24}$$

The modal stiffness is

$$k_n = m_n \omega_n^2, \quad \text{n= 1,2,....,} \tag{4.25}$$

4.5 Bond Graph Model

A simple free-free bond graph model is created to test the assumption of whether a rigid body model is valid up to a certain range of load and road roughness. It was discussed in Chapter 2 why inclusion of excess structure such as unnecessary flexible modes is potentially undesirable. The model partitioning technique of Section 4.3 is used to determine if flexible mode responses have an insignificant effect on the dominant system dynamics that excite them. If so, then the partitioned modes can be eliminated.

In Figure 4.4 below, a free-free beam model is represented with bond graph elements. More details on this bond graph will be discussed on next chapter. Note that the three flexible modes appear as a 1-junction corresponding to the modal velocity, and attached to these 1-junctions are modal mass I element and modal stiffness C element. Velocity at discrete points such as the suspension locations and load location, are arrived at by summing each modal velocity times the mode shape value at those locations. The mode shape values are the moduli of the transformer (TF elements) in the bond graph. The TF elements also take input forces from the suspension elements and load, and multiply them by the respective mode shape amplitudes to get the contribution of the forces to each mode.

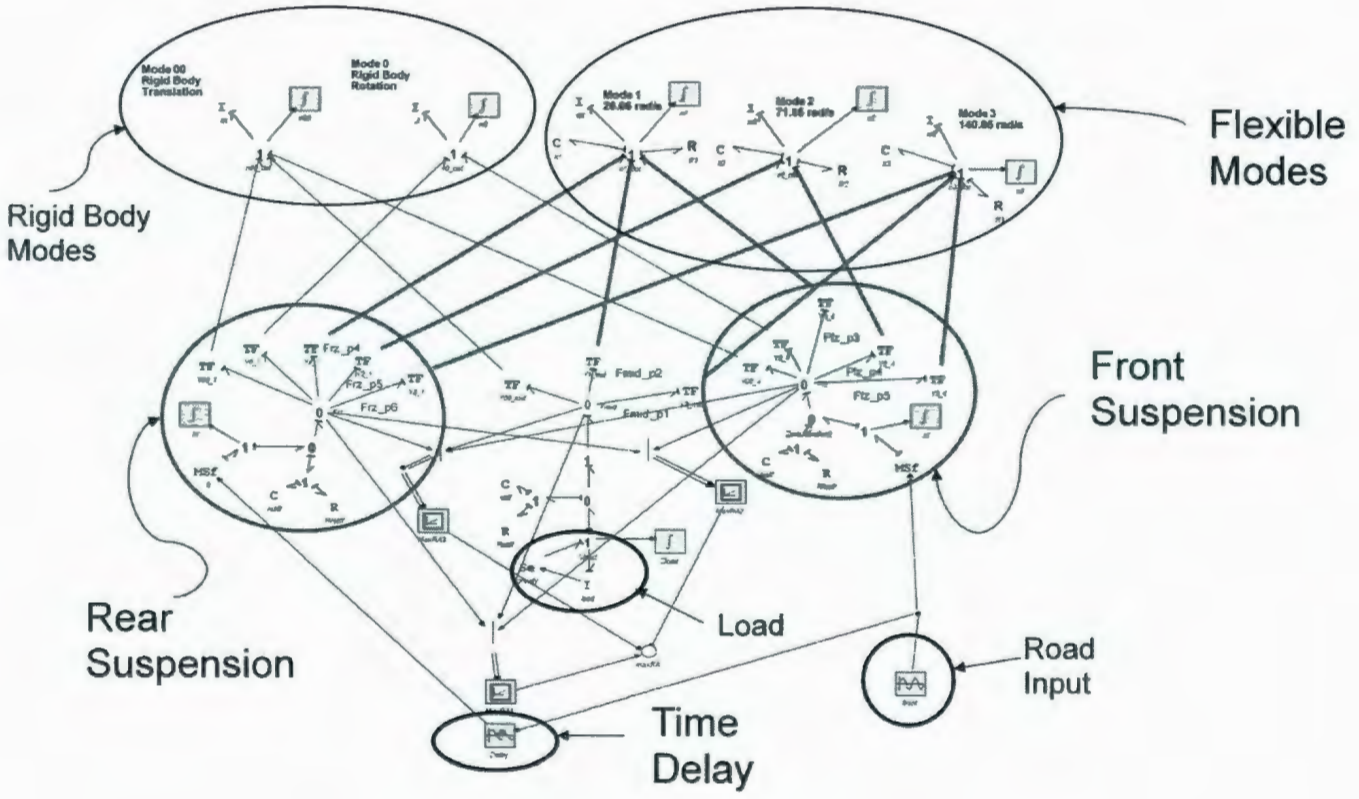

Fig. 4.4: Bond Graph Model of Free-Free Beam

Chapter 5 incorporates the free-free beam bond graph model into a nonlinear half-car model of a Class VI truck, and uses partitioning to find the range of validity of a rigid model subject to road roughness and load parameters. Chapter 6 uses the simpler example system of Figure 4.3 to similarly find the rigid model range of validity, and then compares the results with those obtained with a new algorithm for refining the range of validity search process.

Chapter 5

Range of Validity Case Study: Nonlinear Pitch Plane Truck Model

5.1 Introduction

In this chapter a nonlinear half-car model will be studied. The non-linear half-car model is actually an extension of the free-free beam that was discussed in Chapter 4. The range of validity of rigid models will be studied for varying payload and road roughness.

Section 5.2 describes the bond graph model. Section 5.3 gives the specific variables that will be changed and gives the extents of the test matrix. Section 5.4 gives contour plots of rigid model range of validity, based on relative activity partitioning of flexible modes. Section 5.5 investigates the correlation between flexible mode activity and accuracy of a rigid model, and discusses the results.

5.2 Model Description

A more realistic model was created using the free-free beam as a flexible frame submodel, and including realistic parameters of a Class VI truck. A nonlinear, pitch-plane half-car model of a truck was modeled in the 20SIM bond graph software environment. The model is based on the schematic diagram shown in Fig 5.1.

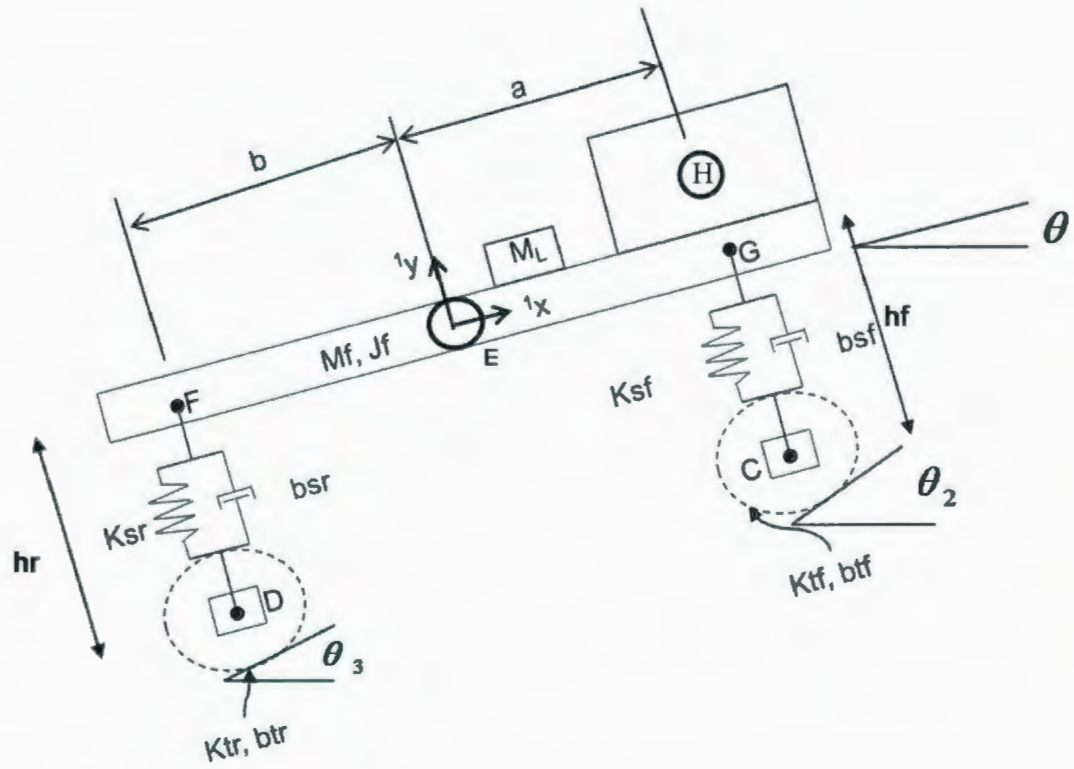

Fig. 5.1: Schematic Diagram of Half-car Model

The vehicle model consists of frame, load, engine, sprung mass and unsprung mass. Velocity components of the sprung mass are expressed in a body fixed frame which is ${}^1x$ and ${}^1y$. The parameters values are-

Frame mass= M_F=5080 kg

Frame inertia = J_F = 21969 kg.m^2

Engine mass = M_E =2177 kg

Rotational inertia of engine block = J_E = 2177 kg-m^2

θ = pitch angle (rad)

θ_2 = Road angle at front wheel (rad)

θ_3 = Road angle at Rear wheel (rad)

h_r = Distance from rear of frame to unsprung mass, when suspension springs are undeflected

h_f = Distance from front of frame to unsprung mass, when suspension springs are undeflected

The wheel distances from the sprung mass are related to the suspension deflections as follows:

$$FD = h_r + Y_{susp\text{-}r} \tag{5.1}$$

and

$$GC = h_f + Y_{susp\text{-}f} \tag{5.2}$$

Assuming small transverse beam deflection gives:

$$^1v_{GX} = {}^1v_{EX} = {}^1v_{FX} \tag{5.3}$$

$$^1v_{HX} = {}^1v_{EX} - GH\omega \tag{5.4}$$

where ω is rate of change of pitch angle θ.

$$^1v_{GY} = {}^1v_{EY} + EG\,\omega \tag{5.5}$$

$$^1v_{FX} = {}^1v_{EY} - EF\,\omega \tag{5.6}$$

GE= 2.115 m and FE= 1.615 m

Bond Graph model

A top level model of the bond graph is shown in Fig. 5.2 below. Explanations of the sub models will follow.

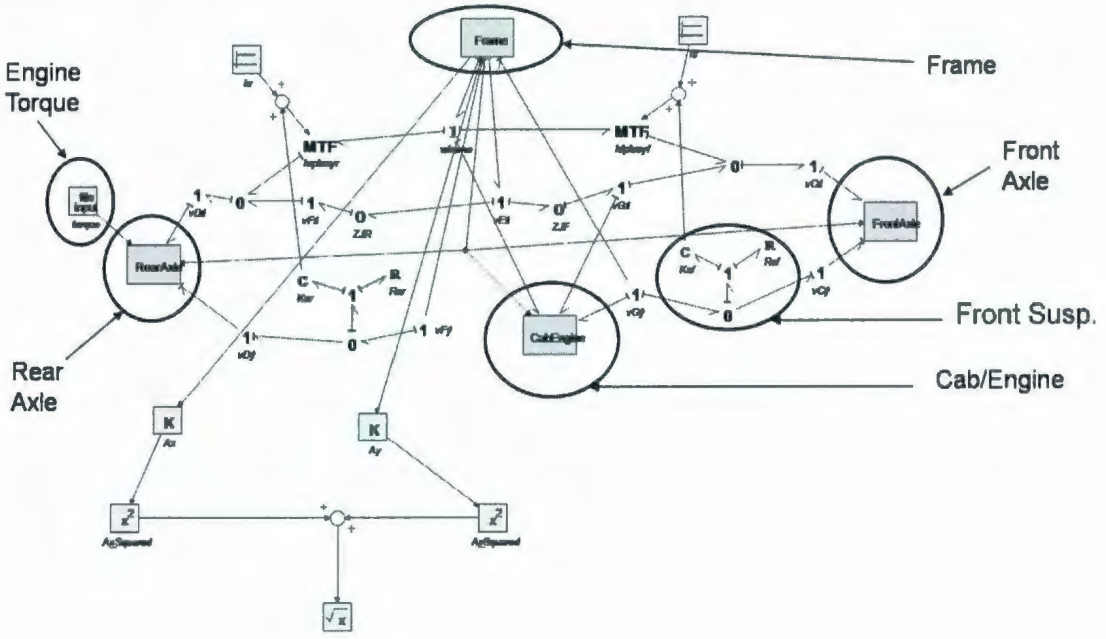

Fig. 5.2: Top Level Model of Nonlinear Half-car

In Figure 5.2, the suspensions are modeled as linear springs (K_{sf}, K_{sr}) and dampers (b_{sf}, b_{sr}) connected in parallel, the extension velocities of which are defined by zero junctions that calculate the differences (v_{Fy}-v_{Dy}) and (v_{Gy}- v_{Cy}) in the bond graph. The axles are constrained to move rigidly (with sprung mass) along the lines DF and GC (along the body fixed ^{1}y axis). The velocities of points C, D, F, and G in the sprung mass frame are

defined using the center of gravity velocities, fixed distances a and b from the Centre of Gravity (C.G) and distances (DF- h_r) and (GC- h_f).

Front and Rear Axle Sub models (Fig. 5.3 and 5.4)

The tire spring (K_{tf}, K_{tr}) and damper (b_{tf}, b_{tr}) forces are functions of displacements and velocities along lines normal to the road. In lieu of a road height velocity profile, the road is input to the model as a slope (the arctangent of which is road inclination angle θ_2 or θ_3), that varies as a function of distance x_f or x_r traveled by the front or rear of the vehicle. The drive torque was generated from an engine model referenced in Sendur et. al.(2002). Front and rear wheel hub forward velocities are integrated with the resulting displacements serving as inputs to road slope. [Rideout et.al. 2007]

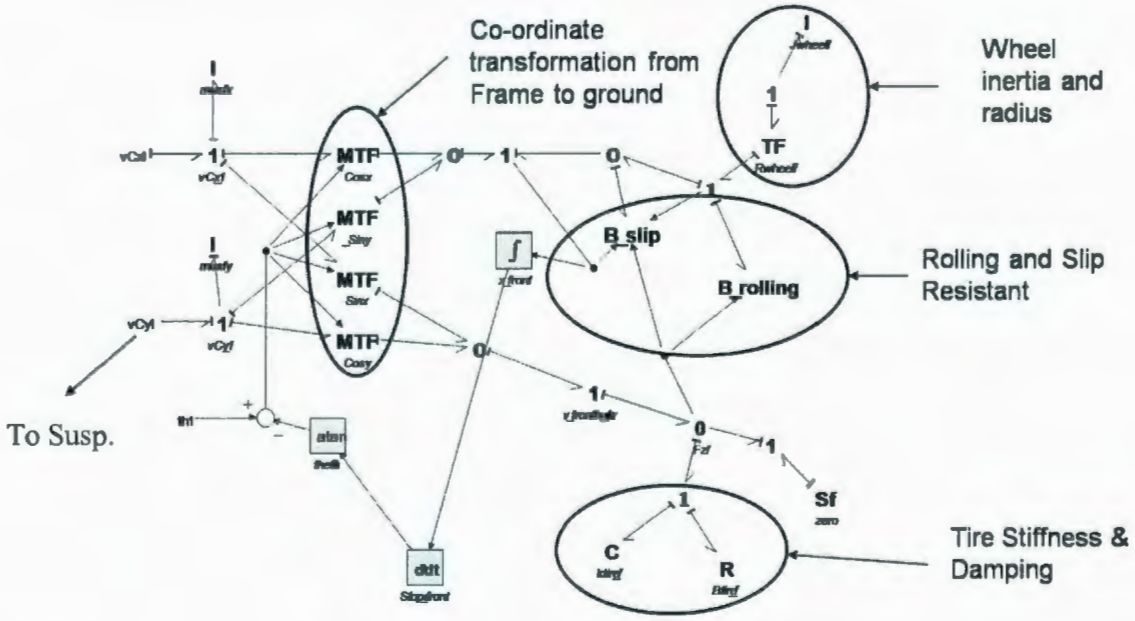

Fig. 5.3: Front Axle Bond Graph Submodel

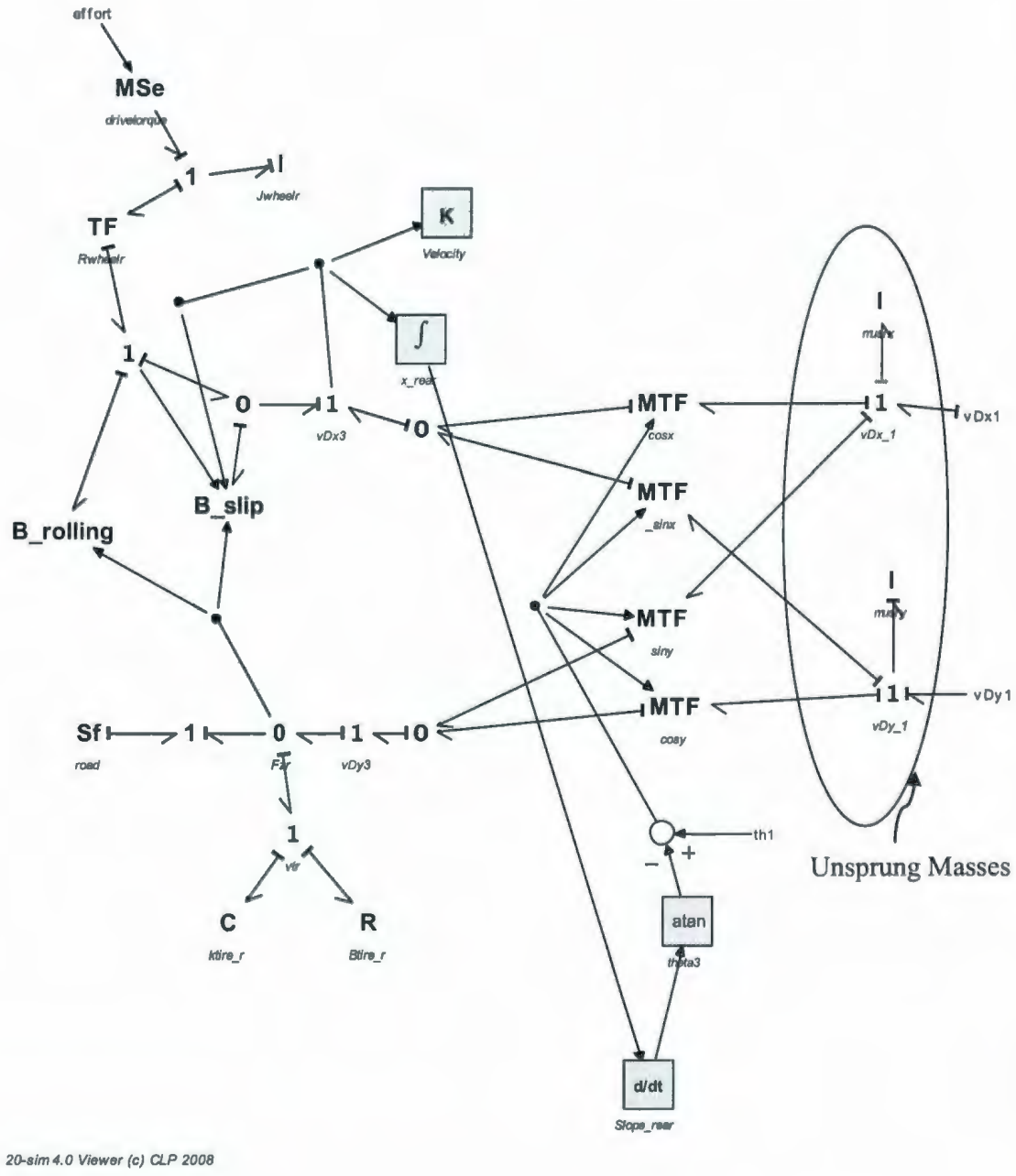

Fig. 5.4: Rear Axle Bond Graph Submodel

The velocity vectors ${}^1v_C$ and ${}^1v_D$ are transformed from sprung mass frame to frames $({}^2x\text{-}{}^2y)$ and $({}^3x\text{-}{}^3y)$ respectively, the x axes of which are instantaneously parallel

to the road surface. The transformation equations below are functions of angles θ_2 and θ_3 defined in the Fig 5.1, and are represented by sets of four MTF elements in Fig 5.3 and 5.4.

From frame 1→2 (frame to front tire ground plane)

$$ {}^{2}v_C = \begin{bmatrix} \cos(\theta - \theta_2) & -\sin(\theta - \theta_2) \\ \sin(\theta - \theta_2) & \cos(\theta - \theta_2) \end{bmatrix} {}^{1}v_C \tag{5.7} $$

From frame 1→3 (frame to rear tire ground plane)

$$ {}^{3}v_D = \begin{bmatrix} \cos(\theta - \theta_3) & -\sin(\theta - \theta_3) \\ \sin(\theta - \theta_3) & \cos(\theta - \theta_3) \end{bmatrix} {}^{1}v_D \tag{5.8} $$

Rolling resistance and longitudinal traction forces are aligned with the road surface i.e. along the x axes of coordinate frames 2 and 3. The traction force is associated with a wheel slip resistance element in which force is a nonlinear function of wheel slip and normal load. The slip resistance arises due to tire compliance and the resulting difference that can occur between the actual forward velocity of a wheel hub and the velocity if the tire were rigid, i.e., tire radius r multiplied by wheel angular velocity ω. Defining slip ratio κ as

$$ \kappa = \frac{rw - v}{v} \tag{5.9} $$

The slip resistance force is [Rideout et. al., 2007]

$$F_{slip} = \frac{\text{sgn}(\kappa)|F_z\|\mu\|\kappa|}{\kappa_{\max}} \tag{5.10}$$

Where F_z = tire force normal to the road, μ = coefficient of friction, $\kappa_{\max}$ = slip ratio at tire saturation, and "sgn" is the signum function, which returns the algebraic sign of its argument.

Rolling resistance is also a function of normal load F_z and longitudinal velocity, along with tire inflation pressure P and empirical constants c_i. In general,

$$F_{rolling} = \text{sgn}(v)\left[c_1 + c_2 F_z + c_3 F_z/P + c_4 F_z^2/P\right] \tag{5.11}$$

Cab and Engine Sub model (Fig. 5.5)

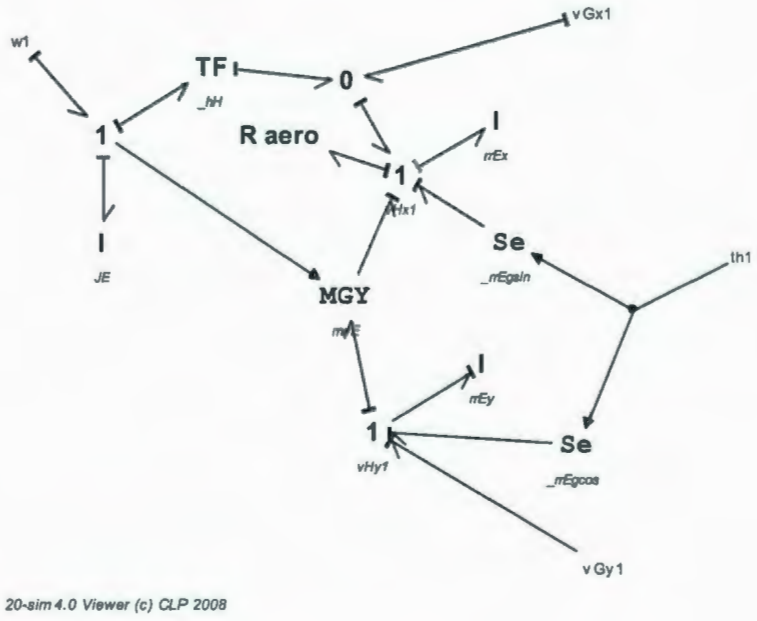

Fig. 5.5: Cab and Engine Bond Graph Submodel

In the cab and engine submodel four different connections are attached. One is "w1" which is angular velocity of the frame, which is assumed to be the same as the angular velocity of cab and engine. ${}^{1}v_{GX}$ and ${}^{1}v_{GY}$ are the velocity components of the centre of gravity. JE is the rotational inertia of engine and m_x is the mass. The two effort sources represent components of the gravity force along axes ${}^{1}x$ and ${}^{1}y$. Aerodynamic drag is introduced in the cab and engine section. The aerodynamic drag constitutive law used is

$$F_{aero} = 0.5\rho A C_d \left|{}^{1}v_{Ox}\right| {}^{1}v_{Ox} \tag{5.12}$$

Where

ρ = air density [kg/m^3]

A = frontal area [m^2]

C_d=drag coefficient (dimensionless)

${}^{1}v_{Ox}$ = Longitudinal velocity [m/s]

The resulting drag force is proportional to the square of the body fixed x-component of the sprung mass longitudinal velocity. The drag coefficient is thus assumed constant regardless of changes in the pitch attitude of the vehicle, which will be small.

Frame Submodel

Two rigid body modes (transitional mode and rotational mode) are expressed as Mode 0 and Mode 00 as shown in Figure 5.6. In addition, two flexible modes are also shown in the sub model. Velocity of point F and G along the frame direction is

$$^{1}v_{FX} = {}^{1}v_{EX} - w_F\omega \tag{5.13}$$

$$^{1}v_{GX} = {}^{1}v_{EX} - w_G\omega \tag{5.14}$$

w_F and w_G are flexible displacement of the beam at F and G and ω is frame angular velocity. The final terms in the equation represent change in relative velocity of the point due to beam deflection, which should be negligible. This was confirmed by comparing the activity of each term in Equations 5.13 and 5.14. The "wω" terms were then removed. Before creating the sub model it was assumed that flexible deflections occur only along the ^{1}y axis. In the forward motion direction the mass of load and frame are lumped together. For vertical motion the frame mass was considered separately from the load, in order to create a force input from the load to the frame

In order to create a force input from the load to the frame (even though they are rigidly constrained) stiff springs are inserted between the load and frame (c: stiff and R: Rstiff in the figure). This decouples the momenta of the load and frame and allows explicit equations to be written (Karnopp et.al., 2006).

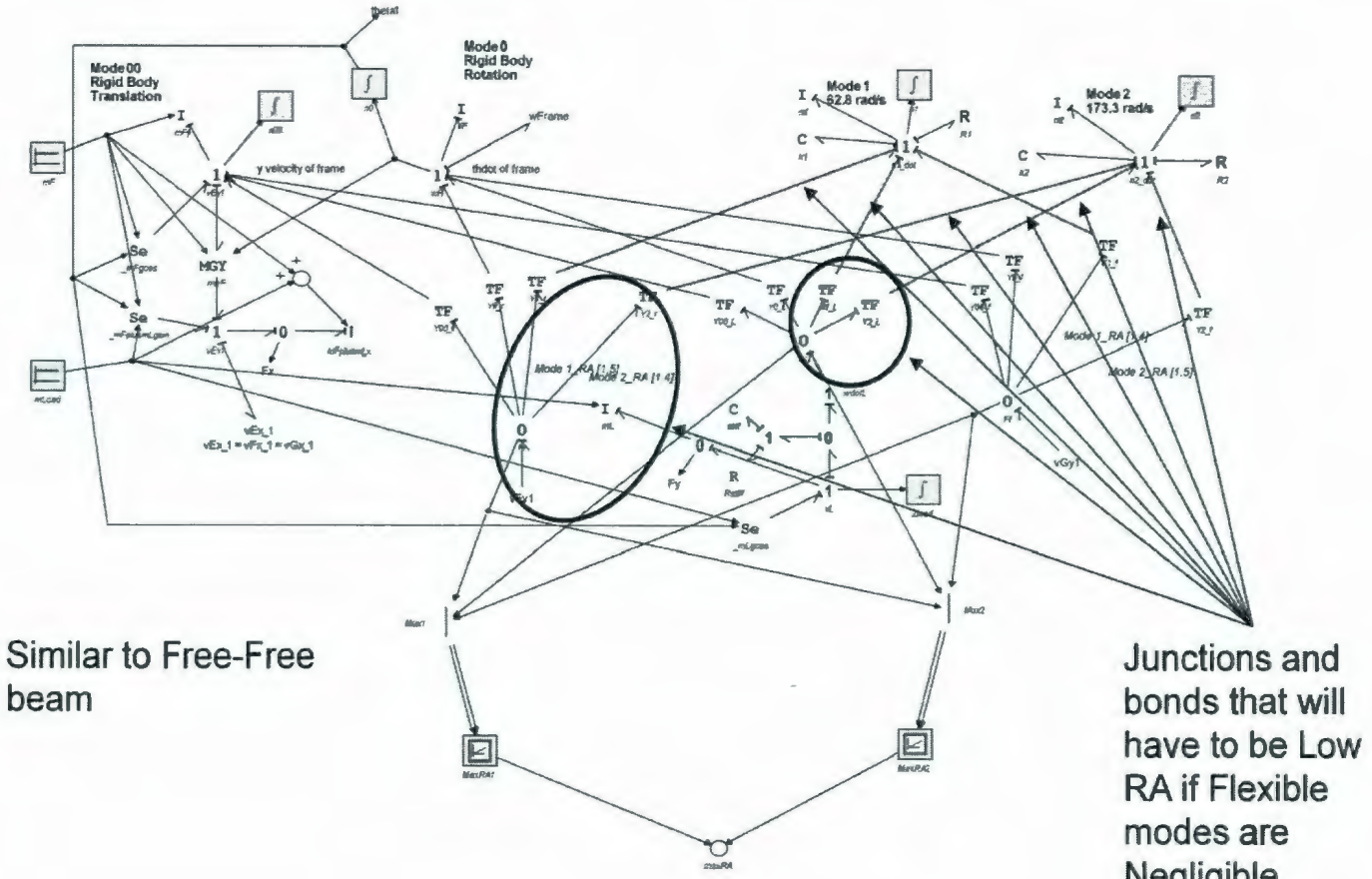

Fig. 5.6: Frame Bond Graph Submodel

5.3 Test Matrix

Range of validity of rigid models was studied subject to variation in three parameters: payload mass, wavelength of sinusoid road bumps and bump amplitude. See Fig 5.7.

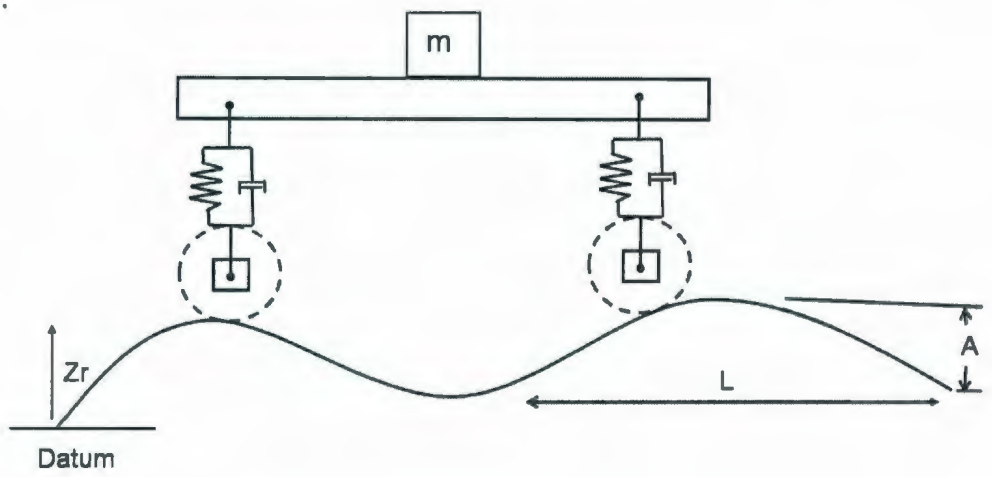

Fig. 5.7: Road Roughness Parameters

Road profile was generated using the equation

$$y = A\sin\left(\frac{2\pi}{L}\right)x \tag{5.15}$$

Because the bond graph requires the road slope as an input as discussed earlier, the equation above was differentiated with respect to distance to give

$$\frac{dy}{dx} = \frac{2\pi}{L}A\cos\left(\frac{2\pi}{L}\right)x \tag{5.16}$$

Where, A = amplitude of the bump and L = length of the bump.

Amplitude and length were varied and load was varied as in Table 5.1. If the maximum Relative Activity (RA) of all flexible modes is lower than the threshold value,

which was set to 0.05, then for that point a rigid model is valid. The flexible modes then form driven partitions and can be eliminated. Because range of validity will be plotted as a response surface, only two parameters can be varied at a time. Three combinations of two parameters were studied as summarized in Table 5.1.

Table 5.1: Combinations of Parameters A, L and m for Simulation

Combination #	**Amplitude (m)**	**Length (m)**	**Load (Kg)**
1	0.05	1-20	10-1500
2	0.001-0.03	3	100-1500
3	0.001-0.4	1-20	1000

5.4 Results

The tables below give, for each combination of parameters, the maximum RA of any bond from a flexible mode to the indicated 0-junctions in Figure 5.6. Maximum RA values below the threshold are shown in bold.

Results for Combination # 1:

Table 5.2: Maximum Relative Activity Values for Combination #1

L (m)	**Load (Kg)**															
	10	100	200	300	400	500	600	700	800	900	1000	1100	1200	1300	1400	1500
1.00	1.00	1.00	0.95	0.79	0.66	0.57	0.43	0.66	0.24	0.21	1.00	0.68	0.72	0.75	0.66	0.64
3.11	0.45	0.34	0.28	0.22	0.26	0.25	0.30	0.31	0.33	0.29	0.29	0.31	0.45	0.39	0.41	0.40
5.22	0.12	0.17	0.31	0.48	0.90	1.00	1.00	1.00	0.57	0.78	0.44	0.49	0.39	0.39	0.36	0.22
7.33	***0.02***	***0.02***	***0.04***	0.06	0.07	0.09	0.11	0.11	0.08	0.08	0.07	0.09	0.12	0.13	0.14	0.14
9.44	***0.02***	***0.02***	***0.03***	0.07	0.09	0.11	0.14	0.16	0.14	0.15	0.13	0.10	0.12	0.11	0.11	0.09
11.56	***0.02***	***0.02***	***0.02***	***0.05***	0.09	0.15	0.18	0.17	0.17	0.15	0.14	0.12	0.11	0.10	0.09	0.09
13.67	***0.02***	***0.02***	***0.02***	***0.02***	***0.02***	***0.03***	***0.04***	***0.05***	0.09	0.14	0.17	0.19	0.18	0.16	0.14	0.12
15.78	***0.01***	***0.01***	***0.02***	***0.01***	***0.01***	***0.01***	***0.01***	***0.02***	***0.02***	***0.02***	***0.02***	***0.03***	***0.03***	***0.03***	***0.03***	***0.03***
17.89	***0.00***	***0.01***	***0.01***	***0.01***	***0.01***	***0.01***	***0.01***	***0.01***	***0.01***	***0.01***	***0.01***	***0.01***	***0.01***	***0.01***	***0.01***	***0.00***
20.00	***0.00***	***0.01***	***0.01***	***0.01***	***0.01***	***0.01***	***0.01***	***0.01***	***0.01***	***0.01***	***0.01***	***0.01***	***0.01***	***0.01***	***0.00***	***0.00***

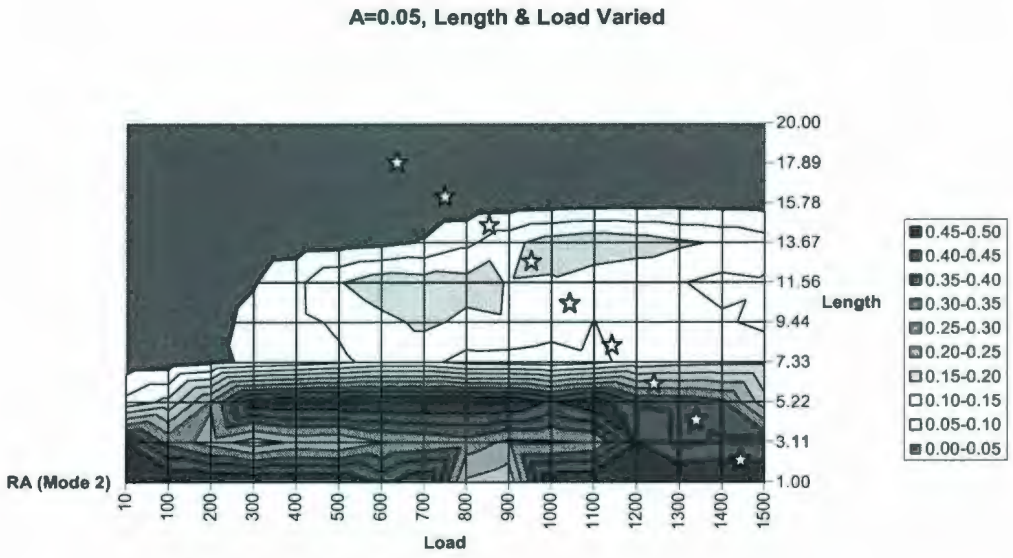

Fig. 5.8: Contour Plot for Combination 1

Figure 5.8 shows that a rigid model is recommended for suitably long road wavelengths (smooth roads). The threshold road wavelength decreases as load decreases, which mean that a rigid model can be used for rougher roads as long as load is decreased.

As with all the contour plots in this thesis, if the modeler wants to vary parameters beyond the extents of the plot, then this can be easily done. It is likely that if load was increased beyond 1500 kg, that the minimum road wavelength for use of a rigid model would continue to rise.

Results for Combination # 2:

Table 5.3: Maximum Relative Activity Values for Combination #2

Load (kg)	**Amplitude (m)**				
	0.001	***0.005***	***0.01***	0.02	0.03
100	***0.000336***	***0.005336***	***0.021324***	0.086656	0.150133
200	***0.000345***	***0.00508***	***0.020486***	0.082526	0.145545
300	***0.000361***	***0.004897***	***0.019913***	0.07938	0.14919
400	***0.000437***	***0.005885***	***0.021807***	0.080362	0.146864
500	***0.000642***	***0.010537***	***0.037854***	0.089594	0.149774
600	***0.000682***	***0.011021***	***0.04527***	0.114574	0.170026
700	***0.000718***	***0.011035***	***0.045423***	0.150213	0.181468
800	***0.000764***	***0.011059***	***0.045203***	0.174797	0.191915
900	***0.000806***	***0.011062***	***0.044936***	0.185342	0.201138
1000	***0.000847***	***0.011065***	***0.044772***	0.18698	0.205264
1100	***0.000892***	***0.011085***	***0.044646***	0.185171	0.204996
1200	***0.000935***	***0.011084***	***0.044462***	0.181878	0.19787
1300	***0.000969***	***0.011044***	***0.044268***	0.176998	0.188856
1400	***0.001002***	***0.011008***	***0.044091***	0.170843	0.179314
1500	***0.001037***	***0.010999***	***0.043948***	0.163793	0.170498

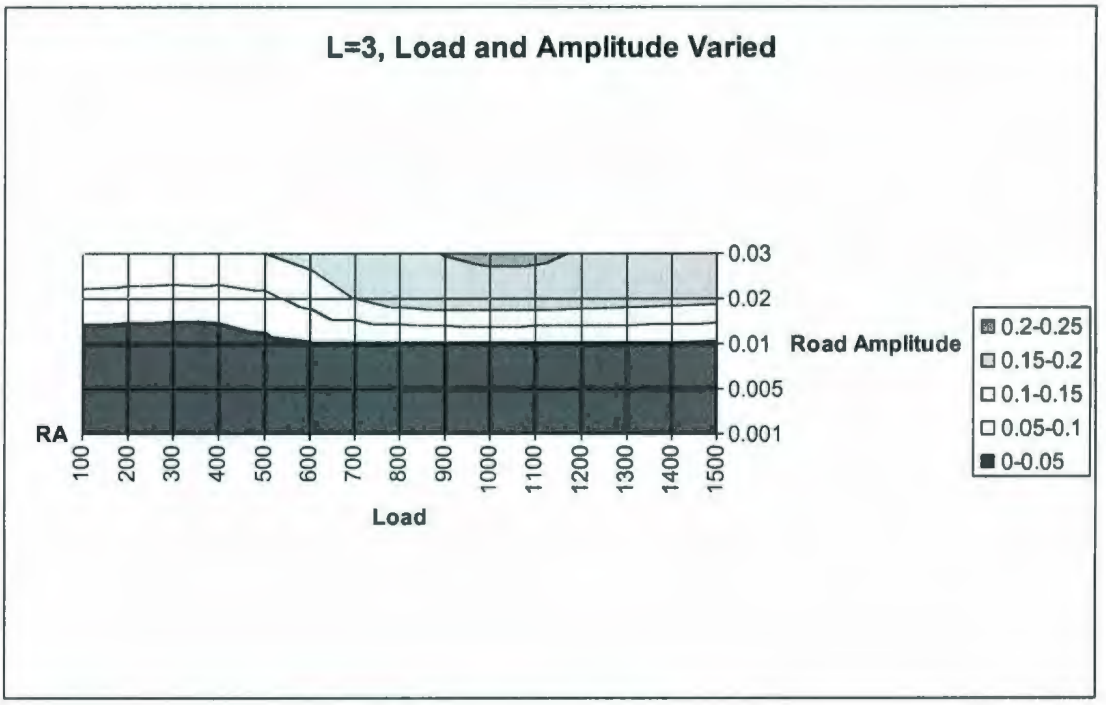

Fig. 5.9: Contour Plot for Combination #2

Figure 5.9 shows that below a threshold road bump height of 0.01 m, with a wavelength of 3 m, a rigid model is valid, and the validity is insensitive to load. For lower loads, slightly higher road amplitudes are permissible with a rigid model. These results are what would be expected qualitatively.

The parameter ranges chosen in Table 5.1 are arbitrary, but demonstrate the application of the partitioning algorithm and the graphical depiction of a range of validity with contour plots. If the analyst is interested in parameters outside the ranges in Figures 5.8-5.10, then they can choose their own range of parameters and generate activity values.

Results for Combination # 3:

Table 5.4: Maximum Relative Activity Values for Combination #3

L (m)	**Amplitude (m)**										
	0.00	0.01	0.01	0.05	0.10	0.15	0.20	0.25	0.30	0.35	0.40
1.00	***0.00***	***0.03***	0.05	1.00	0.52	0.56	0.47	0.10	0.10	0.08	0.08
2.00	***0.00***	***0.01***	***0.03***	0.32	0.40	0.13	0.16	***0.05***	***0.04***	***0.03***	***0.03***
3.00	***0.00***	***0.01***	***0.04***	0.17	0.23	***0.03***	0.14	***0.04***	0.07	0.06	***0.03***
4.00	***0.00***	***0.02***	0.06	1.00	0.19	***0.03***	***0.03***	***0.05***	***0.04***	0.06	***0.05***
5.00	***0.00***	***0.02***	0.08	0.78	0.21	0.06	***0.03***	***0.02***	***0.04***	0.06	0.07
6.00	***0.00***	***0.02***	0.09	0.52	0.20	0.07	***0.02***	***0.03***	***0.03***	***0.05***	0.06
7.00	***0.00***	***0.02***	***0.05***	0.07	0.20	***0.05***	***0.03***	***0.02***	***0.02***	***0.02***	***0.05***
8.00	***0.00***	***0.00***	***0.01***	0.08	0.08	***0.05***	***0.04***	***0.02***	***0.02***	***0.02***	***0.01***
9.00	***0.00***	***0.00***	***0.01***	0.14	0.06	***0.02***	***0.02***	***0.03***	***0.03***	***0.03***	***0.02***
10.00	***0.00***	***0.00***	***0.01***	0.13	***0.01***	***0.04***	***0.02***	***0.03***	***0.02***	***0.02***	***0.02***
11.00	***0.00***	***0.00***	***0.01***	0.14	***0.01***	***0.02***	***0.02***	***0.04***	***0.02***	***0.02***	***0.02***
12.00	***0.00***	***0.00***	***0.01***	0.16	***0.01***	***0.01***	***0.01***	***0.03***	***0.02***	***0.02***	***0.02***
13.00	***0.00***	***0.00***	***0.00***	0.25	***0.01***	***0.02***	***0.01***	***0.04***	***0.02***	***0.02***	***0.02***
14.00	***0.00***	***0.00***	***0.00***	0.13	***0.03***	***0.01***	***0.01***	***0.03***	***0.03***	***0.02***	***0.02***
15.00	***0.00***	***0.00***	***0.00***	***0.05***	0.07	***0.01***	***0.01***	***0.02***	***0.03***	***0.03***	***0.02***
16.00	***0.00***	***0.00***	***0.00***	***0.02***	0.07	***0.01***	***0.02***	***0.02***	***0.02***	***0.03***	***0.02***
17.00	***0.00***	***0.00***	***0.00***	***0.01***	0.06	***0.00***	***0.01***	***0.02***	***0.02***	***0.02***	***0.02***
18.00	***0.00***	***0.00***	***0.00***	***0.01***	***0.04***	***0.01***	***0.01***	***0.02***	***0.02***	***0.02***	***0.03***
19.00	***0.00***	***0.00***	***0.00***	***0.01***	***0.02***	***0.02***	***0.01***	***0.01***	***0.01***	***0.03***	***0.03***
20.00	***0.00***	***0.00***	***0.00***	***0.01***	***0.01***	***0.01***	***0.01***	***0.02***	***0.02***	***0.02***	***0.02***

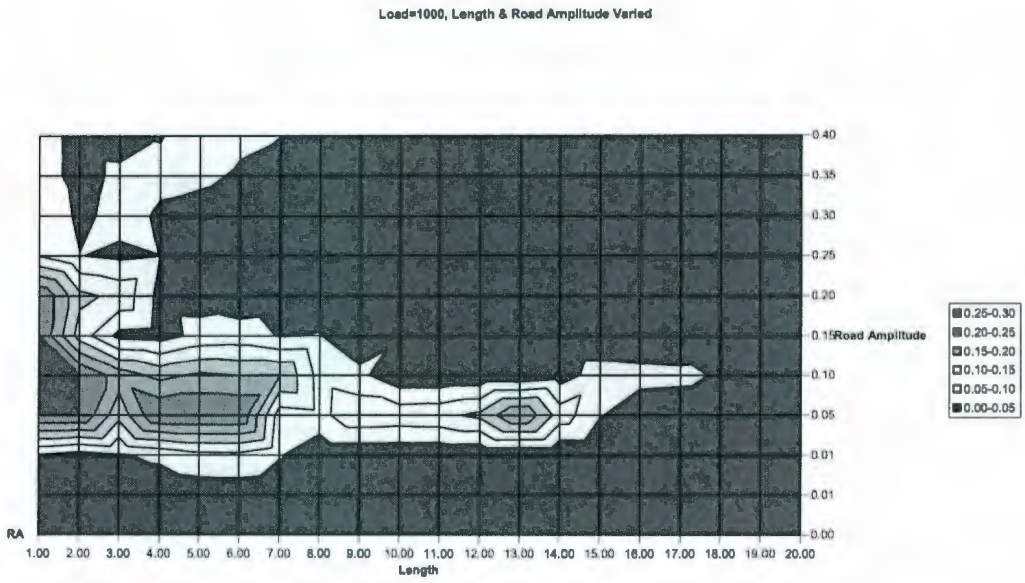

Fig. 5.10: Contour Plot for combination #3

Figure 5.10 shows that in general the range of validity shrinks as road roughness increases. There is an interesting region of low roughness (amplitude 0.05, wavelength 10-17 m) where the maximum relative activity of flexible mode bonds goes above the threshold. This could be due to low-level resonance of one of the flexible modes. The transverse vibration modes were not given damping, which means that any excitation of a mode would take a long time to die out. For smooth roads, there is lower power flow through both rigid and flexible subsystems, which means that any persistent flexible vibration will have relatively higher activity.

Use of the partitioning algorithm allows the modeler to find such zones where eliminating flexible modes might create errors, even though intuition might lead one to assume that a rigid model was proper.

5.5 Correlation of Maximum RA with Model Accuracy

To validate maximum RA as an indicator of how much the flexible modes contribute to overall system response, a comparison was made between rigid and flexible models for parameter combinations inside and outside the validity zones. As maximum flexible mode RA increases, rigid model prediction should be increasingly inaccurate. This section plots max RA versus a quantitative measure of rigid model prediction error.

Residual Sum Calculation

Figure 5.1 shows three possible outputs of interest for the half-car model: forward velocity V, pitch angle θ, and load acceleration magnitude a.

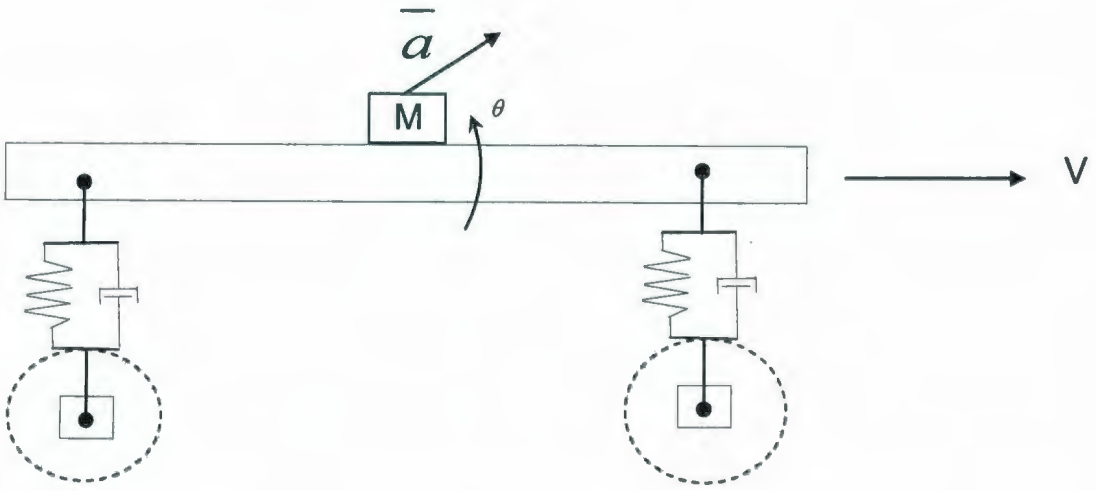

Fig. 5.11: Schematic Diagram of Half-car model with load mass

A Residual Sum (RS) was calculated to estimate overall error of a rigid model compared to a flexible model in predicting these outputs. The flexible models were assumed to be correct "full" models. Residual Sum was calculated to compare the rigid

models ability to predict vehicle forward velocity v, pitch angle θ and load acceleration $|\vec{a}|$ using the following equation-

$$RS = \int_0^T |y_{flex}(t) - y_{rigid}(t)| \cdot dt$$

Where,

RS is the residual sum between the full and reduced model's output,

$y_{flex}(t)$ is the time trajectory for the flexible (full) model

$y_{rigid}(t)$ is the time trajectory for the rigid (reduced) model

T is the time period of interest which was 60 seconds (Torque data was up to 60 seconds)

The model responses were written to data files in 20SIM, and the data points were used to calculate the RS value for velocity, acceleration and pitch angle. Table 5.5 gives the parameters, max RA values of flexible modes, and RS values for the nine sample points. In Figure 5.8, points P1 to P9 are shown on the contour plot, arranged from the upper left to lower right. Points P1, P2 and P3 are in the range of validity, and show lowest RS values for all three outputs.

Table 5.5: Data Points for RS calculation

#	Amplitude (m)	Length (m)	Load (kg)	Combined max RA (Mode 1 & 2)	RS Value (Velocity)	RS Value (Angle)	RS Value (Acceleration)
P9	0.05	2.5	1450	0.15	11.6	0.62	961
P8	0.05	4.5	1350	1	151.3	1.8	3634
P7	0.05	6.5	1250	0.53	10.5	1.2	1744
P6	0.05	8.5	1150	0.13	8	1	1484
P5	0.05	10.5	1050	0.22	12.48	1.137	681
P4	0.05	12.5	950	0.3	7.15	0.71	657
P3	0.05	14.5	850	0.13	4.04	0.57	393
P2	0.05	16.5	750	0.02	2.93	0.41	152.8
P1	0.05	18.5	650	0.017	2.39	0.45	166.9

Analysis of RS vs. RA

Figures 5.13 to 5.39 show the time responses of the outputs of interest for both rigid and flexible models, along with the modal amplitudes of flexible modes 1 and 2. A general trend can be observed for decreasing discrepancy between rigid and flexible models as the points get closer to the range of validity. The plots begin outside the range of validity at P9, and work back towards the model range of validity, ending at P1.

P9 plots, Max RA (combined modes 1 and 2): 0.15

Rigid model

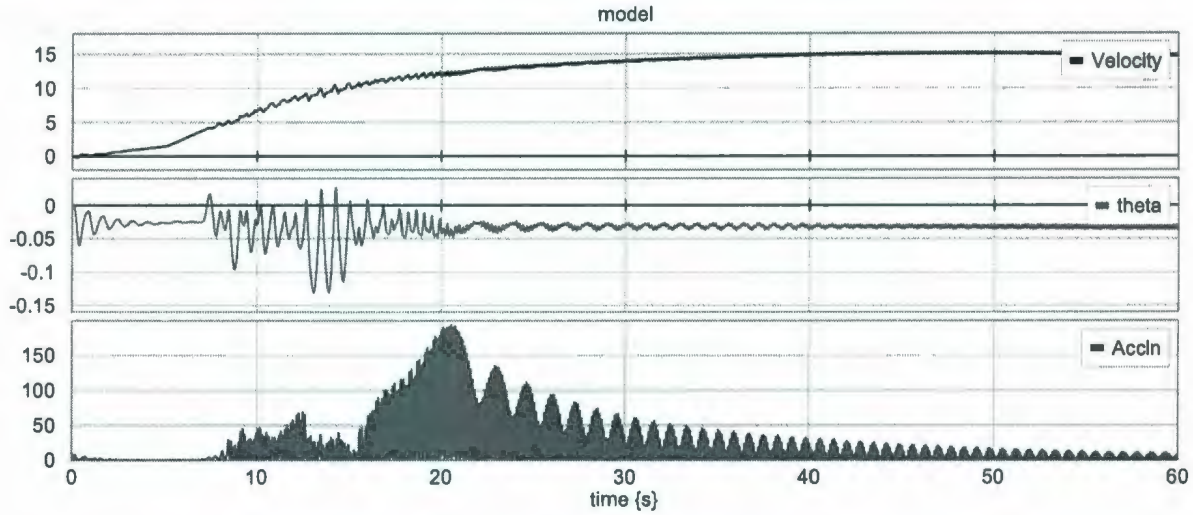

Fig. 5.12: Rigid Model Velocity, Pitch Angle and Acceleration for point P9

Flex model

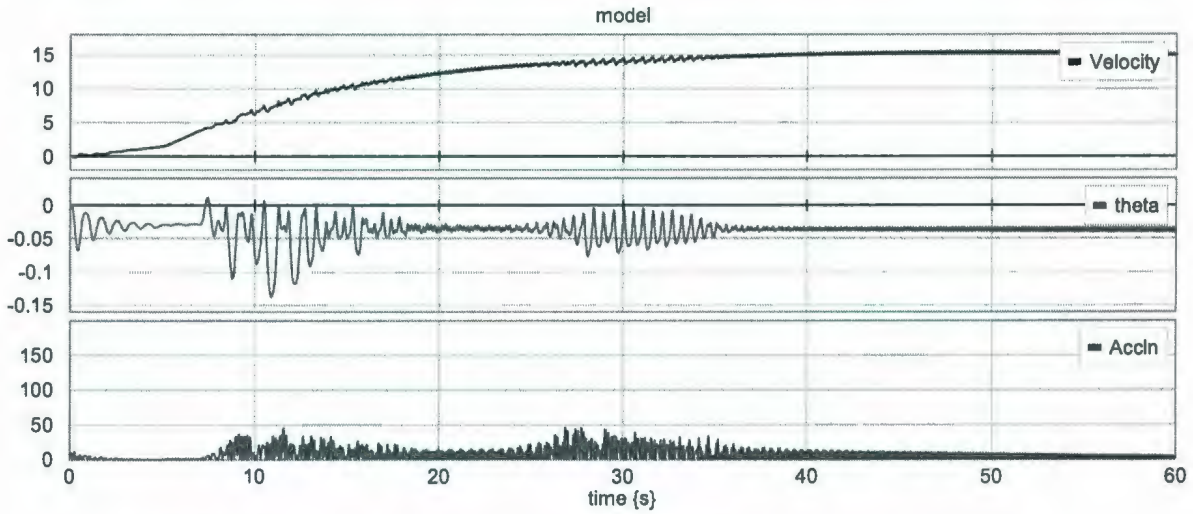

Fig. 5.13: Flex Model Velocity, Pitch Angle and Acceleration for point P9

P9 Modal Amplitudes

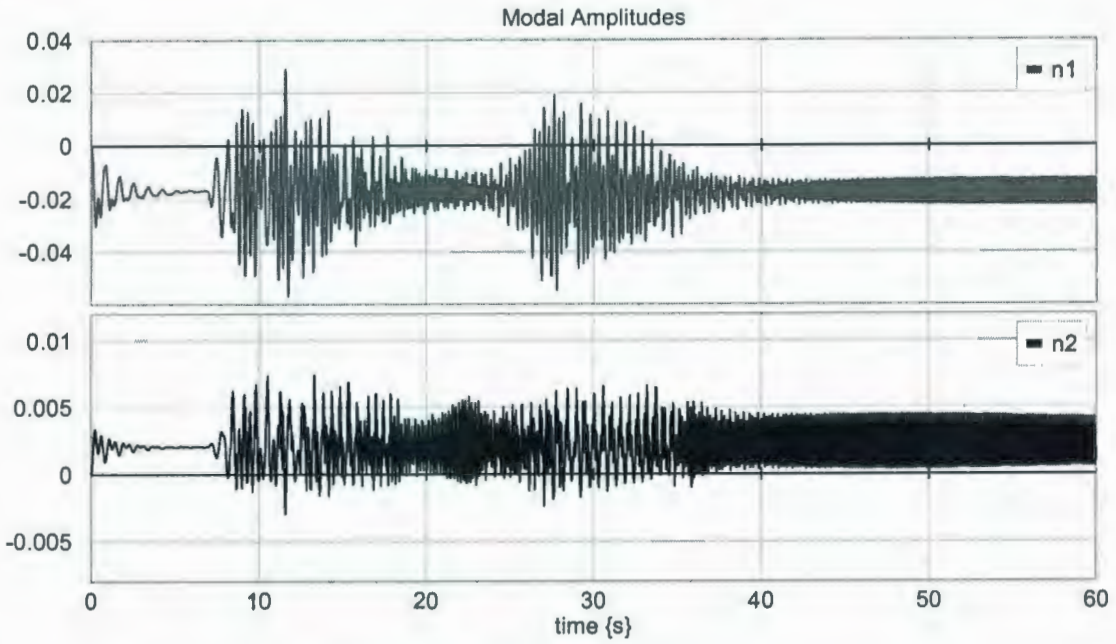

Fig. 5.14: Modal Amplitudes for P9

P8 plots, Max. RA (combined): 1

Rigid model

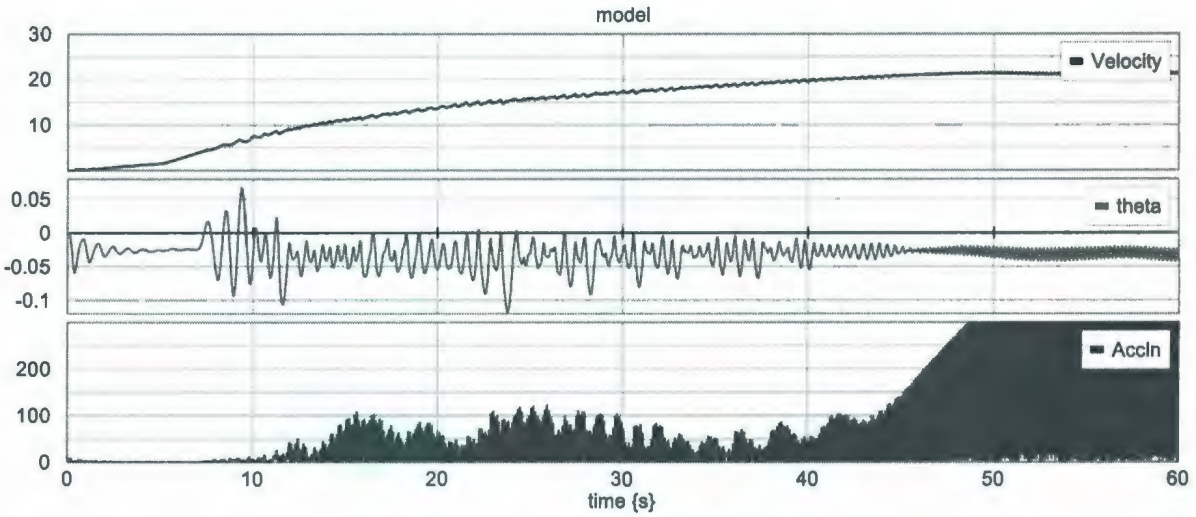

Fig. 5.15: Rigid Model Velocity, Pitch Angle and Acceleration for point P8

Flex model

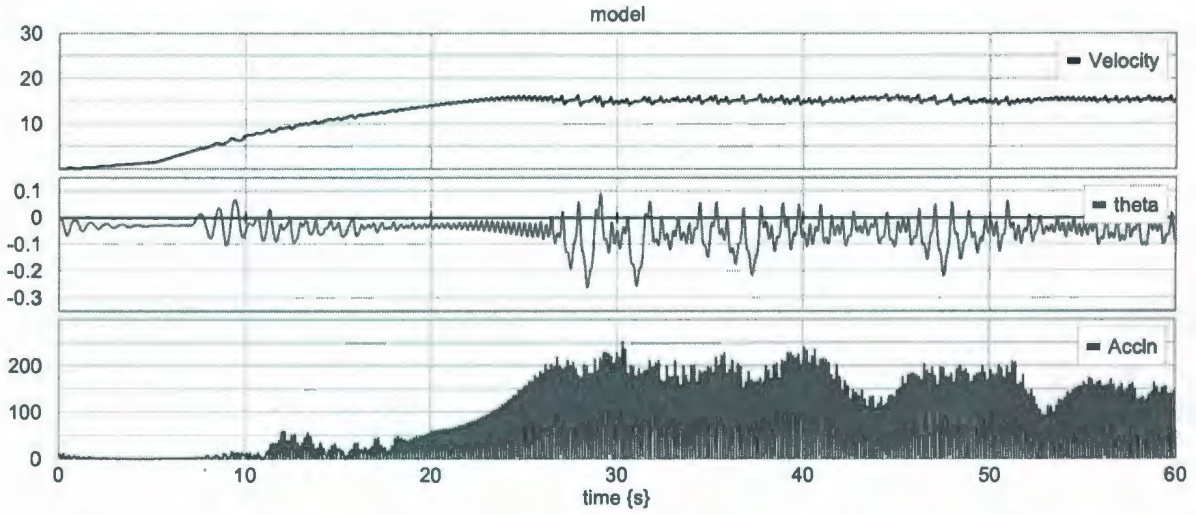

Fig. 5.16: Flex Model Velocity, Pitch Angle and Acceleration for point P8

P8 Modal Amplitudes

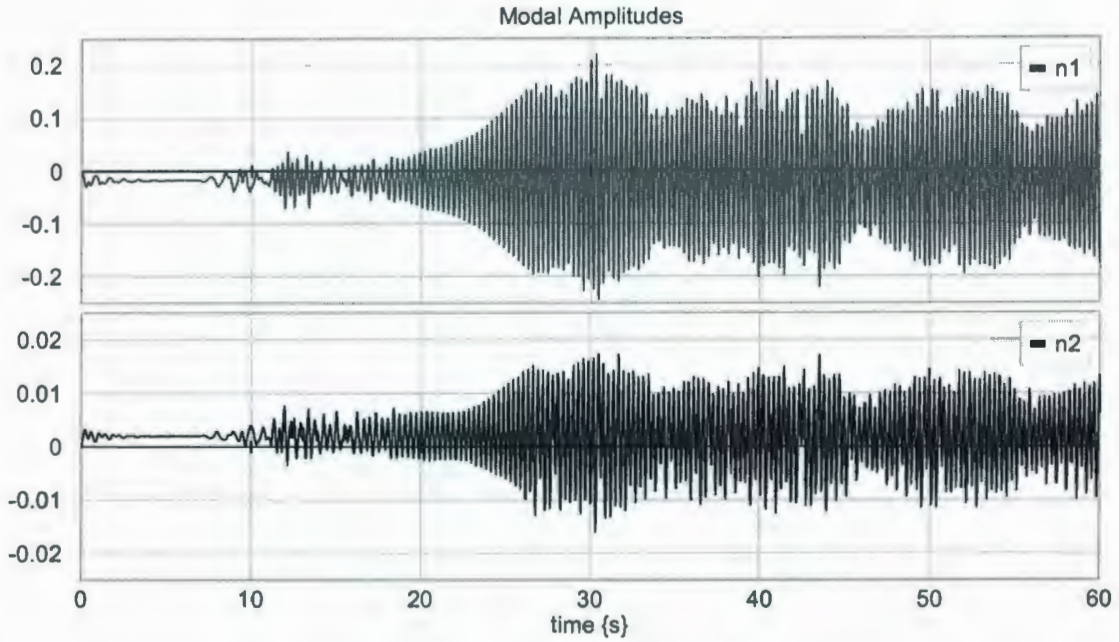

Fig. 5.17: Modal Amplitudes for P8

P7 plots, Max. RA (combined): 0.53

Rigid model

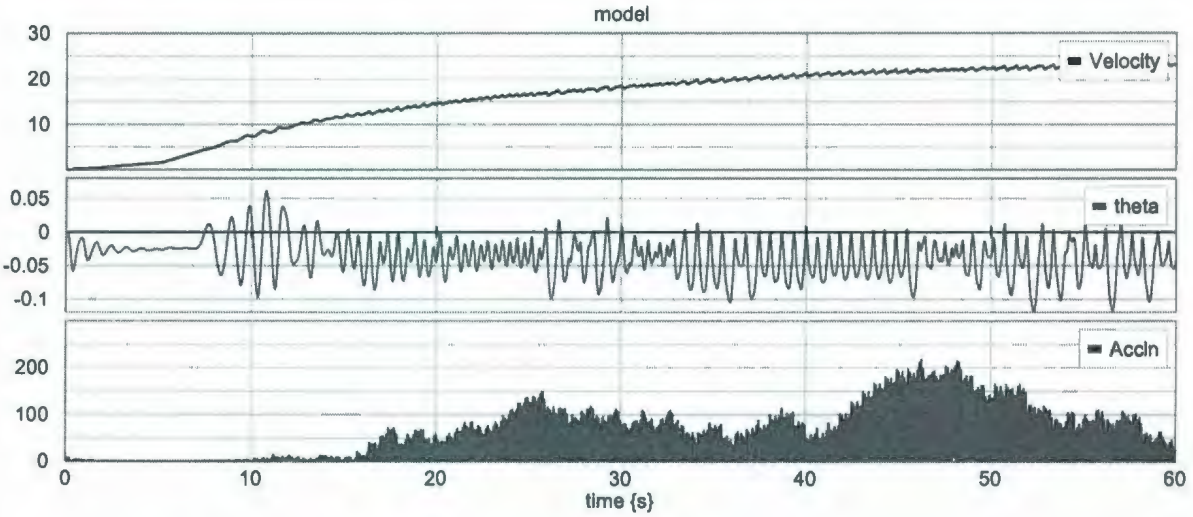

Fig. 5.18: Rigid Model Velocity, Pitch Angle and Acceleration for point P7

Flex model

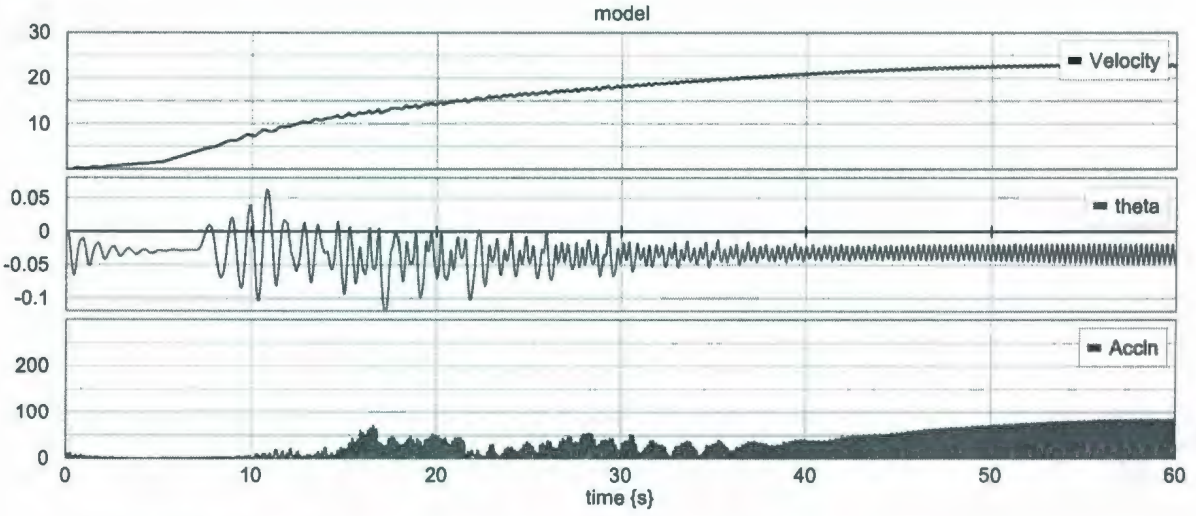

Fig. 5.19: Flex Model Velocity, Pitch Angle and Acceleration for point P7

P7 Modal Amplitudes

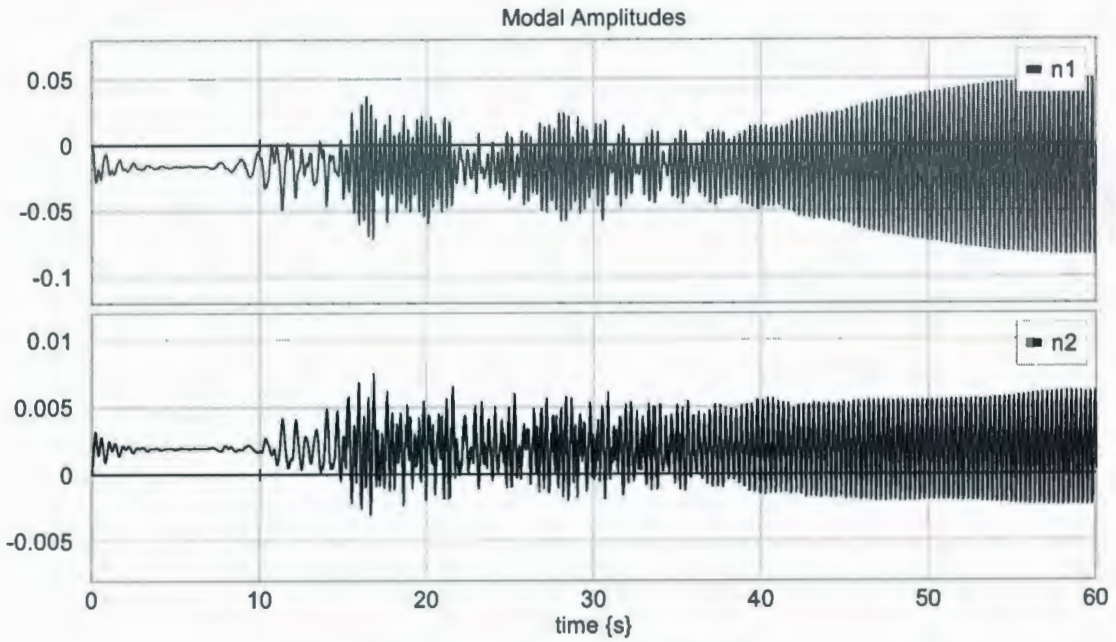

Fig. 5.20: Modal Amplitudes for P7

P6 plots, Max. RA (combined): 0.14

Rigid model

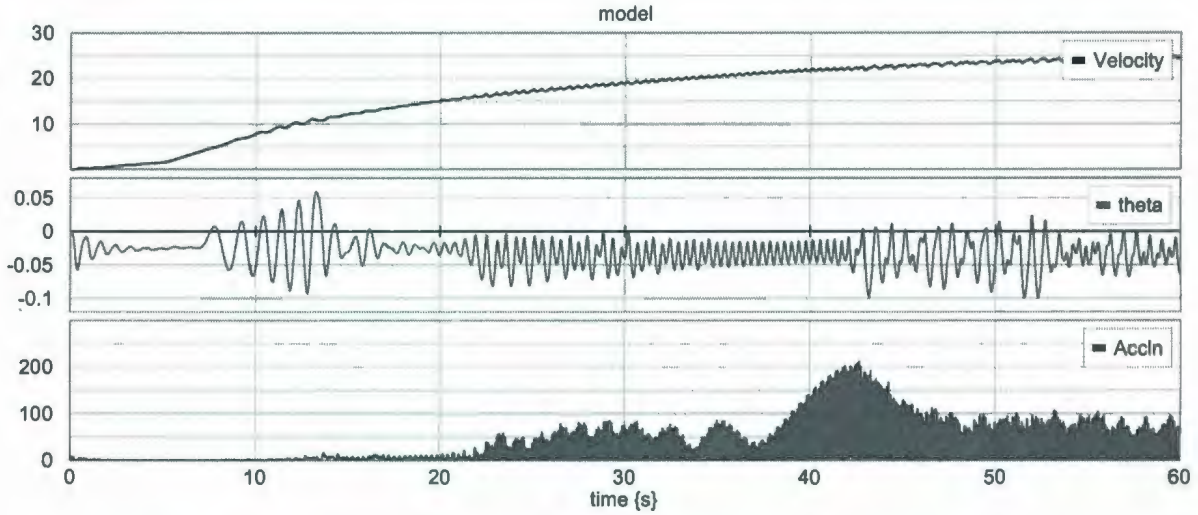

Fig. 5.21: Rigid Model Velocity, Pitch Angle and Acceleration for point P6

Flex model

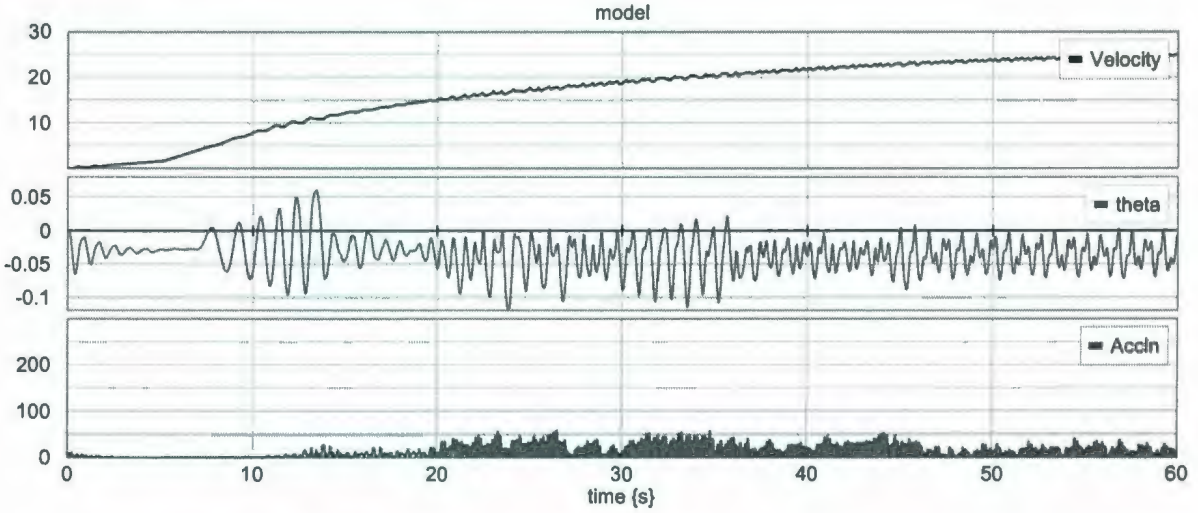

Fig. 5.22: Flex Model Velocity, Pitch Angle and Acceleration for point P6

P6 Modal Amplitudes

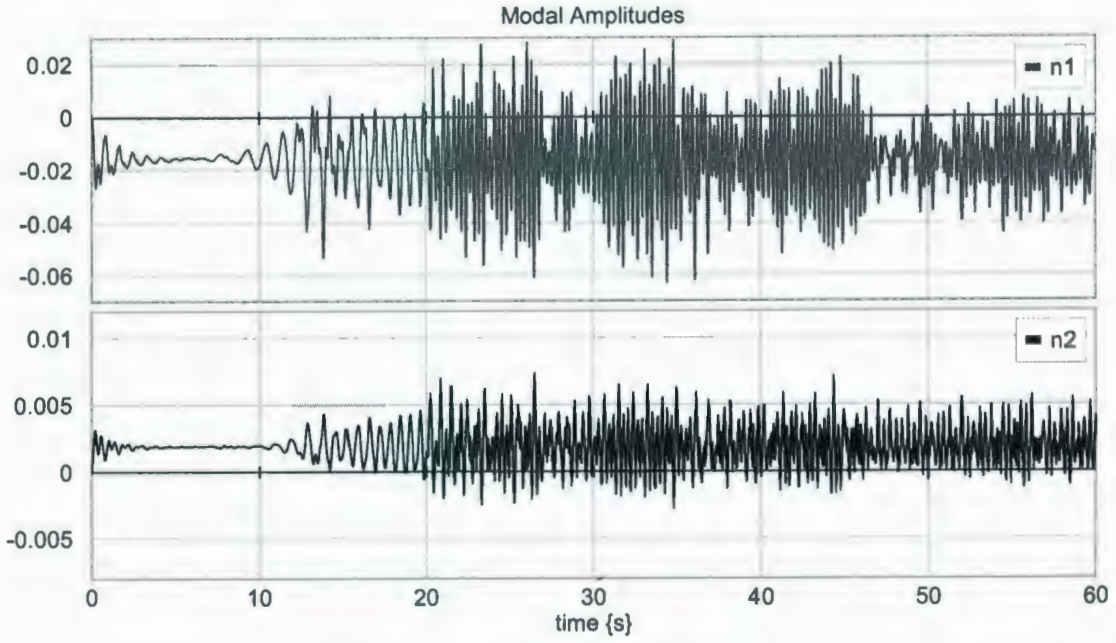

Fig. 5.23: Modal Amplitudes for P6

P5 plots, Max. RA (combined): 0.22

Rigid model

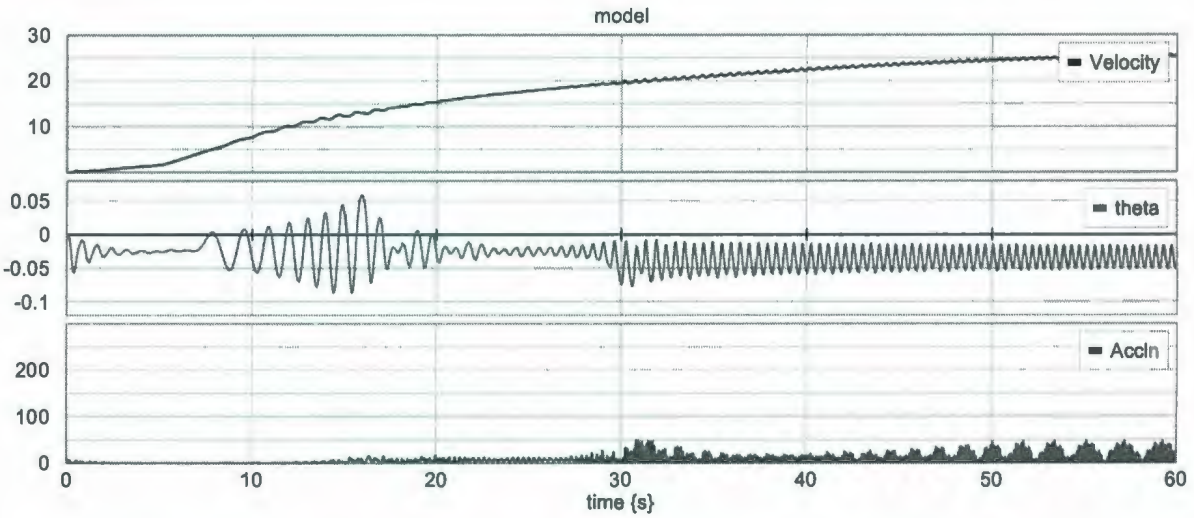

Fig. 5.24: Rigid Model Velocity, Pitch Angle and Acceleration for point P5

Flex model

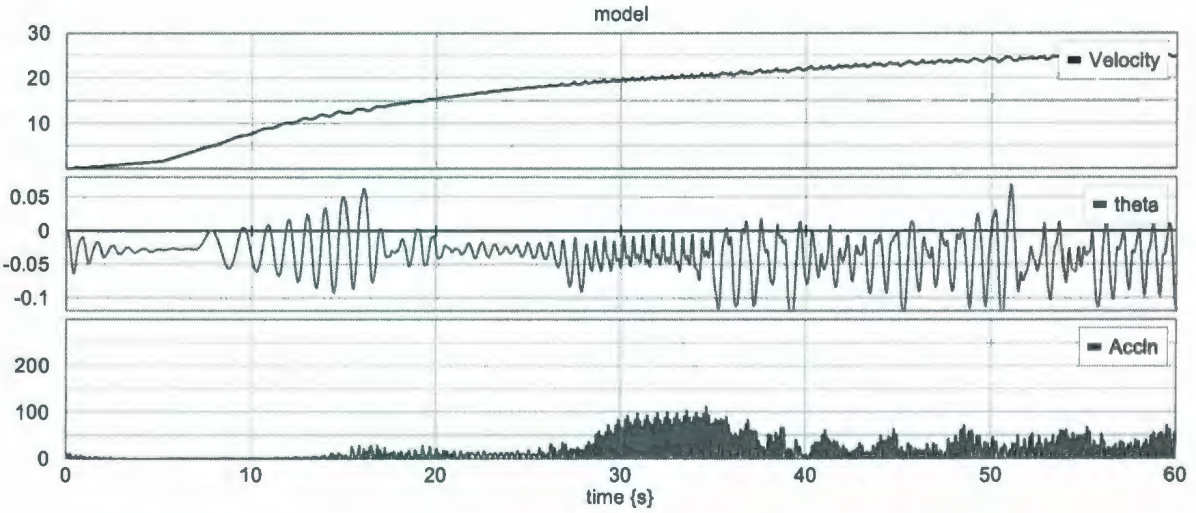

Fig. 5.25: Flex Model Velocity, Pitch Angle and Acceleration for point P5

P5 Modal Amplitudes

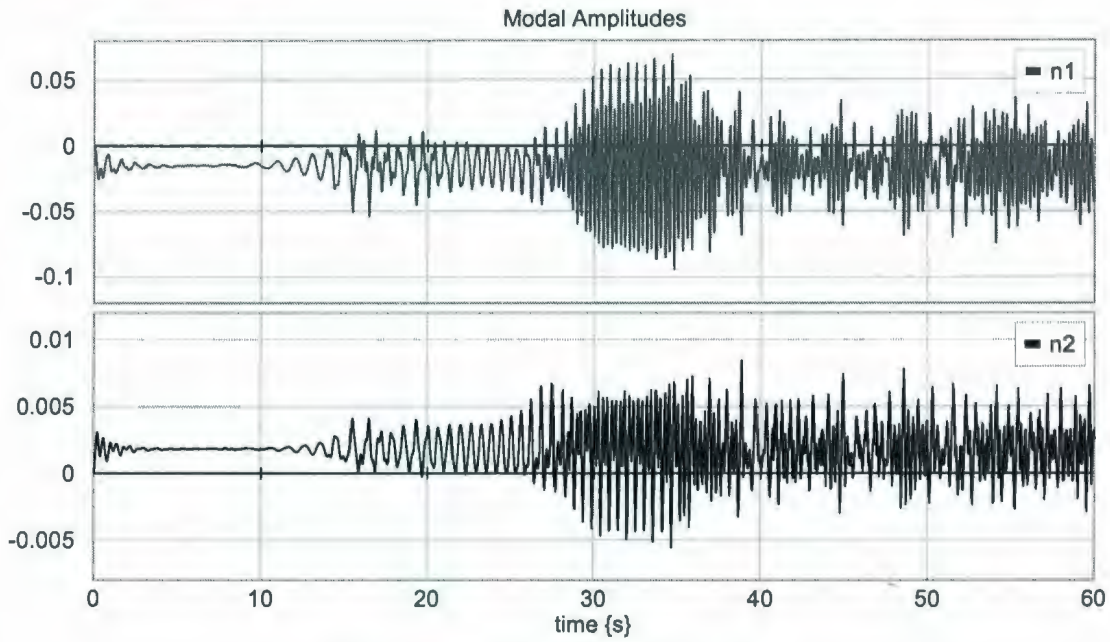

Fig. 5.26: Modal Amplitudes for P5

P4 plots, Max. RA (combined): 0.3

Rigid model

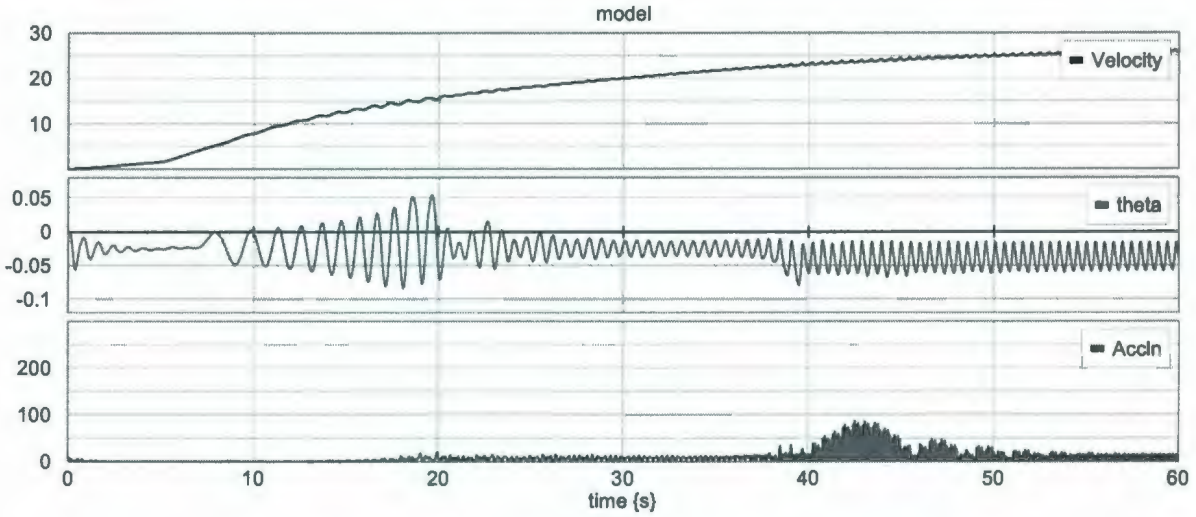

Fig. 5.27: Rigid Model Velocity, Pitch Angle and Acceleration for point P4

Flex model

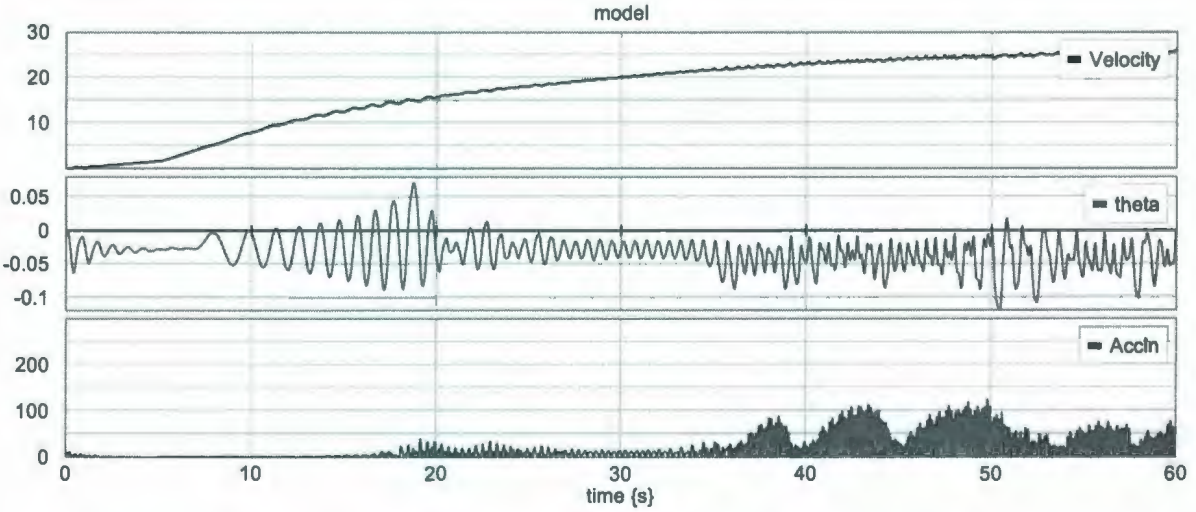

Fig. 5.28: Flex Model Velocity, Pitch Angle and Acceleration for point P4

P4 Modal Amplitudes

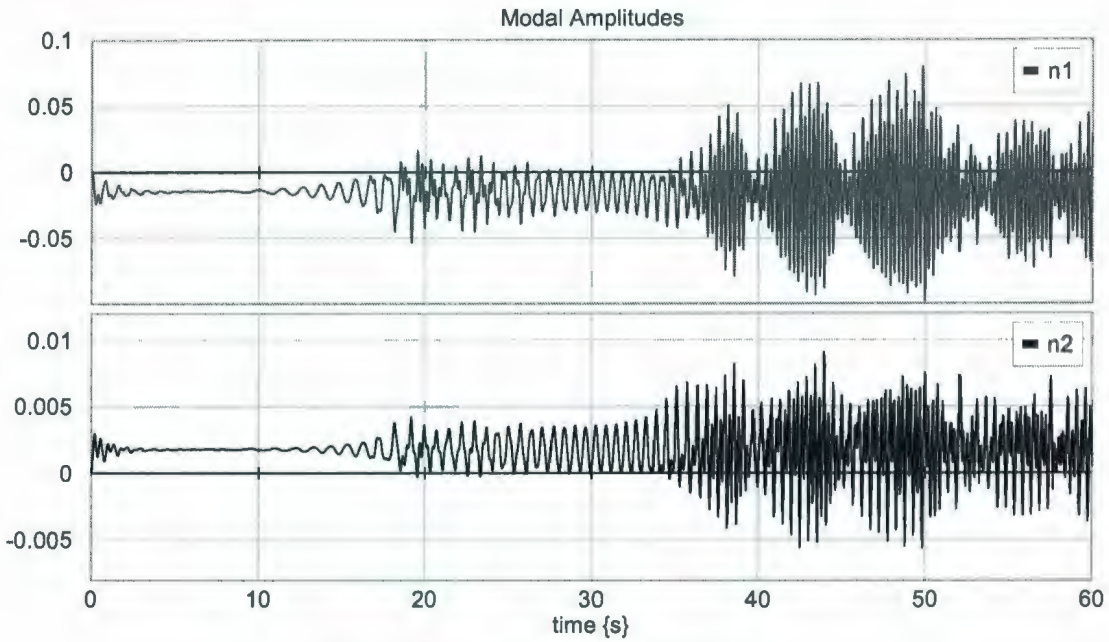

Fig. 5.29: Modal Amplitudes for P4

P3 plots, Max. RA (combined): 0.13

Rigid model

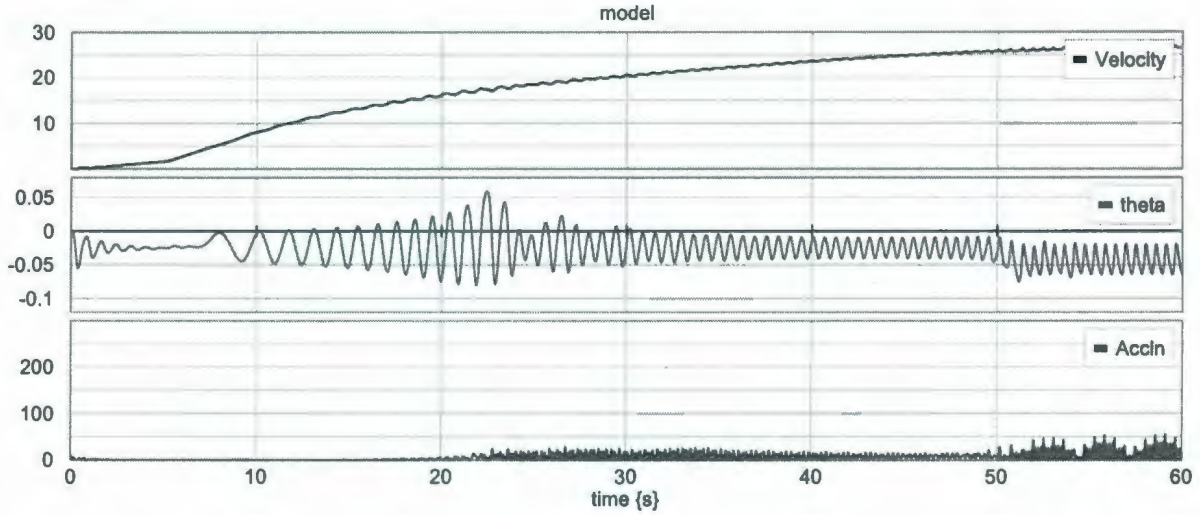

Fig. 5.30: Rigid Model Velocity, Pitch Angle and Acceleration for point P3

Flex model

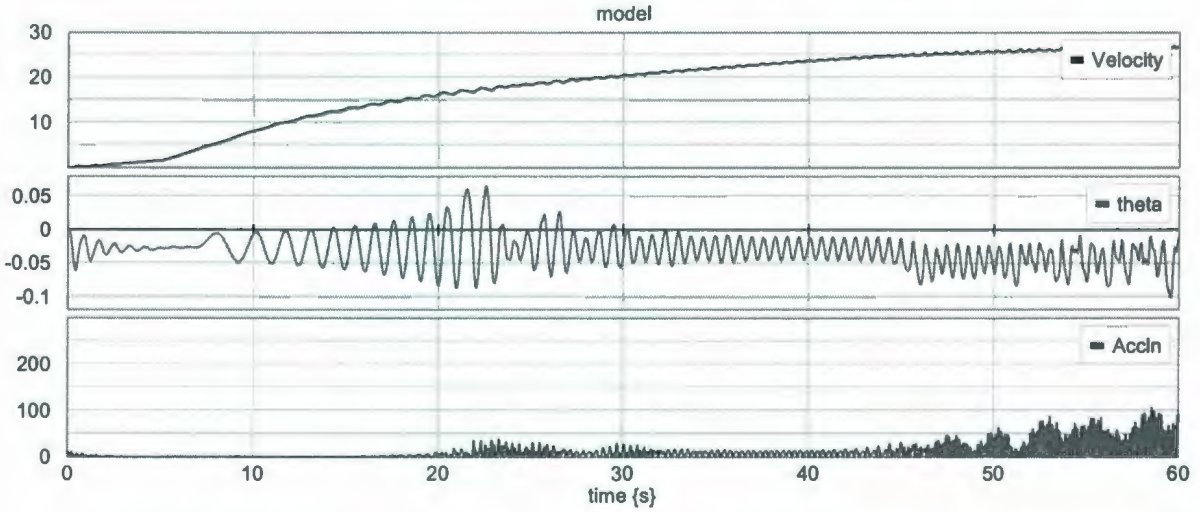

Fig. 5.31: Flex Model Velocity, Pitch Angle and Acceleration for point P3

P3 Modal Amplitudes

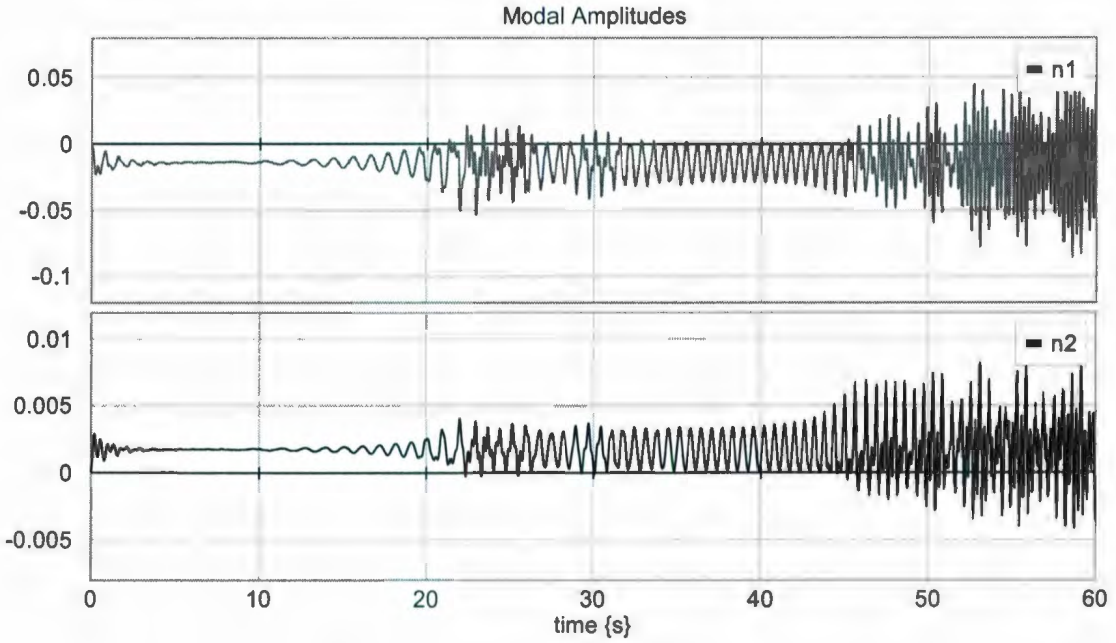

Fig. 5.32: Modal Amplitudes for P3

P2 plots, Max. RA (combined): 0.02

Rigid model

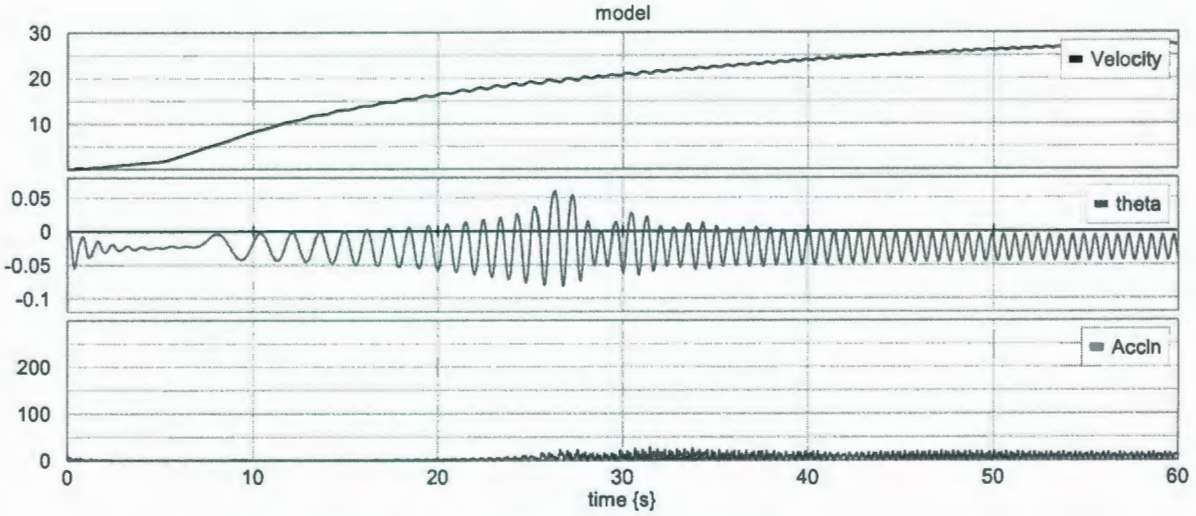

Fig. 5.33: Rigid Model Velocity, Pitch Angle and Acceleration for point P2

Flex model

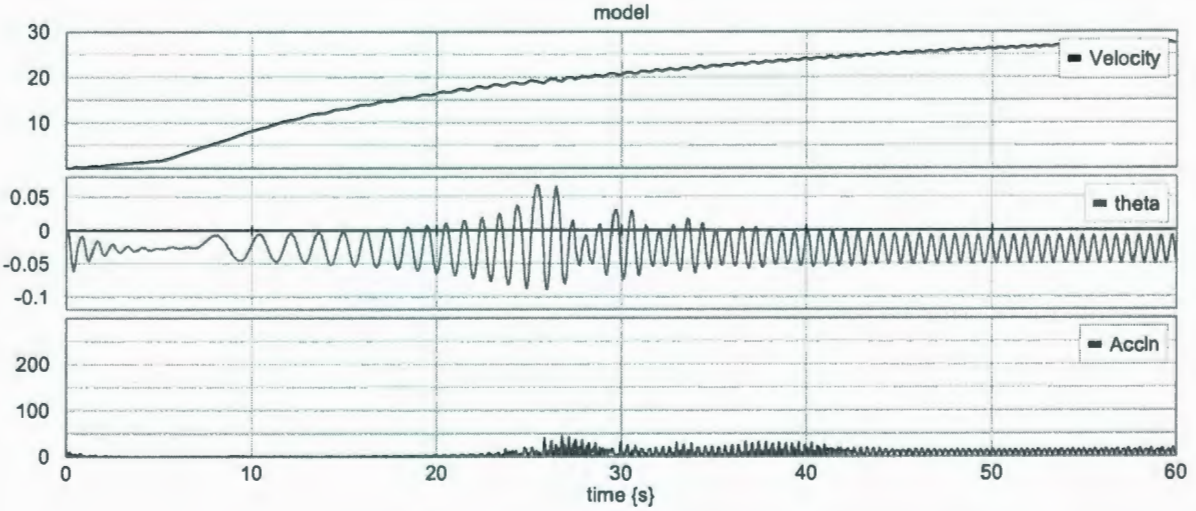

Fig. 5.34: Flex Model Velocity, Pitch Angle and Acceleration for point P2

P2 Modal Amplitudes

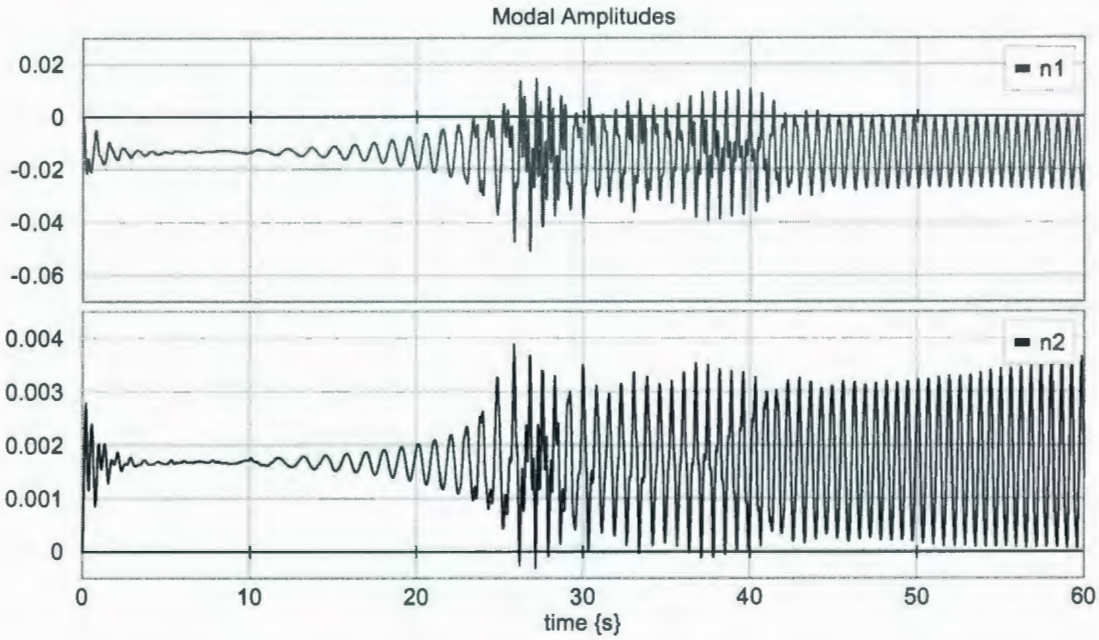

Fig. 5.35: Modal Amplitudes for P2

P1 plots, Max. RA (combined): 0.017

Rigid

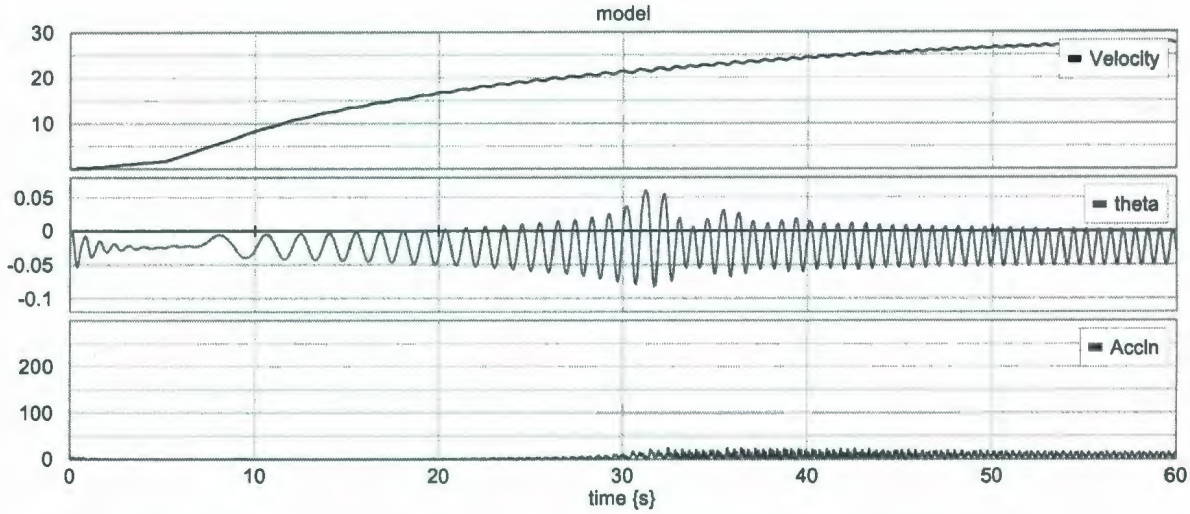

Fig. 5.36: Rigid Model Velocity, Pitch Angle and Acceleration for point P1

Flex

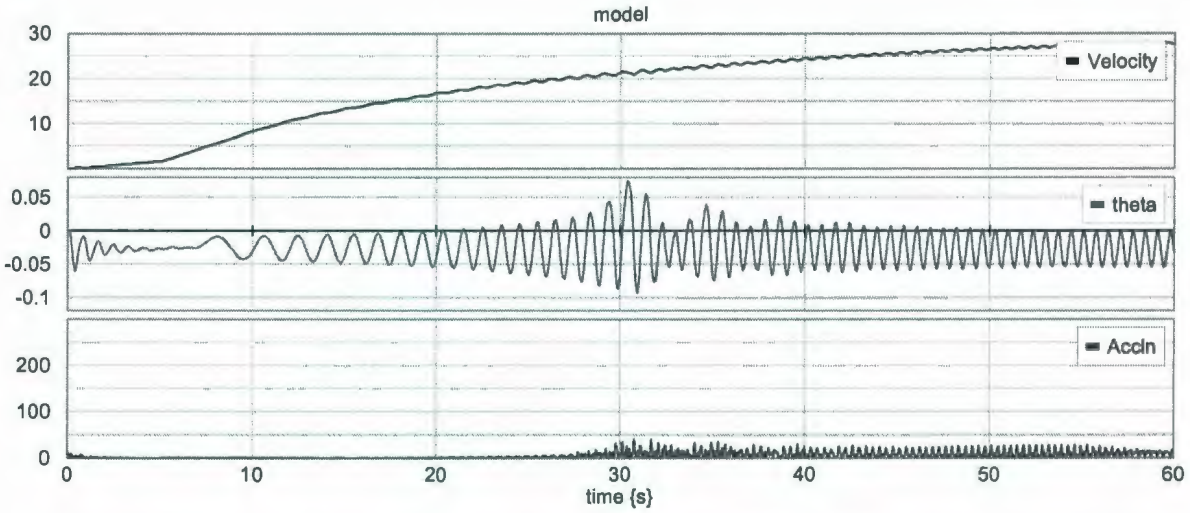

Fig. 5.37: Flex Model Velocity, Pitch Angle and Acceleration for point P1

P1 Modal Amplitudes

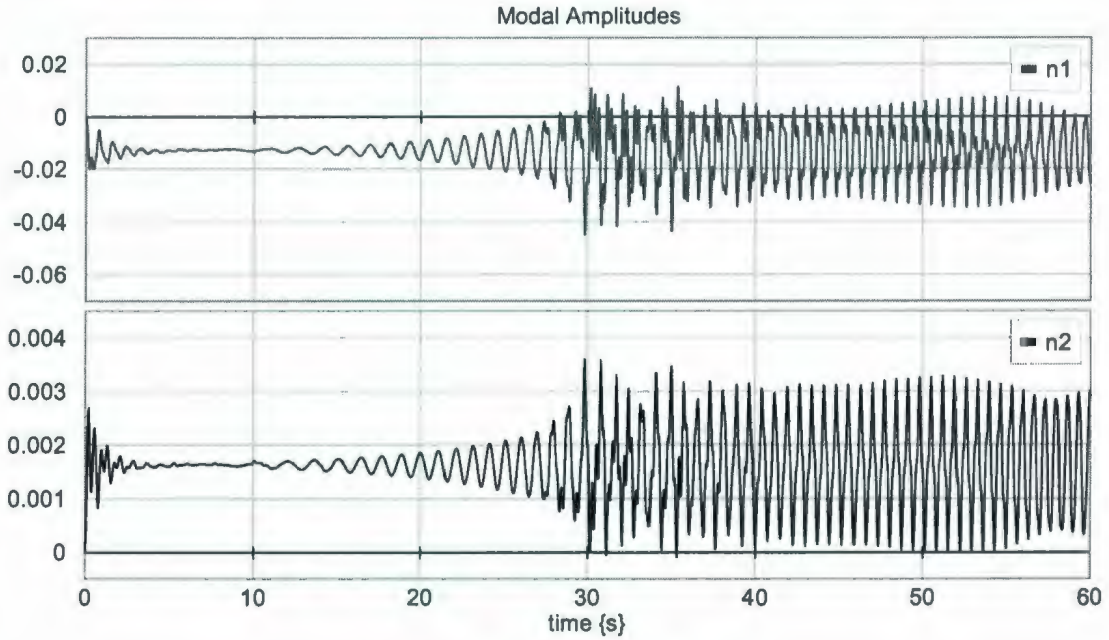

Fig. 5.38: Modal Amplitudes for P1

Figures 5.39 to 5.41 show plots of RS vs. max RA for the three outputs of interest. A correlation between RS and RA is clear.

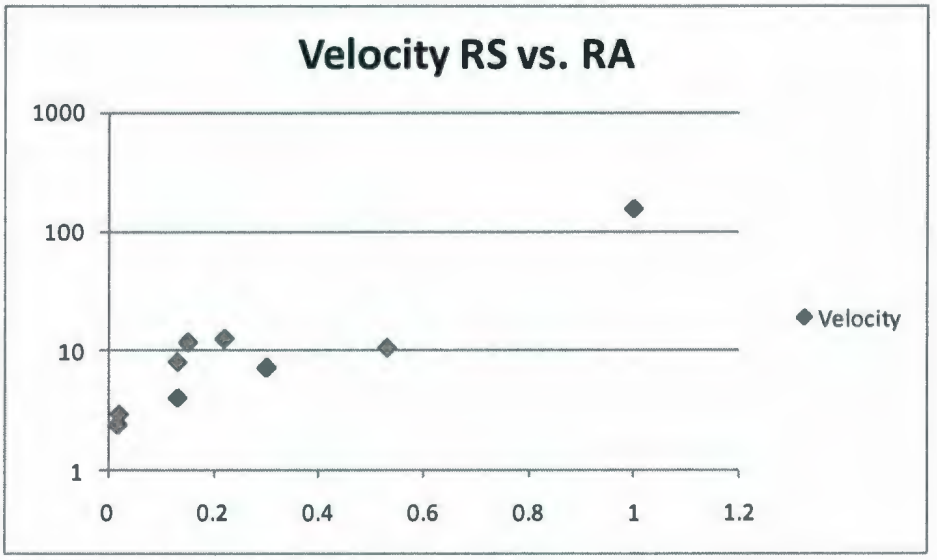

Fig.5.39: RS vs. RA for Velocity

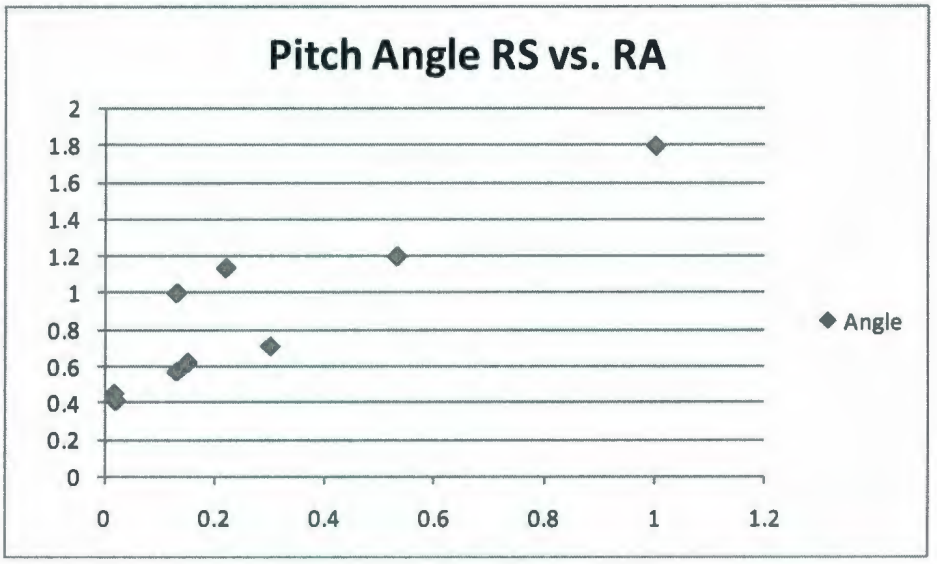

Fig.5.40: RS vs. RA for pitch angle

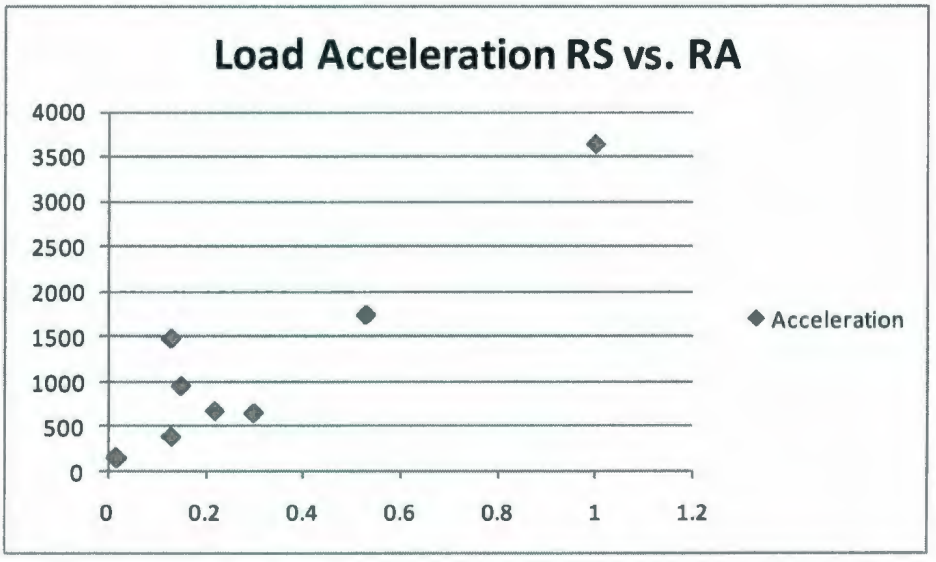

Fig.5.41: RS vs. RA for Load Acceleration

A closer examination of the system response plots can give insight into response for parameter sets such as P9, where one would expect RS to be greater than P8 due to

increased load and road roughness. However, the residual sum errors (and max. RA) for P9 are significantly lower than for P8. At the same time, the RS vs. RA plot for Acceleration shows that RS for P9 is higher than for P3 despite the fact that max RA for P9 and P3 are comparable.

P9 shows significant attenuation of flexible modes, which can be likely attributed to the significant increase in road spatial frequency compared to the other points. Road wavelength reduces from 4.5 m in P8 to 2.5 m in P9, a near doubling of input frequency. Given that the vehicle speed increases with time, the time frequency of the road excitation increases – the road acts as a sine sweep waveform of increasing frequency. For different road roughnesses, different system modes will be excited at different times. There are several vibration modes in the system, making prediction of the exact nature of discrepancies very difficult. Additionally, while the flexible and rigid models have the same suspension parameters, the natural frequencies of the rigid model will drift slightly when flexible modes are added. Increasing the system order will shift all previously-existing eigenvalues slightly (Wilson and Stein, 1995).

Consider the following natural frequency analysis for P9, where the load mass is 1450 kg. Frequencies were generated with 20SIM's Linear System Toolbox. The following table summarizes natural frequencies for the flexible and rigid models. Because the load is assumed to be constrained to the frame by a stiff (parasitic) spring, it contributes a natural frequency. This frequency is highlighted in bold in the table.

Table 5.6: Natural Frequencies for 1450 kg Load

Flexible Model [rad/s]	Rigid Model [rad/s]
6.8	7.0
13.3	14.0
22.0 (load on stiff spring)	**29.2**
50.37 (flexible)	
78.1	79.2
110.0	108.7
161.1 (flexible)	

The third frequency is attributed to the load, because when the load is reduced to 1 kg, the frequency shifts to approximately 999 rad/s as shown in the table below.

Table 5.7: Natural Frequencies for 1 kg Load

Flexible Model [rad/s]	Rigid Model [rad/s]
7.15	7.25
14.9	15.07
36.0 (flexible)	
78.1	79.14
110.4	108.6
160.5 (flexible)	
999.3 (load on stiff spring)	998.8

In the P9 rigid model response figure (Figure 5.13), the acceleration spikes around 20 seconds, unlike in the flexible model (Figure 5.14). The frequency of the road input at

20 seconds is approximately 4.8 Hz or 30 rad/s, very close to the 29.2 rad/s resonant frequency of the load on its parasitic spring for the rigid model. Relative damping of the parasitic mode, from 20SIM's Linear System Toolbox, was about 3%. Thus, the load acceleration was much greater in the rigid model and RS error was high. The parasitic spring between load and frame should be stiffened to better approximate a rigid connection.

Meanwhile, the vehicle system appears to begin to act like a filter when the road frequency increases significantly from P8 to P9. Higher-frequency inputs are filtered out, the angular rigid body mode excitation does not persist, and flexible modal amplitudes are lower.

Similar conclusions can be drawn for point P6, in which the rigid model has a resonance that is excited at around 40 seconds. For P6, flexible modes are not as excited as much as for parameter sets P5 and P7, and max RA is low for P6 despite the acceleration errors. The P6 max RA, at 0.13, is still high enough that flexible modes (contributing 13% of the aggregate energy at the junction) would not be eliminated.

The plots show a general trend for increasing error (RS) between the rigid and flexible models as maximum flexible mode relative activity increases. There is no analytical relation between RS and RA. RA is a nonlinear metric, and there are many interacting energetic elements in the model which will be excited to varying degrees as parameters change. Below a certain reasonable threshold, the rigid and flexible models agree. For unreasonable thresholds such as 0.13 and above, it is not feasible to predict exactly how "wrong" a rigid model will be – we can only predict that the rigid model will be incorrect.

Chapter 6

Improving Efficiency of Range of Validity Search Using Design of Experiments (DOE)

6.1 Introduction

Design of Experiments (DOE) is a systematic approach to investigation of a system or process. A series of structured tests are designed in which planned changes are made to the input variables of a process or system. The effects of these changes on a pre-defined output are then assessed. DOE is important as a formal way of maximizing information gained while minimizing resources required. It has more to offer than 'one change at a time' experimental methods, because it allows a judgment on the significance to the output of input variables acting alone, as well as input variables acting in combination with one another. 'One change at a time' testing always carries the risk that the experimenter may find one input variable to have a significant effect on the response (output) while failing to discover that changing another variable may alter the effect of the first (i.e. some kind of dependency or interaction). This is because the temptation is to stop the test when this first significant effect has been found. In order to reveal an interaction or dependency, 'one change at a time' testing relies on the experimenter carrying the tests in the appropriate direction. However, DOE plans for all possible

dependencies in the first place, and then prescribes exactly what data are needed to assess them i.e. whether input variables change the response on their own, when combined, or not at all. In terms of resources the exact length and size of the experiment are set by the design before testing begins [Box, 1978]. DOE can be used to find answers in situations such as "what is the main contributing factor to a problem?", "how well does the system/process perform in the presence of noise?", "what is the best configuration of factor values to minimize variation in a response?" etc. In general, these questions describe the following DOE applications: problem solving, parameter design and robustness study. In each case, DOE is used to find the answer; the only thing that marks them different is which factors would be used in the experiment. DOE starts with identifying the input variables and the response (output) that is to be measured. For each input variable, a number of levels are defined that represent the range for which the effect of that variable is desired to be known. An experimental plan is produced which tells the experimenter where to set each test parameter for each run of the test. The response is then measured for each run. The method of analysis is to look for differences between response (output) readings for different groups of the input changes. These differences are then attributed to the input variables acting alone (called a single effect) or in combination with another input variable (called an interaction).

In the previous chapter, a brute force method for finding model range of validity was used. When studying the range of validity of a model with respect to two parameters, the parameters must be varied over their allowable ranges, and a simulation is required for each parameter combination. The number of simulations can be excessive if all combinations of parameters are simulated. Additionally, the number of intermediate

points between the extreme parameter values can be theoretically infinite. This chapter investigates the suitability of DOE to minimize the number of simulation runs required, by choosing intermediate parameter values according to standard DOE experiment designs.

In Section 6.2, simple DOE factorial experiment designs are discussed. Section 6.3 describes the software tool used in the analysis, and how response surfaces are generated. Section 6.4 proposes a preliminary algorithm to determine response surfaces for maximum flexible mode relative activity (RA) for small sets of parameter values, and then join those response surfaces to create the model validity zones of Chapter 5. The goal is to reduce the number of runs required. Section 6.5 applies the algorithm to the free-free beam model from Chapter 4.

6.2 Factorial Experiment

DOE provides a cost-effective means for solving problems and developing new processes. The simplest, but most powerful, DOE tool is two-level factorial design, where each input variable is varied at high (+) and low (-) levels and the output observed for resultant changes. Statistics can then help determine which inputs have the greatest effect on outputs.

Two level factorial experiments are factorial experiments in which each factor is investigated at only two levels. The early stages of experimentation usually involve the investigation of a large number of potential factors to discover the "vital few" factors. Two level factorial experiments are used during these stages to quickly filter out unwanted effects so that attention can then be focused on the important ones.

This section is divided into the following subsections-

- Two to the k Designs (2^k *Design*)
- The Two Squared Design (2^2 *Design*)
- The Two Cubed Design (2^3 *Design*)

2^k Designs

The factorial experiments, where all combinations of the levels of the factors are run, are usually referred to as full factorial experiments. Full factorial two level experiments are also referred to as 2^k designs where k denotes the number of factors being investigated in the experiment. [Montgomery, 1992]

A full factorial two level design with k factors requires 2^k runs for a single replicate. For example, a two level with three factors will require 2 x 2 x2 = 2^3= 8 runs. The choice of the two levels of factors used in two level experiments depends on the factor. Some factors naturally have two levels. For example, if result is a factor, then pass and fail are the two levels. For other factors, the limits of the range of interest are usually used. For example, if temperature is a factor varying from 45°C to 90°C, then two levels used in the 2^k design would be 45°C and 90°C. The two levels of the factor in the 2^k design are usually represented as -1 (for the first level) and +1 or 1 (for the second level).

2^2 Designs

The simpler of the two level factorial experiments is the 2^2 design where two factors (say factor A and factor B) are investigated at two levels. A single replicate of this design will require four runs ($2^2 = 2 \times 2 = 4$).The effects investigated by this design are the two main effects, A and B, and the interaction effect AB. The treatments for this

design are shown in Figure 6.1(a). In the figure, letters are used to represent the treatments. The presence of a letter indicates the high level of the corresponding factor and the absence indicates the low level. For example, (1) represents the treatment

Treatment Name	Factors	
	A	*B*
(1)	-1	-1
a	1	-1
b	-1	1
ab	1	1

(a)

I	*A*	*B*	*AB*
1	-1	-1	1
1	1	-1	-1
1	-1	1	-1
1	1	1	1

(b)

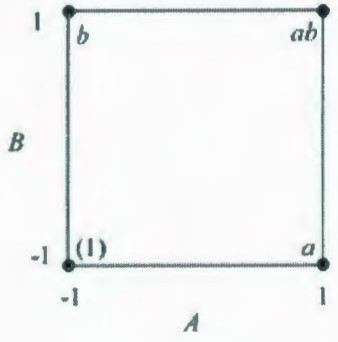

(c)

Fig. 6.1: The 2^2 design- (a) displays the experiment design (b) displays the design matrix (c) displays the geometric representation for the design. In fig (b), the column names *I, A, B* and *AB* are used. Column *I* represents the intercept term. Columns *A and B* represents the respective factor settings. Column *AB* represents the interaction and is the product of columns *A* and *B*. [Montgomery, 1992]

combination where all factors involved are at low level or the level represented by -1, *a* represents the treatment combination where factor *A* is at the high level or the level of 1, while the remaining factors (in this case, *B*) are the low level or the level of -1. Similarly *b* represents the treatment combination where factor *B* is at the high level or the level of 1, while factor *A* is at the low level and *ab* represents the treatment combination where factors *A* and *B* are at the high level or the level of 1. Figure 6.1(b) shows the design matrix for the 2^2 design. It can be noted that the sum of the terms resulting from the product of any two columns of the design matrix is zero. As a result the 2^2 design are orthogonal designs. This property of the 2^k design offers a great advantage in the analysis because of the simplifications that result from orthogonality. The 2^2 design can also be represented geometrically using a square with the four treatment combinations lying at the four corners, as shown in figure 6.1(c). [Montgomery, 1992]

2^3 Design

The 2^3 design is a two level factorial experiment design with three factors (say factors *A*, *B* and *C*). This design tests three ($k = 3$) main effects, *A, B* and *C*; three two factor interaction effects, *AB, BC, AC*; and one three factor interaction effect, *ABC*. The design requires eight runs per replicate. The eight treatment combinations corresponding to these runs are (1), *a,b,ab,c,ac,bc* and *abc*. Note that the treatment combinations are written in such an order that factors are introduced one by one with each new factor being combined with the preceding terms. This order of writing the treatments is called the *standard order* or *Yates' order*. The 2^3 design is shown in Figure 6.2 (a). The design matrix for the 2^3 design is shown in Figure 6.2 (b). The design matrix can be constructed by following the standard order for the treatment combinations to obtain the columns for

the main effects and then multiplying the main effects columns to obtain the interaction columns. [Montgomery, 1992]

Treatment Name	Factors		
	A	*B*	*C*
(1)	-1	-1	-1
a	1	-1	-1
b	-1	1	-1
ab	1	1	-1
c	-1	-1	1
ac	1	-1	1
bc	-1	1	1
abc	1	1	1

(a)

I	*A*	*B*	*AB*	*C*	*AC*	*BC*	*ABC*
1	-1	-1	1	-1	1	1	-1
1	1	-1	-1	-1	-1	1	1
1	-1	1	-1	-1	1	-1	1
1	1	1	1	-1	-1	-1	-1
1	-1	-1	1	1	-1	-1	1
1	1	-1	-1	1	1	-1	-1
1	-1	1	-1	1	-1	1	-1
1	1	1	1	1	1	1	1

(b)

Fig. 6.2: The 2^3 design- Figure (a) shows the experiment design and (b) shows the design matrix. [Montgomery, 1992]

The 2^3 design can also be represented geometrically using a cube with the eight treatment combinations lying at the eight corners as shown in Figure 6.3.

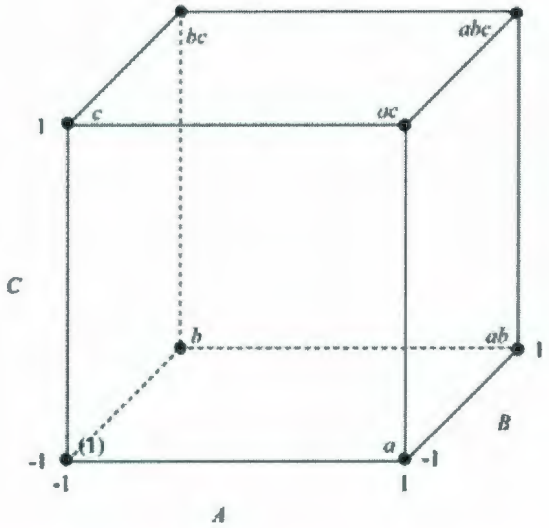

Fig. 6.3: Geometric Representation of 2^3 *Designs*. [Montgomery, 1992]

6.3 Response Surface Designs

Response surface method (RSM) designs help to quantify the relationships between one or more measured responses and the vital input factors. If there are 5 or more factors, doing a two-level factorial screening design is a wise decision to consider. At least some of the factors for RSM must be quantitative, continuous variables. The objective is to find a desirable location in the design space. This could be a maximum, a minimum or an area where the response is stable over a range of the factors. Goals might include meeting a set of specifications for several responses simultaneously. RSM can also be used as a model reduction method. For example, replacing a FEM with a simple regression model could result in a model with several curve fit parameters rather than hundreds or thousands of degrees of freedom. In the present study, the goal is to fit response surfaces to flexible mode activity as a function of payload and road input frequency. While the range of parameters can be found by conducting a "brute force"

batch simulation with many runs, it may be more efficient to take sparse samples of the payload and frequency variables and fit response surfaces to the small samples. If the union of the response surfaces for small regions of the parameter space converges to the brute force surface, then the rigid model range of validity could have been found with fewer simulation runs. An algorithm is proposed, and demonstrated for the free-free beam.

Design descriptions and analyses are best done with coded factors. Coding reduces the range of each factor to a common scale, -1 to +1, regardless of its relative magnitude. Scaling establishes factor levels that can be orthogonal (or nearly so). Also, it is easier to think in terms of changes from low to high for the factors than to think about their actual values - especially when thinking about squared terms and interactions. For example, one factor may vary from 100 to 200 while another varies from 0.1 to 0.5.

The most popular response surface method (RSM) design is the central composite design (CCD). A CCD has three groups of design points:

(a) two-level factorial or fractional factorial design points

(b) axial points (sometimes called "star" points)

(c) center points

CCD's are designed to estimate the coefficients of a quadratic model. All point descriptions will be in terms of coded values of the factors.

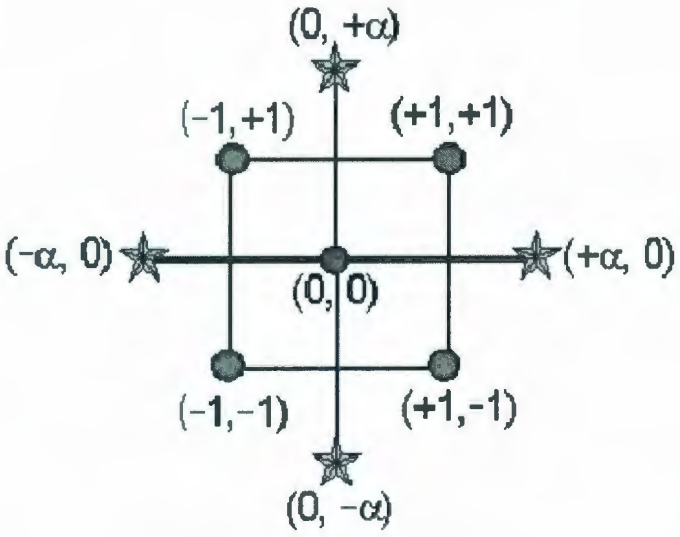

Fig. 6.4: Central Composite Design [Myers, 1995]

(a) Factorial Points

The two-level factorial part of the design consists of all possible combinations of the +1 and -1 levels of the factors. For the two factor case there are four design points: (-1, -1) (+1, -1) (-1, +1) (+1, +1)

(b) Star or Axial Points

The star points have all of the factors set to 0, the midpoint, except one factor, which has the value +/- Alpha. For a two factor problem, the star points are: (-Alpha, 0) (+Alpha, 0) (0, -Alpha) (0, +Alpha) .The value for Alpha is calculated in each design for both rotatability and orthogonality of blocks. The experimenter can choose between these values or enter a different one. The default value is set to the rotatable value.

Another position for the star points is at the face of the cube portion on the design. This is commonly referred to as a face-centered central composite design. You can create

this by setting the alpha value equal to one, or choosing the Face Centered option. This design only requires three levels for each factor.

(c) Center Points

Center points, as implied by the name, are points with all levels set to coded level 0 - the midpoint of each factor range: (0, 0). Center points are usually repeated 4-6 times to get a good estimate of experimental error (pure error). For example, with two factors the design will be created with five center points by default. To summarize, central composite designs require 5 levels of each factor: -Alpha, -1, 0, 1, and +Alpha. One of the commendable attributes of the central composite design is that its structure lends itself to sequential experimentation. Central composite designs can be carried out in blocks.

In this research, User Defined CCD was used to obtain more precise results. The main difference between CCD and User Defined RSM is that User Defined RSM was developed to select design points in a way that minimizes the variance associated with the estimates of specified model coefficients (Myers & Montgomery, 2002). Candidate points are a set of possible points from which to choose the actual design points. The number of possible points may be only a few when there are just a few factors and a small model is desired. Or, there may be thousands of points when there are many factors and the model is quadratic or cubic.

The number of candidate points generated by software which was used in this research depends on the model; here are the types of points that are generated:

- Vertices or Factorial points - A two-level factorial, full or fractional, forms the core. The high and low levels of the factorial come from the high and low level constraints on each factor.
- Axial Check blends - To provide lack of fit points, the factorials are augmented with check points. The check points are embedded within the main factorial, with levels that are the average of the vertices of the design space and the overall centroid.
- Overall Centroid - The center point of the design space is added to the candidate set.

- Centers of edges - Points midway between adjacent factorial points.
- Interior points - Average of centers of edges and with the overall centroid and also averages of constraint plane centroids with the overall centroid.

In this research for each subsection of the total contour plot 4 vertex points, 4 center edge points, 4 axial check blend points. 4 interior points and 1 center point were used to derive the plots in each subsection precisely. After defining the minimum and maximum limit of the load and frequency it automatically selects 17 points for which simulation was done in bond graph software and RA values were obtained and entered as an input in Response field in DOE simulator software. The software package used was Design Experts. Load was varied from 0.1 kg to 300 kg and frequency was varied from 1 rad/s to 12 rad/s. These parameter ranges encompassed the entire range of validity for a particular bump height. The total area was segmented using 13 subsections. A detailed algorithm and discussion will be done in the following section. For each subsection 17

points were generated using user defined RSM method. The goal is to use RSM to find the extents of the range of validity using fewer runs than were required in Chapter 5.

6.4 Algorithm

This algorithm was created based on the work done with the MS Excel and Design Experts software. The algorithm is shown as a flowchart in Figure 6.5 below, to which the reader is referred in the following explanation. The first step of the algorithm, assuming that an exhaustive brute force search had not been done, would be for the analyst to choose parameter ranges that they believed would span the full range of validity or invalidity of the reduced model (see flowchart, *Guess ranges of factors to cover entire validity range*). A DOE experiment is then designed, and response surface generated for a small sample of points in those ranges (*Generate response surface*). Inspection of the contour plot reveals whether or not it covers the entire validity range (*Encompasses entire region?*), if there are no low-activity contours of the surface remaining at the edge. The user may decide that the range of validity has been essentially captured even if the range is not entirely contained on the plot. In Figure 5.8 of Chapter 5, for instance, the contour plot for parameter combination 1 may be assumed to cover the entire range because there appears to be threshold value of road wavelength above which flexible modes are not excited regardless of load. Other inputs such as discrete bumps might excite the flexible modes, but this would require re-calculation of activity and generation of new validity range plots. If the first surface appears to cover the entire range of parameter values for which maximum RA is below the threshold, then that area

is subdivided into "n" smaller segments (*Divide into smaller zones*). For each smaller segment, a DOE experiment is designed and a response surface created after simulating the bond graph model (*Generate surface for each sub region*). Then the contours of those segments were plotted. If the contours are equivalent when the smaller area is overlaid onto the bigger region plot, then it is assumed that no sharp local peaks or valleys occur within that smaller area (*Overlay on overall surface & contours similar?*). The process is repeated for adjacent smaller regions until the entire original parameter area has been explored. Upon completing the finer-resolution analysis of the original region, a check is required to ensure that no other distant regions of the parameter space contain any regions of low maximum RA (*Pick large adjacent region*). Response surfaces for large test regions, with sparsely distributed design points, adjacent to the original region are then generated. If any new regions of maximum RA below the threshold are found (*More points with relative activity below threshold?*), then the same steps are followed again (*Expand validity range*). If not, then the algorithm is terminated (*Stop*) and the original region is considered accurate.

Section 6.5 shows the results of applying the algorithm to the free-free beam model of Chapter 4.

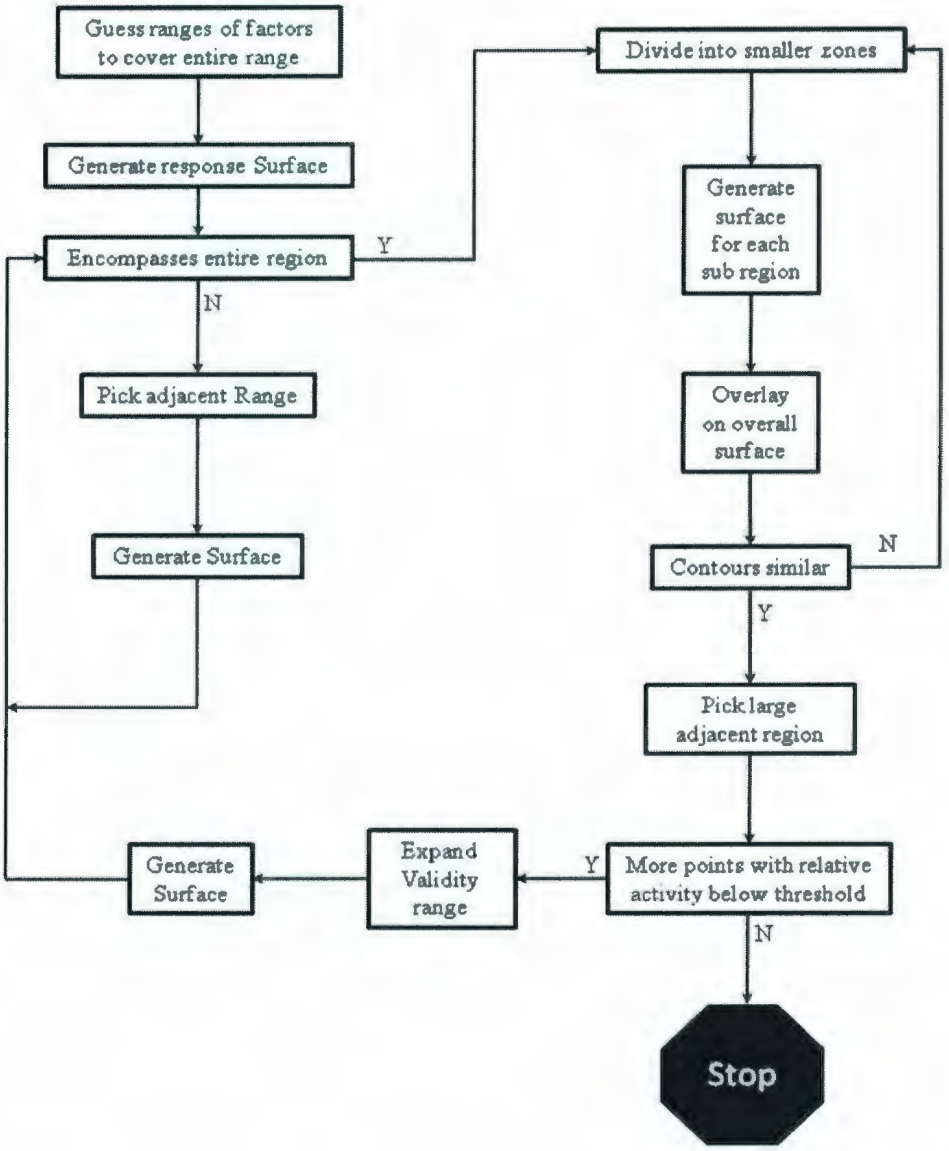

Fig. 6.5: Algorithm for Efficiently Determining Range of Model Validity Using DOE and Response Surfaces.

6.5 Explanation of Plot

The threshold value of Relative Activity was chosen to be 0.05 as before. That means if for any load and frequency combination the maximum Relative Activity for a flexible mode goes higher than this value then for that load and frequency a rigid model is not valid. Figure 6.6 shows a zone (lower left) which is the area below 0.05. In this region the model is assumed to be appropriate. The x axis is load in kilograms and the y axis is frequency in rad/s. There is a legend beside the plots which shows the color code for different area or region.

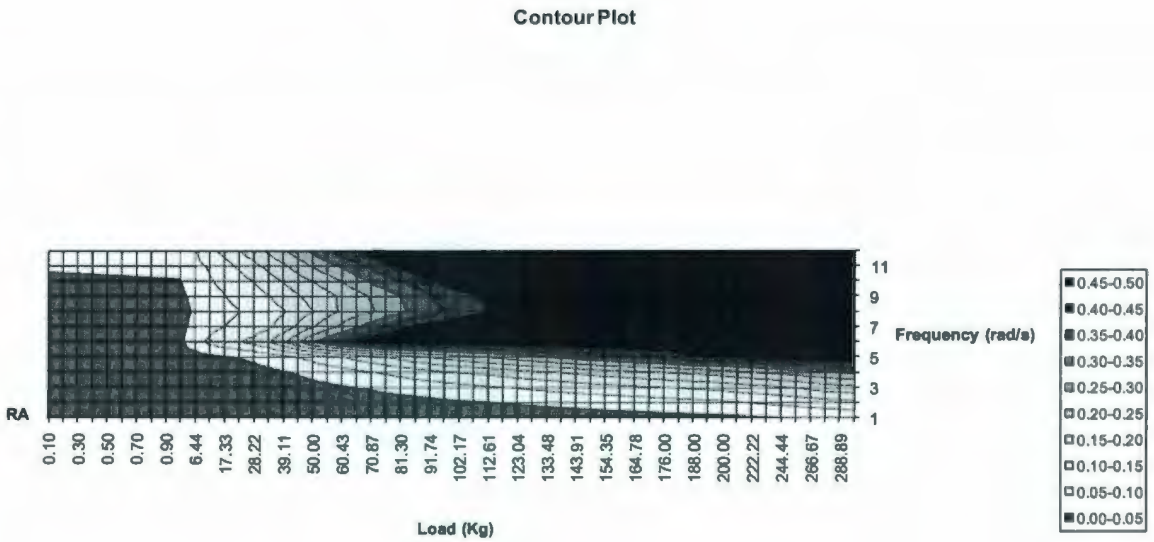

Fig. 6.6: Contour Plot- Range of Validity of Rigid Model

Figure 6.7 shows a 3D surface plot of the range of validity.

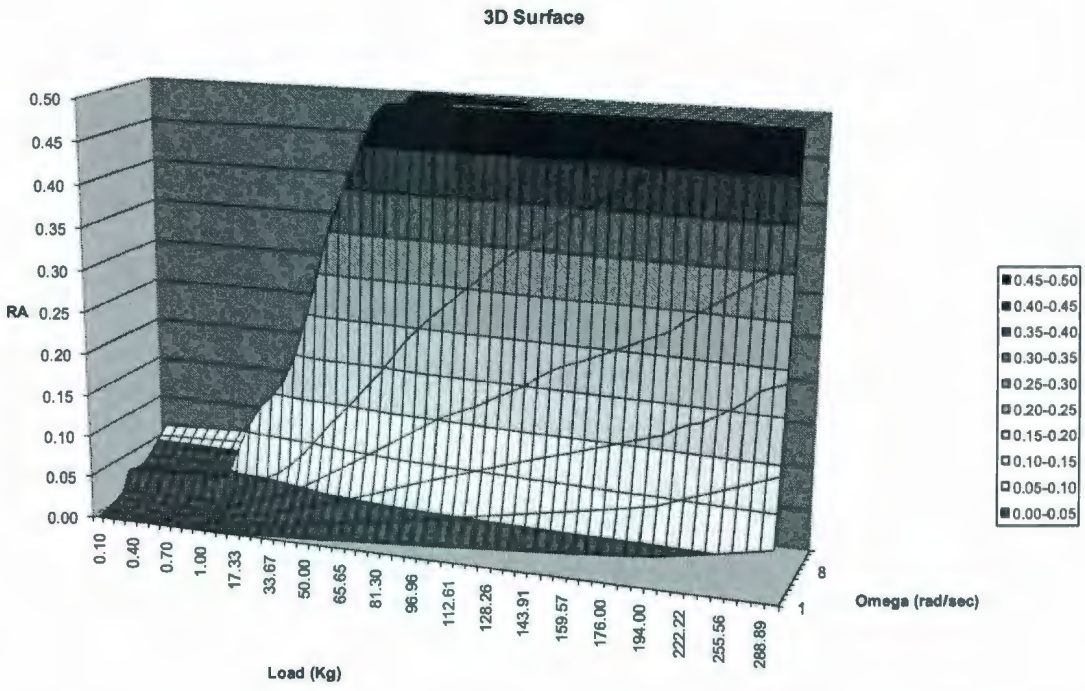

Fig. 6.7: 3D Surface Plot-Range of Validity of Rigid Model

This region was segmented and DOE experiments were designed for the sub-regions. The range of validity zone was divided into 3 main subdivisions: from 0.1 to 1 kg load, 1 to 100 kg load and 100 to 300 kg load. The DOE response surface for the first subdivision is shown in Figure 6.8. The top line is the contour line for threshold value 0.05. It starts from the frequency near 10 rad/sec which exactly same as the Figure 6.7.

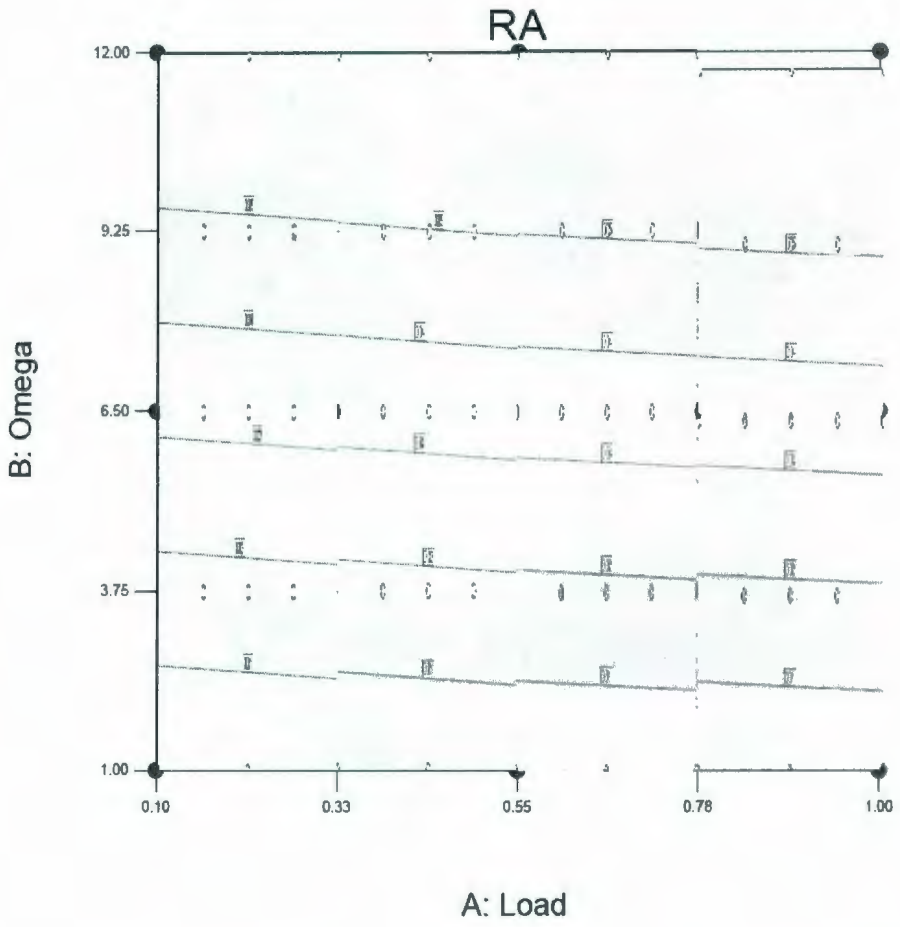

Fig. 6.8: Contour Plot: 0.1 kg-1 kg Range

The medium range of 1-100 kg was also matched by generating and joining five smaller response surfaces, as shown in Figure 6.9 below. In Figure 6.9, note that the DOE sample points are visible. Figure 6.10 shows the 100-300 kg range.

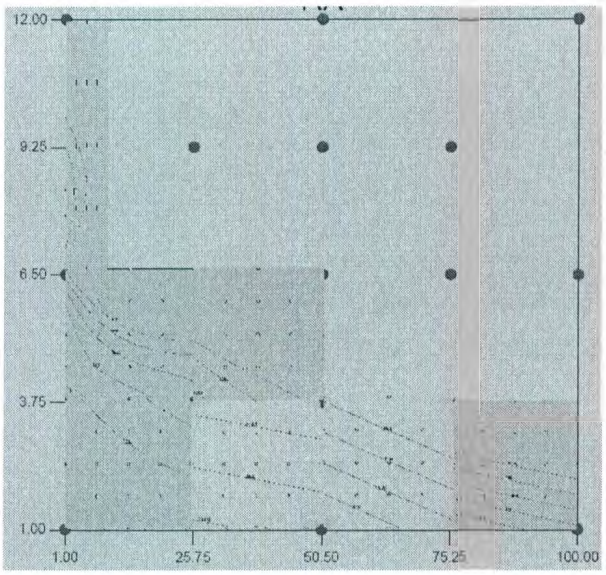

Fig. 6.9: Contour Plot: 1 kg-100 kg Range

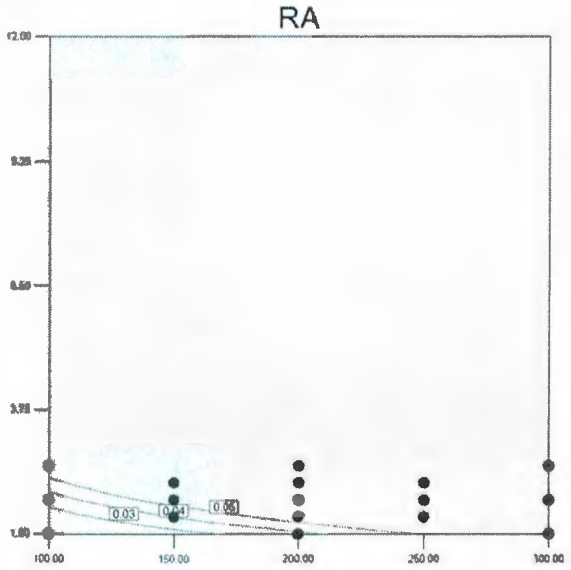

Fig. 6.10: Contour Plot: 100 kg-300 kg Range

As seen from the union of Figures 6.8 through 6.10, the algorithm captures the range of validity of the model. The number of required runs using the algorithm was 220, compared to 660 runs using a brute force, fine grid search of the parameter space in Fig. 6.6. This does not prove that the algorithm will always reduce the number of runs, as one could arrive at the range of validity by chance with a coarse grid of evenly spaced parameter sets. Future work will involve refining the algorithm, and considering alternative approaches such as working outwards from an initial point in the range of validity as opposed to working in from a large region encompassing the range.

Chapter 7

Conclusions and Future Work

This research investigated whether flexible effects must be included in truck models when studying ride quality given the truck parameters and road profile. Finite element modeling of a single rail frame was done to obtain natural frequencies for use in modal expansion bond graphs of the truck frame. A free-free beam bond graph model was developed to represent a flexible truck frame, and the modal parameters were derived theoretically. The flexible model was then incorporated into a nonlinear half-car model of a Class VI truck. A power-based model partitioning algorithm, based on a quantity called "relative activity (RA)" was applied to the free free beam model to find a range of validity of a rigid model when two factors were varied. Residual sum of the error between rigid and flexible models were obtained to quantify the performance of reduced (rigid) model over full model. There was a correlation between maximum relative activity of flexible modes and error of a rigid model. Low relative activity means that the aggregate power flow between flexible modes and rigid elements such as suspension and engine is low, and therefore the rigid elements excite the flexible modes but not vice versa. For the Class VI truck model with a torque input to the rear wheels that represents full-throttle acceleration from rest, the rigid model validity was found for variations in two of the following parameters, with one held constant: sinusoidal road bump height, road wavelength, and payload mass.

Range of validity was found using a fine grid search of a large parameter space. Design of experiments response surface method was used to develop an algorithm which showed potential to reduce the number of simulation runs required to compute model range of validity, by taking sparse samples in parameter space subregions and joining them together.

The research was successful in that a systematic approach was successfully used to determine if frame flexibility can be neglected in truck ride quality models. Relative activity was considered which allows quantitative determination of range of validity of the rigid models, instead of relying on possibly unreliable assumption and intuition of the modeler. The bond graph method was used, because the explicit power flow paths of bond graphs facilitate the power-based partitioning of flexible modes. The free-free beam case study is the first application of the partitioning algorithm to flexible systems. In addition, the vehicle model is a useful extension of typical flexible ride quality models where suspension motion is assumed vertical and the pitch angle is assumed small. The DOE/response surface algorithm shows sufficient potential to reduce simulation runs, that it should be refined as discussed in the future work below.

A limitation of the method is that because activity is a nonlinear metric, it is not feasible to establish an analytical relation between relative activity and the error in actual model outputs between a full and partitioned model. There are many possible outputs of interest, of varying power levels, in a big model, and many element interactions mean that the residual sum error of all individual outputs may not correlate equally well with maximum RA. Some checking and input from the modeler may still be required even though the partitioning method is intended to automate generation of proper models.

Some future work includes:

- Constructing a more complete finite element model of the frame, and studying the effect on modal frequencies when the suspension and cab are mounted. Doing this will result in more accurate natural frequencies for a specific vehicle.
- With the aid of a more complete finite element model, studying the effect of different payload shapes and weight distributions on the beaming mode natural frequencies. A distributed load such as a shipping container would have a different effect than a point load, and long flat loads such as steel beams might act like leaf spring elements and make the truck's flat bed stiffer.
- Currently, by using response surface methods, it is limited to studying the range of validity of a model subject to variations in two parameters. Future work will investigate methods to study range of validity for several parameters. One possible approach is to generate and analyze a collection of surfaces, one for every possible two-parameter combination. Other possible methods include curve-fitting to generate maximum RA as a function of several variables, and using sensitivity analysis to efficiently find the boundaries of the multidimensional parameter space.
- Refining DOE-based algorithm, using optimization techniques such as steepest descent or ascent algorithms. This thesis begins with a parameter range that surrounds the range of validity and then subdivides it. Another possible approach is to start with an arbitrary parameter range and work outward to the range of validity boundary, and then move along the boundary until the range of validity is found.

- Studying the relation between vertical vibration of the frame and longitudinal vibration of the drivers head. This may help in setting maximum RA thresholds less arbitrarily. If certain RA values create longitudinal vibrations that are known to cause fatigue or discomfort, then these values may dictate an appropriate threshold for truck vibration applications. While the goal of proper modeling is to reduce the need for domain experts in generating models, the modeler cannot be completely removed from the process, and continued use of the approach described in this thesis may eventually lead to truck-specific activity thresholds. The mapping between activity and actual physical system response remains an open research topic.

References

1. Boilear, P. E., Pakheja. S, and Liu, P.J. "A Combined Suspension Seat Vehicle Driver Model for Estimating the Exposure to Whole Body Vehicular Vibration and Shock." International Journal of Vehicle Design 24 (4) (1997): 244-65.

2. Boileau, P. E., Turcot D, and Scory, H. "Evaluation of Whole Body Vibration Exposure using a Fourth Power Method and Comparison with ISO 2631." Journal of Sound and Vibration 129 (1989): 143-54.

3. Corbridge, C., and Griffin, M.J. "Vibration and Comfort: Vertical and Lateral Motion in the Range 0.5 to 5.0 Hz." Ergonomics 29 (1986): 249-72.

4. Donati, P., Grosjean A, Mistrot P, and Roure, L. "The Subjective Equivalence of Sinusoidal and Random Whole-Body Vibration in the Sitting Position (An Experimental Study Using The 'Floating Reference Vibration Method')." Ergonomics 26 (1983): 251-73.

5. Ferris, John B. "Factors Affecting Perceptions of Ride Quality In Automobiles." ASME IMECE, DSC 65 (1998).

6. Howarth, H. V., and Griffin, M.J. "The Frequency Dependence of Subjective Reaction to Vertical and Horizontal Whole Body Vibration at Low Magnitudes." Journal of Acoustical Society of America 83 (1988): 1406-413.

7. Ibrahim, I. M. "A Generally Applicable 3D Truck Ride Simulation With Coupled Rigid Bodies and Finite Element Models." International Journal of Heavy Vehicle Systems 11 (2004).

8. Ibrahim, I. M., Crolla, D.A, and Barton, D.C. "Effect of Frame Flexibility on the Ride Vibration of Trucks." Computers & Structures, Elsevier International, 1996, 709-713 (2009).

9. Jiang, Z. "Heavy Vehicle Ride Comfort: Literature Survey." Heavy Vehicle Systems 8 (2001): 258-84.

10. Ledesma, Ragnar H. "Effect of Chassis Frame Compliance on Heavy Truck Ride Quality." ASME Energy Sources Technology Conference (1998).

11. Louca, Loucas S., Stein, J.L, and Hulbert, G.M. "A Physical Based Model Reduction Metric with an Application to Vechicle Dynamics." IFAC Nonlinear Control Systems Symposium, Netherlands (1998).

12. Louca, Loucas S., Stein, J.L, Hulbert, G.M. and Sprague, J. "Proper Model Generation: An Energy-Based Methodology." Proc. International Conference on Bond Graph Modeling, ICBGM'97 (1997).

13. Rideout, Geoff, Stein, J.L, and Louca, Loucas S., "Systematic Identification of Decoupling in Dynamic System Models." Journal of Dynamic Systems, Measurement, and Control 129 (2007): 503-13.

14. Sendur, Polat, Stein, J.L, Peng, H, and Louca, Loucas S. "An Algorithm for the Selection of Physical System Model Order Based on Desired State Accuracy and Computational Efficiency." Proc. ASME IMECE (2003).

15. Yamada, Y., and Watanbe, Y. "Analysis of Heavy Duty Truck Ride." SAE International Pacific Conference On Automotive Engineering p169 (1985).

16. Yamakawa, Junya, Kojima, A, and Watanbe, K. "A Method of Torque Control for Independent Wheel Drive Vehicles on Rough Terrain." Journal of Terramechanics, Elsevier Limited (2007): 371-81.

17. Zhang, Yuan. "Vehicle Chassis/Suspension Dynamics Analysis-Finite Element Model vs. Rigid Body Model." SAE Special Publication 1338 (1998): 113-26.

18. Dahlberg, T. An optimized speed controlled of a 2-DOF vehicle travelling on a randomly profiled road. Journal of Sound & Vibration, *62*, 541-546 (1979).

19. Abdollahi, M, and Olatunbosun, O. "Vehicle ride enhancement using simulation assisted rubber mount design." International Journal of Vehicle Design, *26*, 2 (2001)

20. Gadala, M.E., El-Madany, M.M., and Gadala, M.S.. "Finite element and analytical modeling of a tractor-semitrailer vehicle." Journal of Computers and Structures, *23*, 831-836 (1986).

21. Baum, J.H., Bennett, J.A., and Carne, T.G. "Truck ride improvement using analytical and optimization methods". SAE Paper no. 770609 (1977).

22. Jalali, A, and Goodarzi, A. "An investigation of body flexibility effects on the ride comfort of long vehicles". CANCAM 2006.

23. Gawthrop, P. and Balance, D. "Symbolic Algebra and Physical-Model-Based Control". Bond Graph Digest, 1(1). (1997)

24. Ledesma, R. "Effect of chassis frame compliance on heavy truck ride quality". ASME Energy Sources Technology Conference, 7 (1998)

25. Sendur, P., Stein, J.L., Peng, H., and Louca, L.S. "A Model Accuracy and Validation Algorithm." Proc. 2002 ASME International Mechanical Engineering Conference and Exhibition, New Orleans, LA. American Society of Mechanical Engineers, New York, NY.

26. Stein, J.L. and Wilson, B.H. "An Algorithm for Obtaining Proper Models of Distributed and Discrete Systems". J. Dynamic Systems Measurement and Control, v. 117(4), pp. 534-540. American Society of Mechanical Engineers, New York, NY. (1995)

27. Box, G. E. P., Hunter, W. G., and Hunter, J. S., Statistics for Experimenters, John Wiley & Sons, Inc., New York, (1978).

28. Box, G. E. P., and Behnken, D. W., "Some New Three Level Designs for the Study of Quantitative Variables," Technometrics, Vol. 2, No. 4, pp. 455-475, (1960).

29. Montgomery, Douglas C., Design and Analysis of Experiments, John Wiley & Sons, Inc., New York (2001).

30. Shabana, A. Dynamics of Multibody Systems. Wiley, New York (1989).

31. Tong, Y."Vehicle dynamic simulations based on flexible and rigid multibody models". SAE Technical Paper Series, *01*, 114. (2000)

32. Karnopp, D. C, Margolis, D. L, and Rosenberg, R. C. System Dynamics: Modeling and Simulation of Mechatronic Systems, *4th Edition*. New York: Wiley Interscience (2005).

33.Matsushita, A, Takeda, N, and Naito, T. "An example of body vibration analysis for light-duty truck". Isuzu Technical Journal, 63, 1 (1979).

34. Gillespie, T. "Developments in road roughness measurement and calibration procedures." 5th REAAA Conf. Australian Road Res. Board, 23, 91-112 (1986).

35. Myers, R. H., and Montgomery, D. C., Response Surface Methodology: Process and Product Optimization Using Designed Experiments, John Wiley & Sons, Inc., New York (1995).

36. 20SIM v.4.0. Controllab Products b.v., Enschede, Netherlands (2006).

37. Design-Expert® version 7.1, Stat-Ease, Inc. Minneapolis, MN (2007).